HYDRAULIC FRACTURING STRATEGY IN GAS CONDENSATE RESERVOIRS

Mr. Kuntol Chinrungkhakul

A Thesis Submitted in Partial Fulfillment of the Requirements

for the Degree of Master of Engineering Program in Petroleum Engineering

Department of Mining and Petroleum Engineering

Faculty of Engineering

Chulalongkorn University

Academic Year 2010

กลยุทธการทำไฮโดรลิคแฟรคเจอริงในแหล่งกักเก็บก๊าซธรรมชาติเหลว

นาย กุณฑล ชินรังคกุล

วิทยานิพนธ์นี้เป็นส่วนหนึ่งของการศึกษาตามหลักสูตรปริญญาวิศวกรรมศาสตรมหาบัณฑิต
สาขาวิชาวิศวกรรมปิโตรเลียม   ภาควิชาวิศวกรรมเหมืองแร่และปิโตรเลียม
คณะวิศวกรรมศาสตร์ จุฬาลงกรณ์มหาวิทยาลัย
ปีการศึกษา 2553

Thesis Title   HYDRAULIC FRACTURING STRATEGY IN GAS
           CONDENSATE RESERVOIRS

By   Mr. Kuntol Chinrungkhakul

Field of Study   Petroleum Engineering

Thesis Advisor   Assistant Professor Suwat Athichanagorn, Ph.D.

    Accepted by the Faculty of Engineering, Chulalongkorn University in Partial Fulfillment of the Requirements for the Master's Degree

.... Dean of the Faculty of Engineering

(Associate Professor Boonsom Lerdhirunwong, Dr.Ing.)

THESIS COMMITTEE

..............................Chairman

(Associate Professor Sarithdej Pathanasethpong)

.... Thesis Advisor

(Assistant Professor Suwat Athichanagorn, Ph.D.)

..................................External examiner

(Saifon Daungkaew, Ph.D.)

กุณฑล ชินรังคกุล : กลยุทธ์การทำไฮโดรลิคแฟรคเจอริงในแหล่งกักเก็บก๊าซธรรมชาติ เหลว (HYDRAULIC FRACTURING STRATEGY IN GAS CONDENSATE RESERVOIRS) อ.ที่ปรึกษาวิทยานิพนธ์หลัก: ผศ.ดร. สุวัฒน์ อธิชนากร, 88 หน้า.

แหล่งกักเก็บก๊าซธรรมชาติเหลวมักจะแสดงคุณสมบัติการไหลของก๊าซธรรมชาติเหลวที่ ซับซ้อน แหล่งกักเก็บก๊าซธรรมชาติเหลวนั้นมีสถานะเป็นก๊าซที่สภาวะของแหล่งกักเก็บในตอน แรก ก๊าซธรรมชาติเหลวกลั่นตัวเป็นของเหลวในแหล่งกักเก็บเมื่อความดันก้นหลุมลดลงต่ำกว่า ความดันกลั่นตัว ก๊าซธรรมชาติเหลวที่สะสมบริเวณใกล้เคียงหลุมกีดขวางการไหลของก๊าซและลด ความสามารถในการซึมผ่านของก๊าซ อีกทั้งยังเป็นสาเหตุให้ความสามารถในการผลิตของหลุมและ การผลิตของส่วนประกอบหนักที่ระดับพื้นดินลดลง

การทำไฮโดรลิคแฟรคเจอริงนั้นเป็นวิธีปฏิบัติสามัญที่รู้จักกันดีว่าเป็นวิธีที่ช่วยเพิ่ม ความสามารถการผลิตของหลุม โดยเฉพาะอย่างยิ่งในแหล่งกักเก็บก๊าซธรรมชาติเหลวที่มีค่าความ ซึมผ่านต่ำ หลุมแนวนอนที่ผ่านการทำไฮโดรลิคแฟรคเจอริงนั้นสามารถเพิ่มความสามารถในการ ผลิตเป็นอย่างมากเมื่อเทียบกับหลุมแนวนอนที่ไม่ได้ทำไฮโดรลิคแฟรคเจอริง มีหลุมแนวนอน จำนวนมากในแหล่งกักเก็บก๊าซธรรมชาติเหลวแต่มีเพียงบางหลุมที่ทำไฮโดรลิคแฟรคเจอริง

จุดประสงค์หลักของงานศึกษานี้คือเพื่อศึกษาการทำไฮโดรลิคแฟรคเจอริงสำหรับหลุม แนวนอนในแหล่งกักเก็บก๊าซธรรมชาติเหลวโดยใช้แบบจำลองแหล่งกักเก็บเพื่อให้เข้าใจ ผลกระทบของการทำไฮโดรลิคแฟรคเจอริงต่อการผลิตก๊าซธรรมชาติเหลวมากขึ้น ผลกระทบของ ตัวแปรในการออกแบบรอยแตกในหินต่าง ๆ ต่อศักยภาพของหลุมแนวนอนในแหล่งกักเก็บก๊าซ ธรรมชาติเหลวได้ถูกพิจารณาในงานศึกษานี้ ตัวแปรนั้นได้แก่ระยะห่างระหว่างรอยแตก ความยาว ของรอยแตก ความกว้างของรอยแตก ค่าความซึมผ่านของรอยแตกและจำนวนรอยแตก

ผลลัพธ์ที่พบในงานศึกษานี้แสดงให้เห็นว่าการทำไฮโดรลิคแฟรคเจอริงลดเวลาในการ ผลิตก๊าซธรรมชาติเหลวได้เป็นอย่างมาก การทำไฮโดรลิคแฟรคเจอริงสามารถลดความดันที่ลดลง ได้ ทำให้การกลั่นตัวเป็นของเหลวของก๊าซธรรมชาติเหลวใกล้หลุมน้อยลงและการผลิตของก๊าซ ธรรมชาติเหลวที่ระดับพื้นดินเพิ่มขึ้น

ภาควิชา วิศวกรรมเหมืองแร่และปิโตรเลียม ลายมือชื่อนิสิต ....

สาขาวิชา วิศวกรรมปิโตรเลียม .... ลายมือชื่ออ.ที่ปรึกษาวิทยานิพนธ์หลัก ....

ปีการศึกษา 2553 ....

5071601221 : MAJOR PETROLEUM ENGINEERING
KEYWORDS: /MULTIPLE HYDRAULIC FRACTURES/GAS CONDENSATE RESERVOIR/CONDENSATE BLOCKAGE

KUNTOL CHINRUNGKHAKUL. HYDRAULIC FRACTURING STRATEGY IN GAS CONDENSATE RESERVOIRS. ADVISOR: ASST. PROF. SUWAT ATHICHANAGORN, Ph.D., 88 pp.

Gas condensate reservoirs usually exhibit complex flow behaviors. The gas condensate reservoir is initially gas at the reservoir condition. Liquid forms in the reservoir when the bottomhole pressure drops below the dew point pressure. The accumulated condensate in the vicinity of the well bore causes a blockage effect, reduces the gas effective permeability, and causes reduction in well productivity and recovery of heavy components at the surface.

Hydraulic fracturing is a well known and common practice to improve the well productivity, especially in tight gas condensate reservoirs. Horizontal well with hydraulic fractures can achieve significant productivity improvements over a non-fractured horizontal well. Many horizontal wells have been drilled in gas condensate reservoirs, but a few of them was hydraulically fractured.

The main objective of this paper is to study hydraulic fracturing for horizontal wells in gas condensate reservoirs using reservoir simulation model to obtain better understanding of its effect on gas and condensate recovery. Effect of different hydraulic fracture design parameters on the performance of hydraulically fractured horizontal well was studied. These parameters are fracture spacing, fracture half-length, fracture width, fracture permeability and number of fracture.

The results found in this study show that fracturing the well significantly decreases gas production time. Hydraulic fracturing reduces the pressure drawdown, leading to less liquid condensate dropout near the wellbore and more condensate produced at surface.

Department: Mining and Petroleum Engineering   Student's Signature *ภฑฑล ชินรังคกุล*

Field of Study: Petroleum Engineering   Advisor's Signature *Suwat Athichanagorn*

Academic Year: 2010

Acknowledgements

Contents

Lists of Tables

Lists of Figures

List of Abbreviations

bbl	barrel
bbl/D	barrel per day
BHP	bottomhole pressure
btu	British thermal unit
D	darcy
FVF	formation volume factor
GOR	gas oil ratio
IFT	interfacial tension
lb/ft^3	pound per cubic feet
LGR	local grid refinement
M	thousand (1,000 of petroleum unit)
m^3/h	cubic meter per hour
$MM\ m^3$	million cubic meter
Mscf/D	thousand standard cubic feet per day
Msm^3/D	thousand standard cubic meter per day
OGR	oil gas ratio
OPEX	operational expenditure
psia	pound per square inch absolute
PI	productivity index
PVT	pressure-volume-temperature
PVTO	live oil PVT properties (dissolved gas)
PVTG	wet gas PVT properties (vapourised oil)
SCAL	special core analysis
SGFN	gas saturation function
SOF3	oil saturation function
SWFN	water saturation function
stb	stock-tank barrel
VFP	vertical flow performance

Nomenclature

F_{cd}	fracture conductivity
k	reservoir permeability
k_f	fracture permeability
k_{rg}	gas relative permeability
k_{ro}	oil relative permeability
N_c	capillary number
P_{bub}	bubble point pressure
p	pressure
p_g	gas pressure
R_s	dissolved gas-oil ratio
S_g	gas saturation
S_o	oil saturation
S_w	water saturation
t	time
u	flow rate
v_g	gas velocity
W_f	fracture width
X_f	fracture half-length

GREEK LETTERS

Δ	difference operator
μ	Newtonian viscosity of the fluid
μ_g	gas viscosity
ρ	density of the fluid
ϕ	porosity
σ	interfacial tension
β	non-Darcy flow coefficient
σ	stress

CHAPTER I

INTRODUCTION

Numerous studies have shown that gas condensate reservoirs exhibit a complex near-wellbore behavior where two phases, reservoir gas and liquid condensate coexist and form a bank when the bottomhole flowing pressure drops below the dew point pressure. Under these conditions, three regions of different liquid saturations and mobilities co-exist in the reservoir. The first zone, away from the wellbore, is above the dew point pressure, with reservoir gas only. Next to it, a second zone, where the reservoir pressure reaches the dew point pressure, contains two phases, reservoir gas and liquid condensate. The liquid is immobile as its saturation is below the critical condensate saturation, but only gas flows. The third zone is near the wellbore where the condensate saturation is above the critical condensate saturation, and condensate and gas flow together. In zones 2 and 3, the existence of two phases reduces the relative permeability to gas, thereby reducing the productivity of the well.

Various solutions have been implemented in order to remediate such a production loss. Hydraulic fracturing is a well known and common practice to improve the well productivity especially in tight gas condensate reservoirs. A hydraulic fracture reduces the flow resistance around a well bore, decreasing the pressure drawdown hence, reducing the negative impact of the condensate banking.

This thesis studies the near-wellbore behaviors and productivities of a hydraulically fractured horizontal well in a low permeability gas condensate reservoir. The reservoir simulator, ECLIPSE 100, was used to simulate a horizontal well with multiple hydraulic fractures. Effects of various factors such as fracture half-length, fracture width, fracture permeability, condensate bank size, the optimal fracture coverage and spacing for transverse fractures in horizontal well, on productivity of gas condensate wells were studied.

Horizontal well with hydraulic fractures can achieve significant productivity improvements over a non-fractured horizontal well. Fracturing the well significantly decreases production time. Stimulation reduces the pressure drawdown, leading to less liquid condensate dropout near the wellbore. The length of the fracture controls the productivity. Long fracture yields higher productivity improvement, despite lower

dimensionless fracture conductivity because the reduction in pressure drawdown far exceeds the pressure loss inside the finite conductivity fracture.

The result obtained from this paper help us to enhance understanding of hydraulic fracture in horizontal well and can be used as a guideline to increase productivity of wells drilled in gas condensate reservoirs.

1.1 Outline of Methodology

This thesis is to study the near-wellbore behaviors and productivities of a hydraulically fractured horizontal well in a low permeability gas condensate reservoir. The economics analysis will be used as criteria to determine the optimum hydraulic fracturing design. The studies are separated into four sections as following:

1. A non-fractured horizontal well in a low permeability gas condensate reservoir is modeled to obtain results for evaluating the productivity improvement when a horizontal well is hydraulically fractured.
2. A hydraulically fractured horizontal well is then modeled to evaluate the effects of various factors on well productivity:
   - Fracture spacing
   - Fracture half-length
   - Fracture width
   - Fracture permeability
   - Number of fracture
3. Condensate saturation profile of the hydraulically fractured horizontal well and the non-fracture horizontal well is investigated.
4. Economy analysis is performed in order to investigate the feasibility of hydraulic fracturing project.

1.2   Review of Chapters

This thesis is organized into six chapters, and the outlines of each chapter are listed below.

Chapter II presents a literature review of the research done on gas condensate reservoir behavior, condensate blockage treatment, hydraulic fracturing in vertical well and hydraulic fracturing in horizontal well. In addition, some of the studies on the multiple hydraulic fracturing in horizontal well have been reviewed.

Chapter III describes theory and concepts related to this study.

Chapter IV shows simulation grid model used in this study.

Chapter V presents and discusses the results obtained from the simulation runs with different design parameters to understand the effect of fractures on productivity of gas condensate wells.

Chapter VI provides conclusions of the study and recommendations for further study.

CHAPTER II

LITERATURE REVIEW

This chapter discusses studies related to gas condensate reservoir behavior and hydraulic fracturing. Some works are significant for generating the most realistic simulation model which will be used to determine optimal hydraulic fracturing to enhance productivity. Review of the studies of important parameters such as non-Darcy flow and capillary number is also included.

The literature review has been sub-divided into five parts. The first part contains a review of the research done to study gas condensate reservoir behavior. The second part reviews some of the research done on condensate blockage treatment. The third part reviews the research done on hydraulic fracturing in vertical well. The fourth part reviews the research done on hydraulic fracturing in horizontal well. Finally, research done in the past on multiple hydraulic fracturing in horizontal well is reviewed.

2.1   Gas Condensate Reservoir Behavior

Chen *et al.* [1] studied the condensate behavior for two North Sea gas condensate reservoirs. They found that critical condensate saturation and relative permeability data were sensitive to flow rate. Increasing flow rate could restore the gas relative permeability. In a gas condensate reservoir, gas velocities near the well are generally very high. If the Reynold's number exceeds some value on the order of 1.0, Darcy's law may not be valid. The flow is then governed by Forchcheimer's equation and depends on a non-Darcy flow coefficient that is difficult to determine accurately.

Boom *et al.* [2] found that even at low condensate content, high condensate saturations may build up around the well as many volumes of gas pass through the near-well region. They also observed that the degree of impairment depends on the mobility of the gas and the condensate. Therefore, depending on the gas and condensate relative permeability, a pseudo-steady state develops where condensate

saturation allows the flow of fresh gas and condensate from deep into the reservoir into the near-well region.

2.2   Condensate Blockage Treatment

Settari *et al.* [3] investigated the effect of condensate blockage on the productivity index of hydraulically fractured wells in a complex, highly heterogeneous rich gas condensate reservoir of Smorkbukk field. The authors concluded that in the lower permeability range, proppant fracturing restored 50-70% of the PI loss of an actual well compared to a non-fractured single-phase PI.

Fevang and Whitson [4] proposed a relative permeability model for fitting steady state gas/oil relative permeability behavior, including the effect of capillary number on $k_{rg} = f(k_{rg}/k_{ro})$. The effect of capillary number on gas/oil relative permeability can result in a significant improvement in gas relative permeability and thereby reduce the negative impact of condensate blockage when proper relative permeability model is used. They proposed an empirical model for scaling gas/oil relative permeability for different rock types and regions with varying end-point saturations.

Wheaton and Zhang [5] developed a general theoretical treatment of condensate banking dynamic to show how the compositions of heavy components of a gas condensate change with time around production wells during depletion. An increase in the total molar concentration of heavy components around a well will occur once the flowing bottomhole pressure falls below the dew point. The rate of the change in heavy component composition is higher in rich gas than for lean gas condensate for a given reservoir system. They also observed that reservoir permeability and production rate have significant effects on condensate banking behavior.

Luo *et al.* [6] conducted a series of experiments to investigate condensate recovery based on two different development schemes: one where gas cycling is done above the dew point and the other where gas cycling is done below the dew point. They found that cumulative recovery above the dew point is more than that below the dew point for the same volume of gas injection. However, cost consideration will

come into picture for injection above the saturation pressure. The authors reported that during the gas injection at the reservoir pressure, mass transfer between the dry gas injected and the original gas condensate will lead to a rise in dew point pressure and earlier retrograde condensation, which may reduce the gas condensate recovery.

Chowdhury *et al.* [7] developed a new semi-analytical method to predict the well deliverability of a gas condensate well damaged by condensate banking. The authors divided the near-well region into several small increments and integrated the equation with the radius from the well as independent variable. They included the effect of trapping number and also accounted for non-Darcy flow in the new model. They concluded that the new model is able to accurately capture the effects of condensate banking and non-Darcy flow near the well and that the method is more general than the pseudopressure method of Fevang and Whitson (1999). One other major advantage of this method, according to the authors, is that unlike the pseudopressure method, this method doesn't need producing GOR to make the calculations.

2.3 Hydraulic Fracturing in Vertical Well

Hashemi and Gringarten [8] used reservoir simulation to quantify the increase in well productivity from different remediation solutions such as drilling horizontal wells instead of vertical wells, hydraulically fracturing vertical wells, etc. They found that horizontal wells and hydraulically fractured vertical wells improve well productivity, but the degree of improvement depends on well and reservoir parameters such as horizontal well lengths, permeability anisotropy, fracture length, and fracture conductivity. For the particular case studied, they found that a fracture with a half-length of 50 ft is equivalent to a horizontal well with a drainage hole length of 600 ft. The optimum choice, according to the authors, between horizontal wells and hydraulically fractured vertical wells, when both are technically feasible, can only be made from economic considerations.

2.4 Hydraulic Fracturing in Horizontal Well

Holditch [9] did an optimization study on the well spacing and fracture length of low permeability gas reservoirs. The authors studied three examples that represented a high permeability, a low permeability and a medium permeability gas reservoir. They concluded that the most important parameters in determining the optimum fracture length are the formation gas permeability and gas in place per section. For a high permeability reservoir, they found that short fractures and large well spacing will provide the optimum profit whereas for tight gas reservoirs, long hydraulic fractures and small well spacing are required to optimize the profit.

Baig and Droegemueller [10] studied productivity assessment of fractured and non-fractured vertical wells in a lean/intermediate low permeability gas condensate reservoir. Fracturing the well before the formation of the condensate bank significantly improves productivity. Stimulation reduces the pressure drawdown, leading to less condensate dropout near the wellbore, thus delaying the formation of the condensate bank. Fracturing increases the effective wellbore radius and hence reduces the near-wellbore pressure drawdown. Hydraulic fracturing enhances well productivity.

Medeiros *et al.* [11] studied the performance and productivity of horizontal well with longitudinal fractures and transverse fractures in tight gas formations. Well spacing and drainage area are important issues for tight formations. The surface area of the longitudinal fractures cannot be increased, but the number of transverse fractures may be increased to obtain larger surface area which provides an advantage to improve productivity. However, the incremental recovery per additional fracture should be determined because it may decrease due to interference between a number of fractures. The project economics analysis should be considered to decide the better option between transverse and longitudinal fractures. One important conclusion is that if hydraulic fracturing affects the stress distribution to create fractures around the well, the productivity of the system is increased significantly.

George *et al.* [12] found that in gas reservoir the recovery factor is increased dramatically when the hydraulic fractures are spaced closer together. The open spacing of hydraulic fractures is driven by the ability to physically, continually

propagate hydraulic fractures in close proximity to another. An investigation of theoretical hydraulic fracture spacing provides a lower bound for their proximity. Hooke's Law is used to determine realistic minimum hydraulic fracture spacing. For Hooke's Law equation $\Delta\sigma = E(w/b)$, E is horizontal Young's Modulus, w is hydraulic fracture width, and b is hydraulic fracture spacing. In order for hydraulic fractures to be very close together, very high stresses are required.

2.5 Multiple Hydraulic Fracturing in Horizontal Well

Ehrl and Schueler [13] found that in a deep extremely low permeability (0.01-0.02 mD) gas reservoir; the concept of multiple fractured horizontal wells has been successfully used for the development over conventionally fractured vertical wells. Development started with massive hydraulic fracture treatments in vertical well producing at uneconomic gas rate of 5,000 m^3/h. The Soehlingen Z10 well was drilled with a 640 m horizontal section and four hydraulic fractures providing a constant plateau of 20,000 m^3/h. Cumulative gas production to date is 600 MMm^3. The technical and economical success of the Soehlingen Z10 well was a milestone for the tight gas development and hydraulic fracturing in multiple wells program.

Alberto *et al*. [14] studied the transverse fracturing with multistage completion concept in horizontal well which allows sequential execution of several fracture treatments in a single pumping operation. Close spaced packer solution proved to be very effective in having the fractures placed exactly where they were planned, more specifically, correctly spaced.

Byung Lee *et al*. [15] studied optimization of multiple hydraulic fractures for open hole horizontal wells by numerical modeling. A maximum productivity gain of approximately 15 to 20% was achieved with seven fractures. The oil producers are completed with 6 1/8 inch open hole horizontal wells with 3000 ft to 7000 ft open hole section. The model is a useful qualitative tool in real application in a field in Saudi Arabia. The well was successfully fractured utilizing a seven-stage acid fracturing technique employing open-hole isolation and ball-actuated frac ports. Multistage horizontal open hole completion system was installed to perform multiple fracturing in one continuous efficient operation. The system utilized multiple open

hole packers with frac ports in each of the segment to be treated. Starting from the toe section of the well, each port was opened by dropping ceramic balls from the surface. The ball isolates the horizontal section below each frac port; therefore, only one zone is being treated at a time. Stimulation treatments are performed in separate stages, but as a single continuous operation. The resulting productivity was increased three fold when compared to similar offset wells.

Coghlan and Holland [16] found that in order to obtain commercial flow rates from a low permeability sandstone gas reservoir, Chiswick field development needed horizontal wells with multiple hydraulic fractures. The reservoir has average porosity of 10% and permeability of 1 mD. A program of multiple hydraulic fractures in three horizontal wells was successfully executed. The wells were stimulated using the converted frac-vessel. Coiled tubing operations were intensive and were used for perforating and for cleaning-out. C1y well flowed at 48 MMscf/D against 150 bara, and C2z well flowed at 56 MMscf/D against 200 bara. Target well deliverabilities were met in all cases.

Lolon *et al.* [17] presented the results of a fracture modeling and multi-well simulation study. The optimum number of fracture treatment stages along the horizontal lateral depends largely on reservoir permeability, lateral length and number of wells per section. The relative effect of number of stages is smaller when the permeability is higher. For the 0.013 mD reservoir studied, the cumulative oil production increases from 8 to 9% when the number of stages is increased from 9 to 15.

CHAPTER III

THEORY AND CONCEPT

This chapter discusses fundamental of gas condensate reservoir, its region around the wellbore, condensate blockage and effect of important parameters such as non-Darcy flow and capillary number. Theories related to hydraulic fracturing: mechanics of hydraulic fracturing, characterization of hydraulic fracture, fracture stimulation in horizontal well and transversely fractured and longitudinally fractured horizontal well are also discussed in this chapter.

3.1   Gas Condensate Phase Behavior
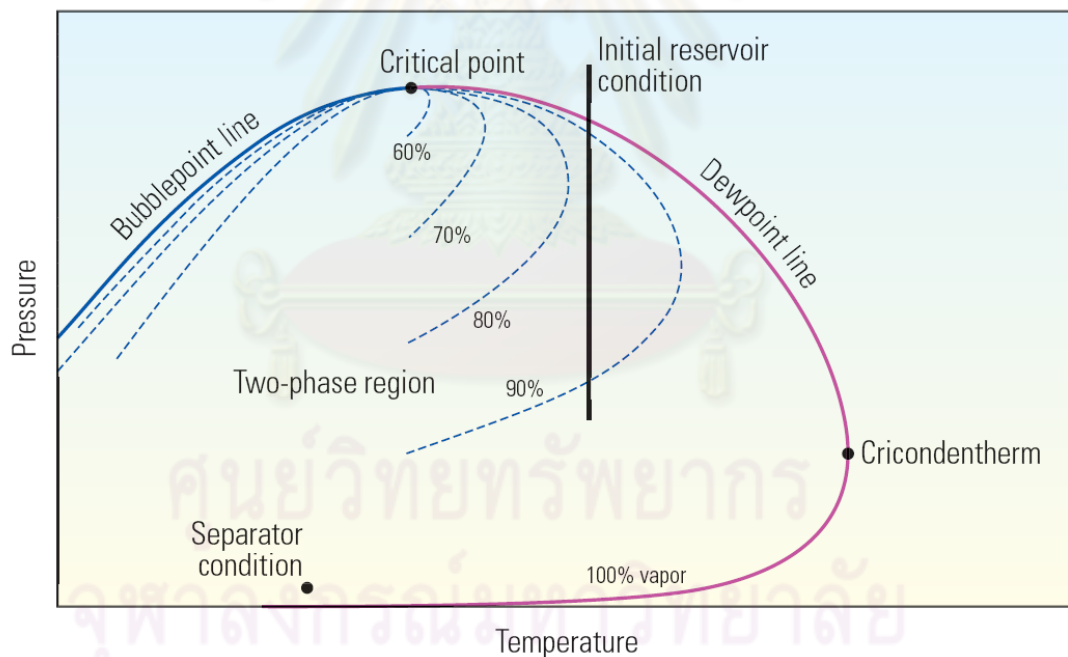
Figure 3.1: Phase diagram of a gas condensate system [18].

Figure 3.1 illustrates phase diagram of a gas condensate system. This pressure-volume-temperature (PVT) plot indicates single-phase behavior outside the two-phase region, which is bounded by bubblepoint and dew point lines. Lines of constant phase saturation (dashed) all meet at the critical point. The numbers indicate the vapor phase

saturation. In a gas condensate reservoir, the initial reservoir condition is in the single-phase area to the right of the critical point. It consists predominantly of methane and other light components, but it also contains some heavy components. As the reservoir pressure declines, the fluid passes through the dew point and separates into two phases, a gas and a liquid that is called a retrograde condensate. The percentage of vapor decreases, but can increase again with continued pressure decline. The cricondentherm is the highest temperature at which two phases can coexist. Surface separators typically operate at conditions of low pressure and low temperature.

As a reservoir produces, formation temperature usually doesn't change, but pressure decreases. A continued decrease in pressure increases the volume of the liquid phase up to a maximum amount of liquid volume then decreases. The amount of liquid phase present depends not only on the pressure and temperature, but also on the composition of the fluid.

3.2 Region around Gas Condensate Wellbore
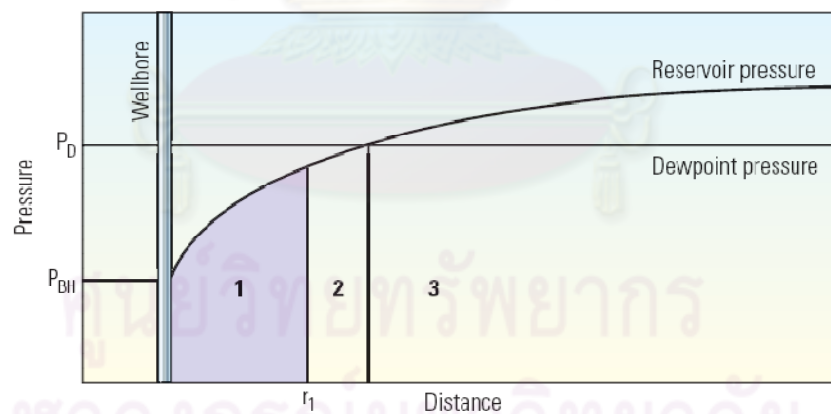
Figure 3.2: Three reservoir regions [18].

Figure 3.2 illustrates three reservoir regions. When the bottomhole pressure, P_{bh}, drops below the dew point pressure, P_d, gas condensate field behavior can be divided into three regions:

- Region 3 is far from the producing well. In this region, the reservoir pressure is greater than P_d. There is only gas phase.

- Region 2 is closer to the well. The condensate reaches the critical saturation for flow at point r_1. The region between the location of the dew point pressure and r_1 is condensate-buildup region. In this region, there are both gas and condensate phases, but only gas flows.

- Region 1 is near the well. Both gas and condensate phases flow toward the well since condensate saturation in this zone exceeds the critical saturation.

3.3 Condensate Blockage
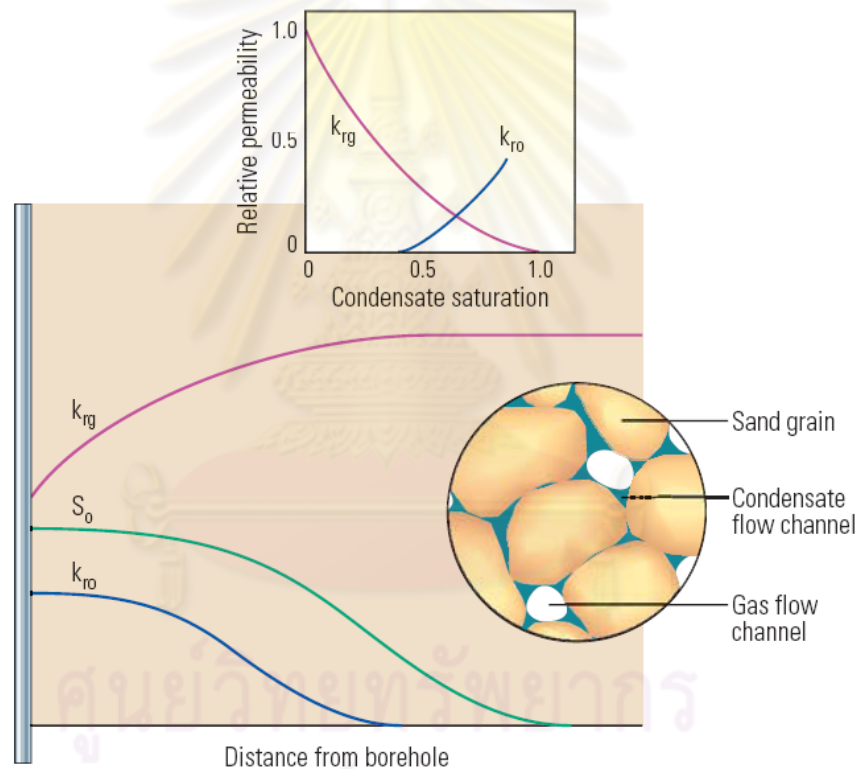
Figure 3.3: Condensate blockage [18].

Figure 3.3 illustrates condensate blockage. Condensate blockage causes a decrease in gas mobility around a producing well when the pressure is below the dew point pressure. Condensate drops out from the gas phase. Capillary forces favor having condensate in contact with the sand grains. After a brief transient period, the region achieves a steady-state flow condition with both gas and condensate flowing. The condensate saturation, S_o, is highest near the wellbore because the pressure is

lower, which means more liquid dropout. The oil relative permeability, k_{ro}, increases with saturation. The decrease in gas relative permeability, k_{rg}, near the wellbore illustrates the blockage effect.

Gas and condensate production decrease because of near-well blockage, and the produced gas contains fewer valuable heavy component because of dropout. The condensate has insufficient mobility to flow toward the well.

3.4 Non-Darcy Flow

The effect of non-Darcy flow on the productivity of a hydraulically fractured gas condensate well has been studied. Henri Darcy [19] proposed a mathematical relationship that is known as Darcy's law after doing an experiment on flow of water through sand filters at relatively low flow rate conditions. This relationship is the fundamental equation governing flow of fluid through porous media. It states that the flow rate is directly proportional to the pressure gradient which can be written as:

$$u = -\frac{k}{\mu}\frac{dp}{dr} \qquad (3.1)$$

where u is flow rate

k is permeability of the rock

p is pressure

μ is Newtonian viscosity of the fluid

Forchheimer [20] observed that Darcy's law did not match the data at high flow rate while doing experiments related to flow of water through linear porous media. Forchheimer correction, which takes into account the inertia effects due to high velocity that may occur in high permeability regions, such as fractures, is considered in this study. When flow velocities are high, turbulent effects as predicted by the Forchheimer model becomes significant. Forchheimer proposed the quadratic equation.

$$u\frac{\mu}{k} + \beta\rho u^2 = -\frac{dp}{dr} \qquad (3.2)$$

where $\qquad \rho \qquad$ is density of the fluid

$\qquad\qquad\quad \beta \qquad$ is non-Darcy flow coefficient

At a very low Reynold's number, the above equation reduces to Darcy's law. For multiphase flow, the appropriate correlation to calculate the non-Darcy flow coefficient, β, which is the property of the porous medium is very important. Geertsma [21] suggested the following correlation for the case of gas flowing in porous media with water saturation. This correlation takes gas relative permeability, water saturation, reservoir permeability and porosity into account.

$$\beta = \frac{0.005}{\left(kk_{rg}\right)^{0.5}[\phi(1 - S_w)]^{5.5}} \qquad (3.3)$$

where $\qquad \beta \qquad$ is non-Darcy flow coefficient

$\qquad\qquad\quad k \qquad$ is reservoir permeability

$\qquad\qquad\quad k_{rg} \qquad$ is gas relative permeability

$\qquad\qquad\quad \phi \qquad$ is porosity

$\qquad\qquad\quad S_w \qquad$ is water saturation

Non-Darcy flow coefficient is very important factor. Neglecting it can overestimate the productivity improvement and the impact of hydraulic fracturing of a gas condensate well.

3.5 Capillary Number Effect

At high gas velocities, in addition to the Forchheimer correction, it is also possible to take into account more complex effects of velocity dependence of the relative permeabilities. The relative permeabilities of the gas and condensate have often been modeled as a function of interfacial tension. This is usually modeled

through correlations in terms of the capillary number, N_c, a dimensionless number which measures the relative permeabilities of gas condensate fluids as a function of viscosity and capillary forces.

These models are intended for gas condensate systems where the expected reduction in Productivity Index (PI) when the well bottomhole pressure drops below the fluid dew point pressure has not been observed in practice. Several theories have been suggested as to why the gas relative permeability in particular remains relatively high but the current consensus seems to imply that a combination of low interfacial tensions (IFT) at reservoir conditions and high velocities as flow converges towards a producer are the main driving forces. Normal engineering practice is to combine IFT and velocity through the so-called Capillary Number. The following equation shows that the capillary number is proportional to gas velocity and gas viscosity, and also inversely proportional to interfacial tension [22].

$$N_c = \frac{v_g \mu_g}{\sigma}$$ (3.4)

where N_c is capillary number

               v_g is gas velocity

               μ_g is gas viscosity

               σ is interfacial tension

The correlations for capillary number can be divided into two classes as follows:

- Corey relative permeability functions.

  A way to include the capillary number that uses part of the general knowledge on relative permeability is to represent the relative permeability functions by a Corey function, whose coefficients depend on the capillary number [23].

$$k_{r\alpha}(S_\alpha, N_C) = k_{r\alpha}^*(N_C)\left(\frac{S_\alpha - S_{r\alpha}(N_C)}{1 - S_{r\alpha}(N_C)}\right)^{\varepsilon_\alpha(N_C)}$$ (3.5)

where k^*_r is the end-point relative permeability

S_r is the residual saturation

ε is the Corey exponent that fixes the curvature of the relative permeability function

α is a phase indicator (condensate, gas)

This approach is designed to fit measured data closely, and do not ensure proper limits of the Corey coefficient at high capillary number. The resulting functions are highly non-linear, so that fitting the functions to a large data set may give problems with convergence.

- Interpolate between immiscible (low capillary number) and miscible (high capillary number) relative permeability functions.

    Relative permeability curves at near-critical conditions have often been represented by a weighted linear function of immiscible and miscible relative permeability curves, where the weighting factor is a function of the capillary number [23].

$$ k_{r\alpha}(S_\alpha, N_C) = f_\alpha(N_C)k_{r\alpha i}(S_\alpha) + \{1 - f_\alpha(N_C)\}k_{r\alpha M}(S_\alpha) \qquad (3.6) $$

where k_{ri} is the conventional relative permeability for capillary dominated (immiscible) flow

k_{rM} is the relative permeability function in the limit of viscous dominated (miscible) flow

f is weighting function

This approach is particularly suitable for fitting large sets of measured data on relative permeability at varying capillary numbers. The N_c-dependence is more explicit than the case of interpolating Corey coefficients, so that convergence causes less problems.

Both capillary number and Forchheimer effects are included in the generalized pseudo pressure equation calculating near wellbore flows exhibiting condensate blockage behavior in a gas condensate reservoir.

Capillary numbers must be used for simulations below the dew point, otherwise, pressure drops and condensate dropout are overestimated and well productivity is underestimated.

3.6   Mechanics of Hydraulic Fracturing

Hydraulic fracturing involves pumping a fluid at high pressure into the formation to exceed the rock strength and open a fracture in the rock. A propping agent is often pumped into the fracture to keep it from closing when the pumping pressure is released.

Brady *et al.* [24] observed that rocks will open in the direction of least resistance. For normal faulting regimes, overburden exerts the greatest stress and the direction of least resistance is horizontal. Fractures will open perpendicular to the direction of least horizontal stress, σ_{hmin} , and vertical fractures form. However, for thrust faulting regimes, the horizontal stress, σ_{hmax} , may exceed the vertical stress, σ_v , and horizontal fractures may form. In slip faulting regimes, the vertical stress, σ_v , is intermediate and the minimum and maximum stresses are horizontal, σ_{hmin} , and σ_{hmax}. Fracture surface is usually near vertical.

Figure 3.4 indicates a hydraulic fracture emanating from a wellbore in a multilayered formation in a normal faulting regime. Here, σ_M denotes the minimum horizontal stress, and σ_v denotes the vertical stress. In this case, the vertical stress is greater, and the fracture opens perpendicular to the minimum horizontal stress. *U*, *R* and *L* denotes the upper, reservoir and lower formation, respectively.
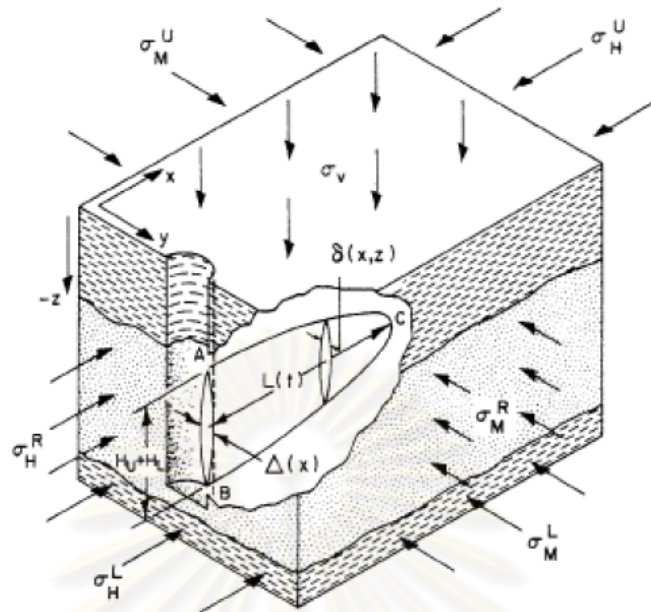
Figure 3.4: Isometric view of a hydraulic fracture emanating in stratified porous media [25].

3.7   Characterization of Hydraulic Fractures

Hydraulic fractures can be characterized by their length and conductivity. The fracture length is the conductive length and not the created hydraulic length and is assumed to consist of two equal half lengths, x_f in each side of the well. Fracture conductivity is defined as:

$$F_{cd} = \frac{k_f w_f}{k x_f}$$ (3.7)

where F_{cd} is fracture conductivity

            k_f is fracture permeability

            w is fracture width

            k is formation permeability

            x_f is fracture half length.

Fracture conductivity affects the distribution of gas production into the fracture. Montgomery *et al.* [26] found that when the fracture conductivity is high, the pressure drops in the reservoir are distributed more uniformly along the fracture, and the fracture will drain the reservoir more effectively because the pressure drop inside the fracture is reduced to a minimum. When the fracture conductivity is low, the pressure drops are greatest near the wellbore. The pressure drop profile in the reservoir will appear to be "radial", and the well behaves more like a well producing under radial flow conditions.

Two fracture types occur in hydraulically fractured wells: finite conductivity fracture and infinite conductivity fracture.

- Finite conductivity fractures are the fractures with significant pressure drop along the axis. This model is very common case, unless formation permeability is extremely low in microdarcy range.

- Fractures with infinite permeability and conductivity have little or no pressure drop along the axis. These fractures are referred as infinite conductivity fractures. They exist in highly propped tight-gas formations. Usually, fractures with dimensionless conductivity greater than 300 are treated as infinite conductivity fractures.

3.8 Fracture Stimulation in Horizontal Well

A horizontal well can be considered as a limiting case of an infinite-conductivity fracture with a fracture height equal to the wellbore diameter. One of the main advantages of drilling a horizontal well in a tight reservoir is the fact that it allows placing more fractures in the main wellbore and consequently obtaining a better coverage of the reservoir. There are many ongoing researches on the efficiency improvement of horizontal well.

One of the most recent approaches that have been developed was to use a system that becomes a permanent completion liner. This system is a series of packers that are integral to the deployed liner. The use of the packers allows the wellbore to be segmented into selected areas for stimulation. Between each of the packers is a sliding sleeve referred to as a fracport. The isolation packers are set just before and after the

fracport. The method of selectively opening the fracport is to drop larger diameter ceramic balls that land on a beveled seat below each of the ports. The seating ball controls the sleeve to the open or close position. Close spaced isolation packer solution is very effective in having the fractures placed exactly where it was planned. Also, the planned fracture spacing and long lasting fracture-to-fracport flow-path can be achieved [14].

Figure 3.5 illustrates close spaced isolation packers, and Figure 3.6 illustrates hydraulic fractures in horizontal well.
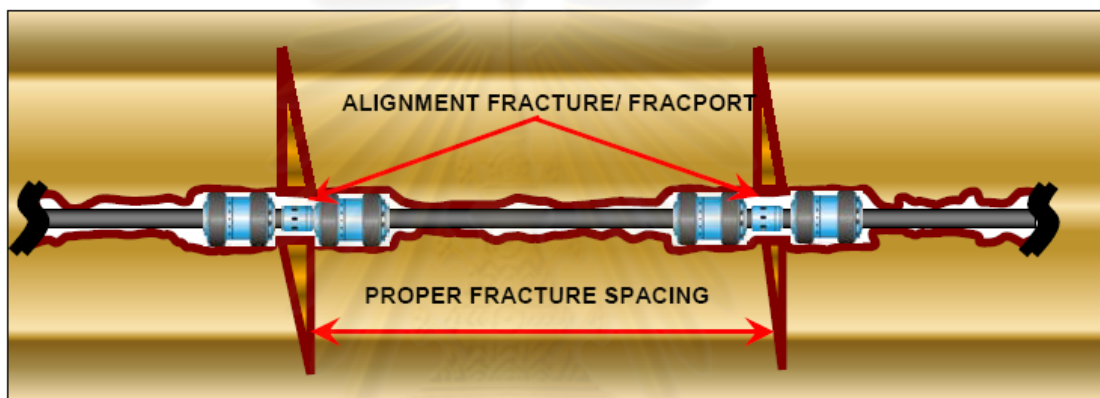
Figure 3.5: Close spaced isolation packers [14].
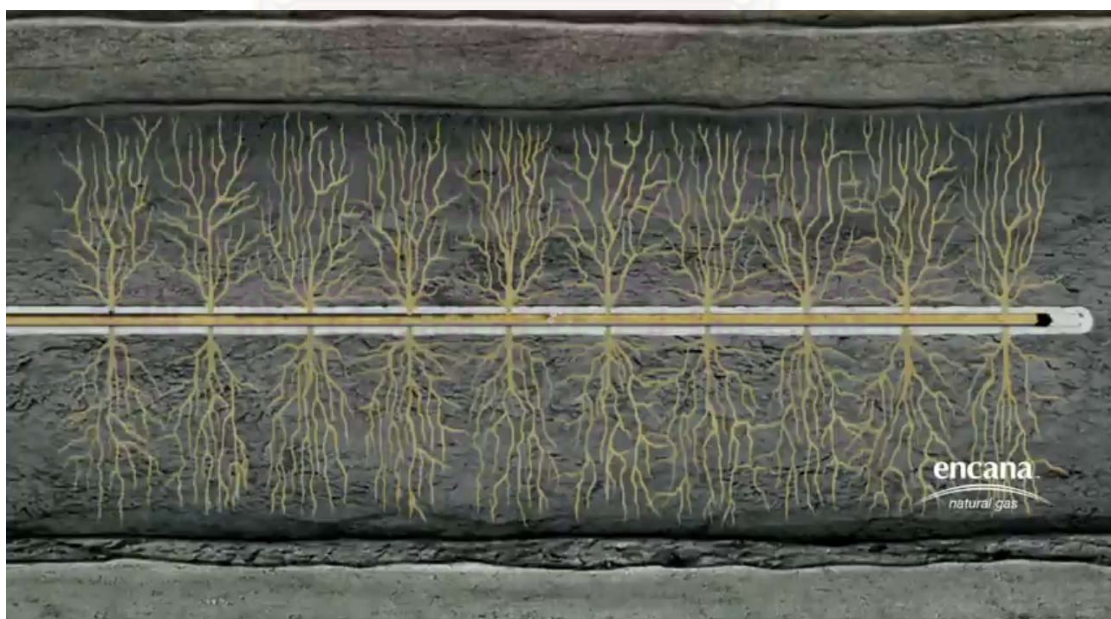
Figure 3.6: Hydraulic fractures in horizontal well [27].

3.9 Transversely Fractured and Longitudinally Fractured Horizontal Well

When considering the fracture plane, the fracture is assumed to be on the plane identified by the well trajectory and the maximum horizontal stress direction. The fracture-to-well interface is practically a straight line corresponding to the perforated interval. This means that the flow in the fracture will be linear. In general, it is assumed that the fractures are not overlapping or interfering each others.

For a horizontal well, the fracture direction can be longitudinal or transverse. Longitudinal fractures can be generated if the well is drilled along the maximum horizontal stress direction. When the well is drilled in the direction of minimum principal stress, multiple transverse fractures can be induced by hydraulic fracturing. Transverse hydraulic fractures extending away from the wellbore will orient themselves perpendicular to the minimum principal stress direction.

Figure 3.7 and 3.8 illustrates simulation grid for longitudinally fractured horizontal well and transversely fractured horizontal well, respectively.
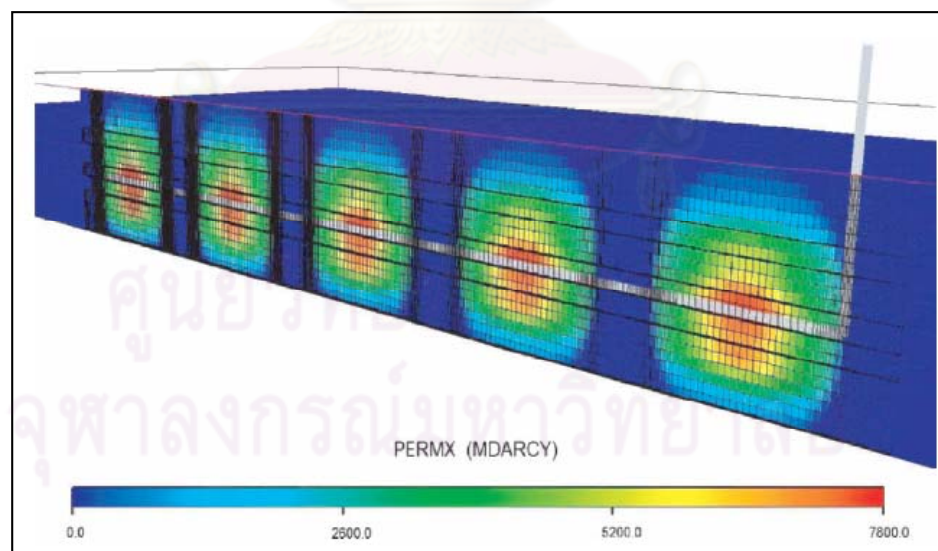
Figure 3.7: Simulation grid for longitudinally fractured horizontal well [28].
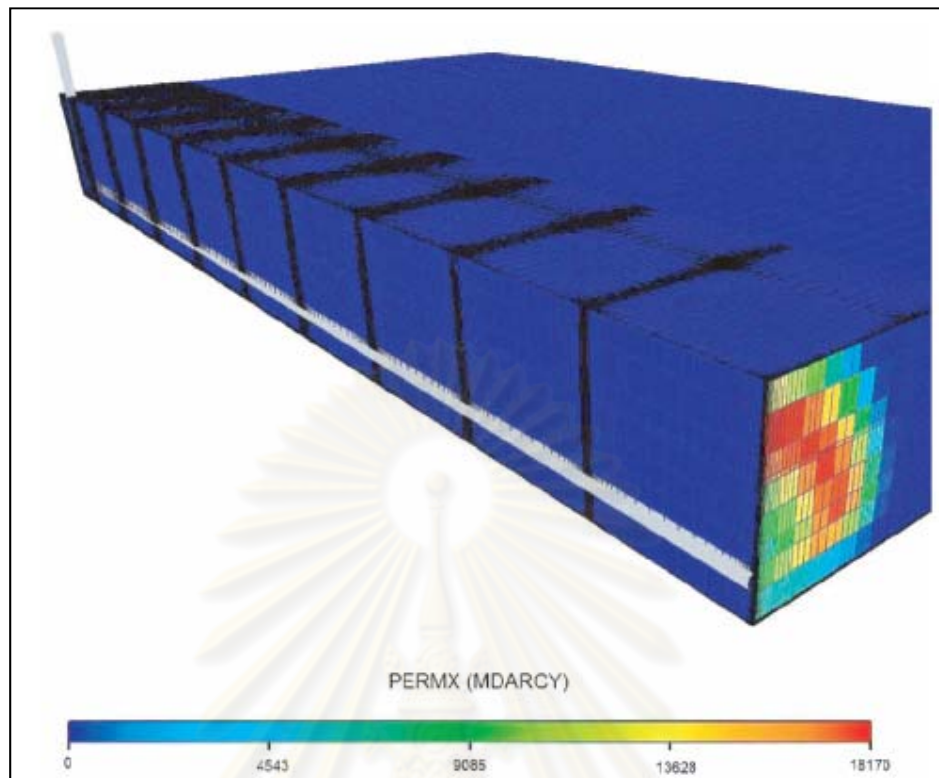
Figure 3.8: Simulation grid for transversely fractured horizontal well [28].

ศูนย์วิทยทรัพยากร

จุฬาลงกรณ์มหาวิทยาลัย

CHARPTER IV

RESERVOIR SIMULATION MODEL

In order to use hydraulic fracturing to enhance gas and condensate recovery, reservoir simulator is used as a tool to predict gas and condensate production. The reservoir simulator, ECLIPSE 100, is used to simulate performance of hydraulic fractures for horizontal well in a gas condensate reservoir. The reservoir simulation model setup is categorized into four main sections: grid, fluid, special core analysis, and wellbore sections. First, the grid section specifies the geometry of the reservoir and its permeability and porosity. The fluid section specifies the reservoir fluid property and initial reservoir condition. The special core analysis or SCAL section specifies the three-phase relative permeabilities. Finally, the wellbore section specifies the wellbore model and the vertical flow performance model. The description of simulation input and how properties were gathered are presented in this chapter.

4.1 Grid Section

4.1.1 Reservoir Model Description

The field is a low permeability gas condensate reservoir. A black oil numerical reservoir simulator, ECLIPSE 100 from Schlumberger, was used to simulate fluid flow in the reservoir. The reservoir model is assumed to be homogeneous. The top of reservoir is located at a depth of 8,000 ft. The key reservoir and model parameters used in the simulation are listed in Table 4.1.

Table 4.1: Key reservoir and model parameters.

Characteristic parameter	Value
Average porosity	20 %
Horizontal permeability	0.2 mD
Vertical permeability	0.01 mD
Water saturation	5 %
Initial reservoir pressure at 8050 ft	3500 psia
Reservoir temperature	260 ^{o}F
Dew point pressure	2610.61 psia
Horizontal well length	2700 ft
Wellbore diameter	0.29 ft (3.49 inch)

4.1.2 Gridding

Cartesian grid model, which is commonly used to simulate a full field simulation model and block centered geometry are used. A rectangular drainage area with a horizontal well is modeled. The reservoir model dimensions are 3200 ft x 1300 ft x 100 ft with 32 x 21 x 7 cells in the x-, y- and z- directions, respectively. Table 4.2 shows the sizes of the gridblocks.

Table 4.2: Sizes of gridblocks

x-dir	size (ft)	y-dir	size (ft)	z-dir	size (ft)
1 to 32	100	1	100	1	20
		2	90	2	15
		3	80	3	10
		4	70	4	10
		5	60	5	10
		6	50	6	15
		7	40	7	20
		8	40		
		9	40		
		10	30		
		11	100		
		12	30		
		13	40		
		14	40		
		15	40		
		16	50		
		17	60		
		18	70		
		19	80		
		20	90		
		21	100		
Total	3200		1300		100

4.1.2 Local Grid Refinement

Local grid refinement (LGR) is used in the simulation. Some of the gridblocks on the main grid will be replaced by a refined grid. Each refined grid will be made up of several small gridblocks that fill the space previously occupied by a parent gridblock. These refined gridblocks can be of variable size and can be assigned different reservoir properties. LGR is particularly helpful for simulating hydraulically fractured reservoirs. Single-well simulations with a LGR grid were performed to model condensate banking in order to capture the important changes in condensate

saturation and relative permeabilities near gas condensate wells when the pressure drops below the dew point pressure. This is required for accurate calculation of liquid dropout around the wellbore.

To minimize computation time, only a sector of the model is locally refined. The 100-ft wide parent gridblocks around the wellbore are locally refined into 10-ft wide gridblocks in the x- and y- directions. In ECLIPSE, we need to specify LGR name, coordinate, and the number of refined cells as shown in Table 4.3.

Table 4.3: Local grid refinement.

LGR Name	LGR Coordinate			Number of refined cells		
	I	J	K	X	Y	Z
WELL1	1-32	1	1-7	320	10	1-7

4.1.3 Fracture Grid Modeling

In this study, fractures are modeled as Erwin *et al.* [29] suggested in his paper. The authors studied fracturing a horizontal well in a gas condensate reservoir. They indicated that the best method for simulating near-wellbore effects was to use very small size gridblocks with high permeability to represent the hydraulic fracture and gridblocks with sizes gradually increasing away from the fracture to represent the reservoir.

The 10-ft wide gridblocks are locally refined into small size fracture gridblocks of 0.02083, 0.05, 0.1 and 0.2 ft in the x-direction depending on fracture width in each designed case. The fracture length was modified by changing the number of local gridblocks in the y-direction containing fracture properties. Different fracture designs with different fracture spacings, lengths, widths and permeabilities were simulated.

The 10-ft wide refined gridblocks around the wellbore within the LGR WELL1 are locally refined to model fracture gridblocks. Two of the 10-ft wide gridblocks are locally refined to seven gridblocks in the x-direction having fracture gridblocks in the middle as shown in the Table 4.4.

Table 4.4: Sizes of locally refined fracture gridblocks for 10-ft wide gridblocks.

Fracture width (ft)	Size (ft)						
	x-dir#1	x-dir#2	x-dir#3	x-dir#4	x-dir#5	x-dir#6	x-dir#7
0.02083	9	0.5	0.489585	0.02083	0.489585	0.5	9
0.05	9	0.5	0.475	0.05	0.475	0.5	9
0.1	9	0.5	0.45	0.1	0.45	0.5	9
0.2	9	0.5	0.4	0.2	0.4	0.5	9

The 100-ft wide gridblocks along the fracture plane which is in the y-direction away from the wellbore, are locally refined to model fracture gridblocks. The 100-ft wide gridblocks are locally refined to seven gridblocks in the x-direction having fracture gridblocks in the middle as shown in Table 4.5.

Table 4.5: Sizes of locally refined fracture gridblocks for 100-ft wide gridblocks.

Fracture width (ft)	Size (ft)						
	x-dir#1	x-dir#2	x-dir#3	x-dir#4	x-dir#5	x-dir#6	x-dir#7
0.02083	49	0.5	0.489585	0.02083	0.489585	0.5	49
0.05	49	0.5	0.475	0.05	0.475	0.5	49
0.1	49	0.5	0.45	0.1	0.45	0.5	49
0.2	49	0.5	0.4	0.2	0.4	0.5	49

Figure 4.1 shows areal view of the simulation grid used. Fracture planes are in the y-direction. A horizontal well of 2700 ft long is in the middle of the reservoir penetrating in the x-direction. Figures 4.2, 4.3 and 4.4 show magnified view of the fracture grid, side view of the simulation grid, and 3D view of the simulation grid, respectively.
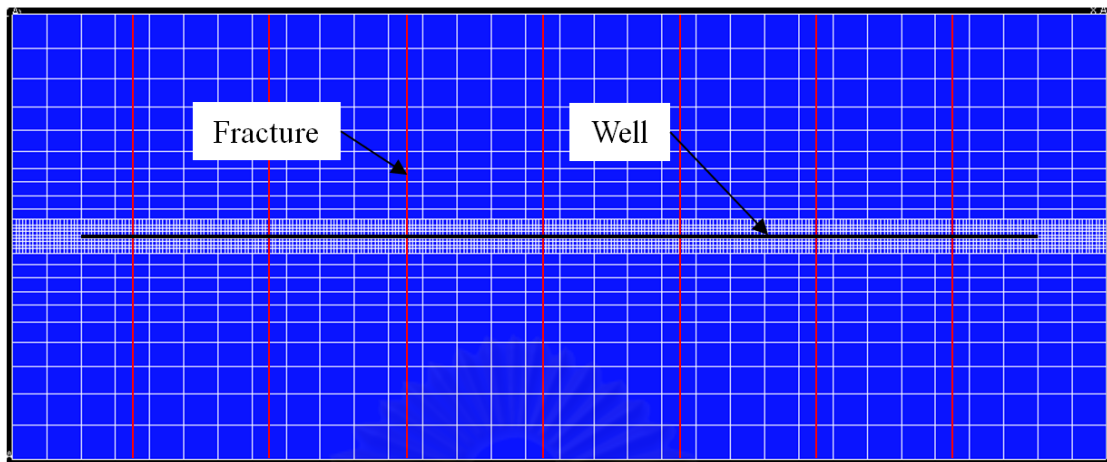
Figure 4.1: Areal view of the reservoir model with seven fractures.
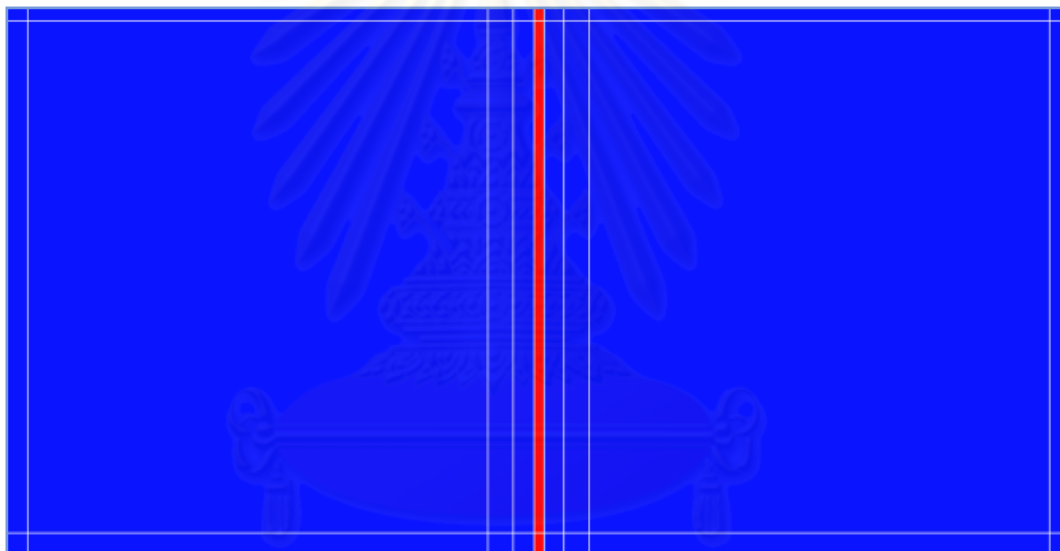
Figure 4.2: Magnified view of the fracture grid.
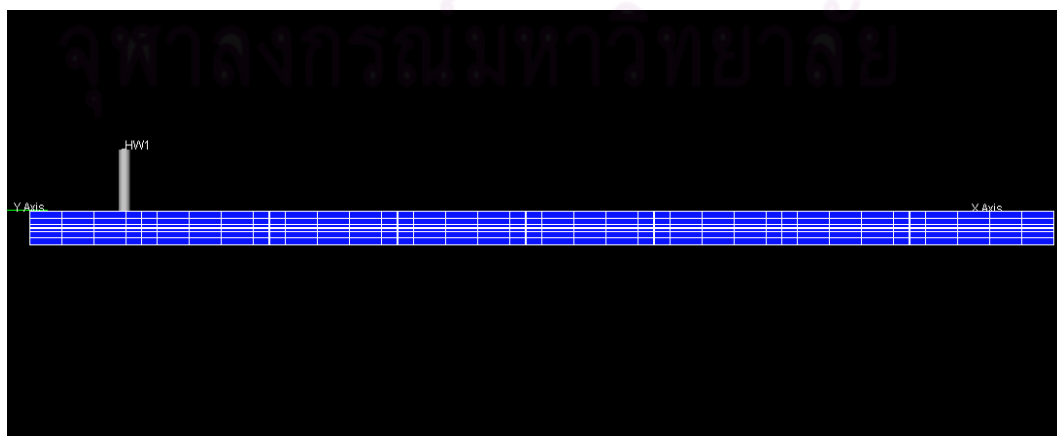
Figure 4.3: Side view of the reservoir model.
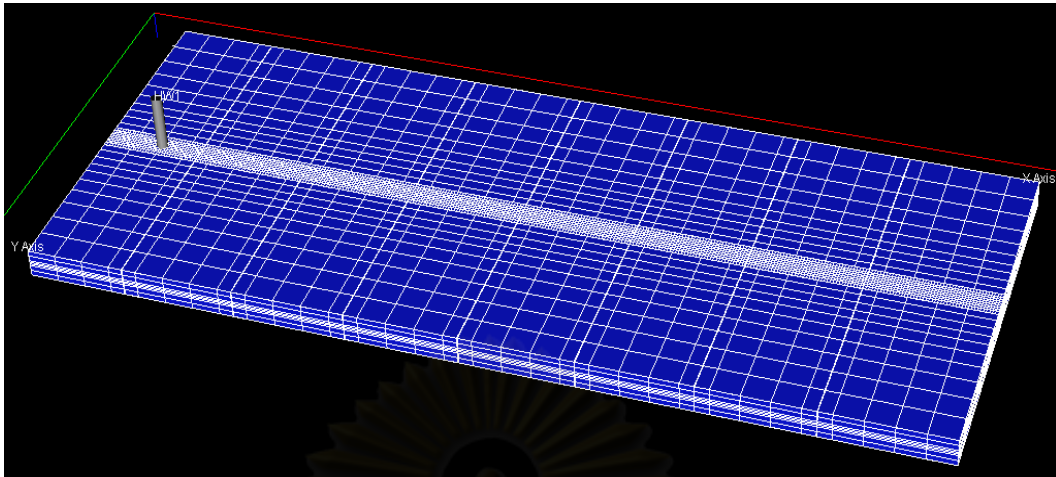
Figure 4.4: 3D view of the reservoir model.

4.2 Fluid Section

4.2.1 PVT Modeling

In this study, the reservoir temperature is assumed to be constant at 260 ^{o}F. The dew point pressure at reservoir temperature is 2610.61 psia. PVT properties for gas and condensate are modeled by two ECLIPSE keywords: PVTG and PVTO, as shown in Tables 4.6 and 4.7. Table 4.8 shows water PVT, fluid densities and rock properties. The source of data is from one of the gas condensate reservoir studies provided by Schlumberger.

Table 4.6: PVTG wet gas PVT properties (vapourised oil)

P_g (psia)	OGR (stb/Mscf)	FVF (rb/Mscf)	Visc (cp)
125	0.03	2.3652689	0.01526
	0	2.3599257	0.01532
285	0.028	1.7401113	0.0166
	0	1.732987	0.01634
445	0.027	1.3767718	0.01818
	0	1.3696475	0.01752
870	0.029031539	1.1445194	0.01994
	0	1.1407792	0.01883
1305	0.034018552	0.98689422	0.02181
	0	0.98903151	0.02021
1740	0.04007421	0.87611129	0.0237
	0	0.88198884	0.02163
2175	0.048445267	0.79631908	0.02559
	0	0.80344339	0.02305
2610.61	0.063050091	0.74698328	0.02714
	0	0.75250461	0.02423
3045	0.071777363	0.71795174	0.02806
	0.063050091	0.72293875	0.02768
	0	0.72685712	0.02492
3480	0.083532465	0.69070128	0.02925
	0.063050091	0.69640072	0.02832
	0	0.69693504	0.02583
5687	0.085313541	0.6889202	0.02935
	0.063050091	0.69461964	0.02842
	0	0.69515397	0.02593

Table 4.7: PVTO live oil PVT properties (dissolved gas)

R_s (Mscf/stb)	P_{bub} (psia)	FVF (rb/Mscf)	Visc (cp)
0.011229167	100	1.02	0.975
0.028072918	725.18869	1.028	0.91
0.056145835	1450.3774	1.036	0.83
0.111	2900.7548	1.051	0.695
0.135	3625.9434	1.06	0.641
0.16843751	4351.1321	1.067	0.594
0.22458334	5801.5095	1.08	0.51
	7251.8869	1.076	0.549
	13053.396	1.063	0.74
0.28072918	7262.0395	1.09	0.449
	13063.549	1.08	0.605

Table 4.8: PVT Modeling

Parameter		Value
Water PVT properties	Reference pressure	4439.6 psia
	Water FVF at reference pressure	1.03 rb/stb
	Water compressibility	2.8269E-6 /psi
	Water viscosity at reference pressure	0.3 cp
	Water viscosibility	0 /psi
Fluid densities at surface conditions	Oil density	49.992 lb/ft^3
	Water density	62.801 lb/ft^3
	Gas density	0.061847 lb/ft^3
Rock properties	Reference pressure	3000 psia
	Rock compressibility	8.430027E-6 /psi

4.2.2 Initialization

The initial reservoir pressure is 3500 psia at 8050 ft which is above the dew point pressure. There is no liquid condensate present at initial conditions. The well is assumed to be operated at a constant rate of 10,000 Mscf/D.

4.3   SCAL (Special Core Analysis) Section

The oil saturation and oil relative permeabilities are tabulated in Table 4.9 and shown in Figure 4.5. Two types of relative permeability, k_{row} and k_{rowg}, are used. k_{row} is the oil relative permeability for a system with oil and water only, and k_{rowg} is the oil relative permeability for a system with oil, water, and gas. The source of data is from one of the gas condensate reservoir studies provided by Schlumberger.

Table 4.9: Oil saturation and oil relative permeabilities.

S_o	k_{row}	k_{rowg}
0	0	0
0.2	0	0
0.32	0.00463	0.015625
0.44	0.037037	0.125
0.56	0.125	0.421875
0.68	0.296296	1
0.95	1	1
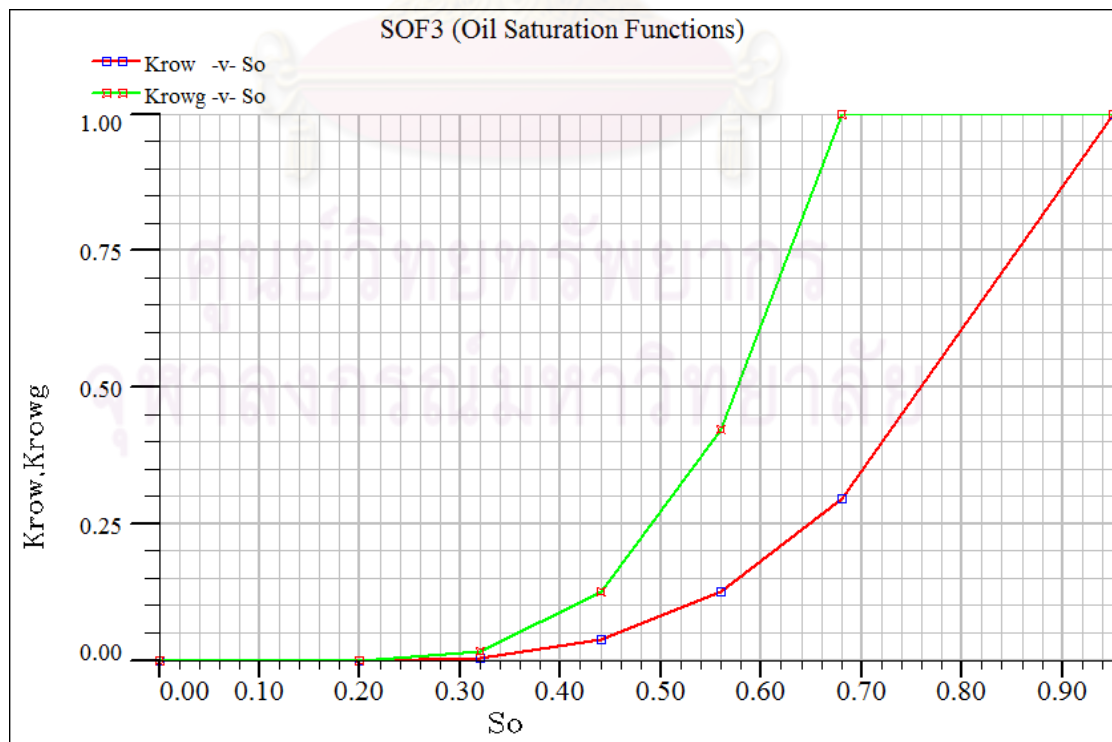
Figure 4.5: Oil relative permeability function.

The gas saturation and gas relative permeability are tabulated in Table 4.10 and shown in Figure 4.6.

Table 4.10: Gas saturation and relative gas permeability.

S_g	k_{rg}
0	0
0.1	0
0.2	0
0.3	0.2
0.4	0.4
0.6	0.85
0.7	0.90
0.8	0.92
0.9	0.95
0.95	0.95
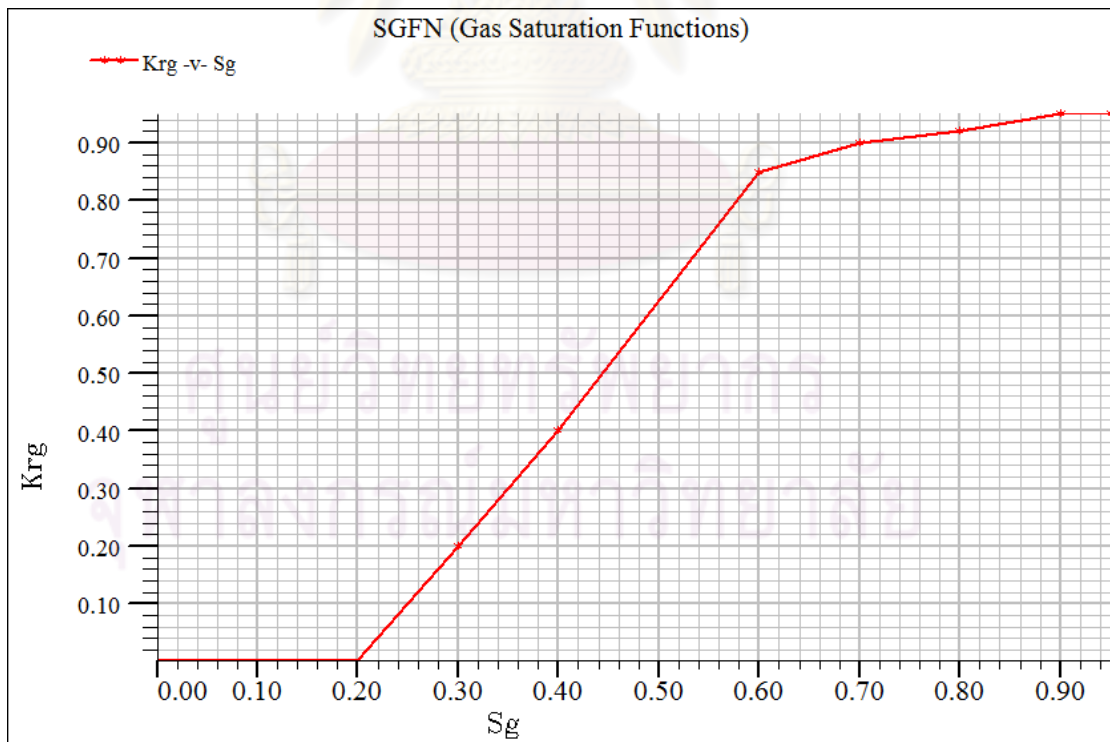
Figure 4.6: Gas relative permeability as a function of gas saturation.

The water saturation and water relative permeability are tabulated in Table 4.11 and shown in Figure 4.7.

Table 4.11: Water saturation and water relative permeability.

S_w	k_{rw}
0.05	0
0.157	0
0.216	0
0.313	0.02
0.44	0.06
0.56	0.10
0.68	0.15
0.80	0.30
0.90	0.65
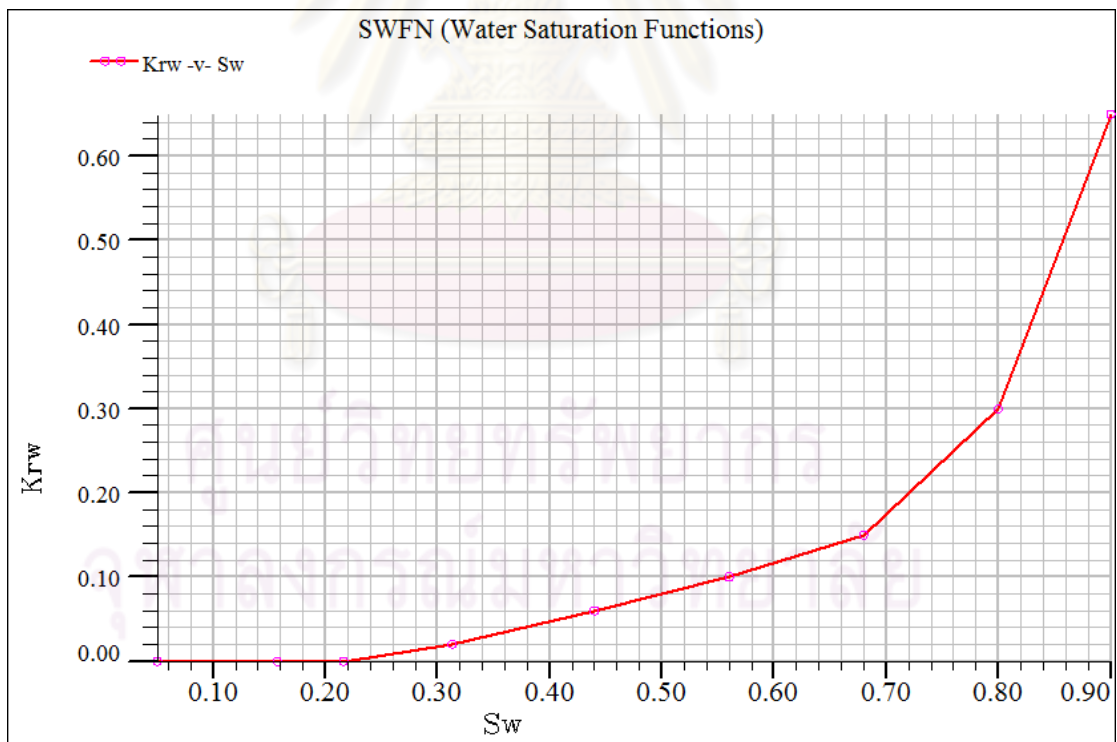
Figure 4.7: Water relative permeability as a function of water saturation.

4.4 Wellbore Section

4.4.1 Wellbore Model

The production well in this study has the wellbore inside diameter of 0.29 ft and is located at depth 8050 ft. The well is designated to be a multi-segment horizontal well. Well production is controlled by gas production rate target of 10,000 Mscf/D. Minimum gas production rate is set at 500 Mscf/D. If the gas production rate falls below the minimum, the well is shut in. Tubing head pressure target is set to 500 psia.

The generalized pseudo-pressure inflow equation which alters both gas and oil mobilities and takes account of the effects of condensate dropout is used in this model. Vertical flow performance and multi-segment are also used in this model. They are discussed in detail in the following sections.

4.4.2 Inflow Performance Relationship in ECLIPSE 100

In ECLIPSE 100, the inflow performance relationship is written in terms of the volumetric production rate of each phase at stock tank conditions. The flow path is defined between the well bore and a single reservoir gridblock as a connection. The flow rate of a phase (oil, water or gas) across a connection is given by the Inflow Performance Relationship,

$$q_{p,j} = T_{wj} M_{w,j} \left(P_j - P_w - H_{wj} \right) \tag{4.1}$$

where q_{pj} is the volumetric flow rate of phase in connection at stock tank conditions. The flow is taken as positive from the formation into the well and negative from the well into the formation

T_{wj} is the connection transmissibility factor defined below

M_{pj} is the phase mobility at the connection defined below

P_j is the nodal pressure in the gridblock containing the connection

P_w is the bottomhole pressure of the well

H_{wj} is the well bore pressure head between the connection and the
                well's bottomhole datum depth

4.4.3 Connection Transmissibility Factor

The connection transmissibility factor depends on the geometry of the
connecting gridblock, the well bore radius, and the rock permeability. Its value may
be specified directly or it can be calculated by the program using the formula below.
In a Cartesian grid, ECLIPSE uses the relationship

$$T_{wj} = \frac{0.001127\theta kh}{ln\left(\frac{r_o}{r_w}\right) + S} \tag{4.2}$$

where θ is the angle of the segment connecting with the well, in radians.
                In a Cartesian grid its value is 6.2832

            kh is the effective permeability times net thickness of the
                connection

            r_o is the "pressure equivalent radius" of the gridblock defined
                below

            r_w is the well bore radius

            S is the skin factor

The pressure equivalent radius of the gridblock is defined as the distance from
the well at which the local pressure is equal to the nodal average pressure of the
block. In a Cartesian grid, we use Peaceman's formula [30], which is applicable to
rectangular gridblocks in which the permeability may be anisotropic. The well is
assumed to penetrate the full thickness of the block through its center, perpendicularly
to two of its faces. The pressure equivalent radius is expressed as:

$$r_o = 0.28 \frac{\left[D_x^2 \left(\frac{k_y}{k_x}\right)^{1/2} + D_y^2 \left(\frac{k_x}{k_y}\right)^{1/2} \right]^{1/2}}{\left(\frac{k_y}{k_x}\right)^{1/4} + \left(\frac{k_x}{k_y}\right)^{1/4}} \tag{4.3}$$

where D_x and D_y are the x- and y- dimensions of the gridblock, and K_x and K_y are the x- and y- direction permeabilities.

Equations 4.2 and 4.3 are intended for vertical wells. Horizontal wells may penetrate the block in either the x- or y- direction, and the appropriate components of permeability and block dimensions are substituted in these equations. For a well penetrating in the x-direction, for example, the quantities k_y, k_z, D_y, D_z will be used in Equations 4.2 and 4.3.

$$k_h = D_x \left(k_y k\right)^{1/2} \tag{4.4}$$

4.4.4 Phase Mobilities

The term M_{pj} in Equation 4.1 represents the mobility of the phase p at the connection. In producing connections, where the flow is from the formation into the well bore, the mobility depends on the conditions in the gridblock containing the connection. The mobility of a free phase (free oil, water, or free gas) is given by

$$M_{fp,j} = k_{p,j} \lambda_{p,j} \tag{4.5}$$

where $\quad k_{p,j} \quad$ is the relative permeability of the phase

$\quad\quad\quad\ \lambda_{p,j} \quad$ is defined by

$$\lambda_{p,j} = \frac{1}{B_{p,j} \mu_{p,j}} \tag{4.6}$$

where $\quad \mu_{p,j} \quad$ is the phase viscosity

$\quad\quad\quad\ B_{p,j} \quad$ is the phase formation volume factor

The quantities in Equations 4.5 and 4.6 are determined from the pressure and saturations in the gridblock. The total gas and total oil mobilities are obtained by including the dissolved gas and vaporized oil content of the phases

$$M_{o,j} = M_{fo,j} + R_{v,j}M_{fg,j}$$
$$M_{g,j} = M_{fg,j} + R_{s,j}M_{fo,j} \tag{4.7}$$

4.4.5 Generalized Pseudo-pressure Method

ECLIPSE 100 has an option to use special inflow equation, the generalized pseudo-pressure equation, to provide a more accurate model of the flow of gas condensate into the well. This method takes into account the pressure-dependence of between the gridblock pressure and the well bore pressure. The generalized pseudo-pressure method is intended for use by gas condensate producers. It provides a means of taking into account of condensate dropout, as well as compressibility, in the calculation of the mobility integral. It is based on the method described by Fevang and Whitson [4].

At the beginning of each timestep, the integral of the total oil and gas mobility is evaluated between the gridblock pressure and the well bore pressure at the connection. This is compared with the total oil and gas mobility at gridblock conditions multiplied by the drawdown, and the ratio of the two quantities is stored as a "blocking factor" for each gridblock connection in the well.

$$\beta_j = \frac{\int_{(P_w+H_{wj})}^{P_j}(M_g + M_o)dP}{(M_{g,j} + M_{o,j})\left(P_j - (P_w + H_{wj})\right)} \tag{4.8}$$

The integrand is fundamentally a function of two independent variables: the pressure P and the gas saturation, S_g. The oil saturation is equal to $1-(S_g + S_w)$ and S_w is regarded as fixed at the gridblock value. However, S_g is eliminated as an independent variable, making it a function of P at pressures below the dew point by

requiring that the local total mobility ratio should be the same as the total mobility ratio at gridblock conditions,

$$M_o/M_g = M_{o,j}/M_g \qquad (4.9)$$

This requirement assumes that within the gridblock the flows are in steady state and there is no zone of immobile dropped-out oil. The integral in Equation 4.8 is evaluated by applying the trapezoidal rule to a set of pressure values between the gridblock and connection pressures. At each pressure value below the dew point, the gas saturation is determined by solving Equation 4.9 using Newton's method.

The blocking factor, β_j, is then used to multiply both the oil and gas mobilities in the inflow performance relationship, Equation 4.1. Note that the free oil mobility is modified by this treatment.

The blocking factor for each connection is retained for the duration of the timestep and recalculated at the beginning of each subsequent timestep. This degree of explicitness should cause oscillations. These may be damped by averaging the calculated blocking factor with its value at the previous timestep.

$$\beta_{used} = f\beta_{new} + (1-f)\beta_{previous} \qquad (4.10)$$

where f is the weighting factor

4.4.6 Capillary number

In this study, the interpolation between immiscible and miscible relative permeability functions is used. A capillary number modified gas relative permeability is given by

$$k_{rg} = f_I k_{rgI} + (1-f_I)k_{rgM} \qquad (4.11)$$

where
k_{rg} is the capillary number modified gas relative permeability

k_{rgM} is the straight-line miscible relative permeability

k_{rgI} is the immiscible relative permeability

f_I is the capillary number dependent transition function

The capillary number dependent transition function depends on the gas capillary number, N_{cg}, and is given by

$$f_I = \frac{1}{\left(\alpha \cdot N_{cg}\right)^n + 1} \tag{4.12}$$

where $\alpha = \alpha^0 / \overline{k_{rg}}$, with $\overline{k_{rg}} = \frac{k_{rgM} + k_{rgI}}{2}$, and α^0 is a constant depending only on rock properties and is obtained from Equation 4.13.

$$\alpha^0 = \frac{\alpha_c^0}{\sqrt{k \cdot \varnothing}} \tag{4.13}$$

where k is the rock permeability

ϕ is the porosity

This model depends on two parameters: the exponent n in Equation 4.12 and the α_c^0 coefficient in Equation 4.13. These parameters are typically defaulted to 0.65 and 10^4, respectively. These default values are used in this study.

4.4.7 VFP (Vertical Flow Performance) Table

Pressure losses between the bottomhole pressure reference depth and the tubing head are handled by VFP tables. VFP tables offer the most flexible and potentially the most accurate means of determining the pressure drop across each segment.

VFP tables can be constructed to describe the pressure drop along a certain length of tubing at the appropriate angle of inclination, using a suitable multi-phase flow correlation. The pressure drop along a segment is interpolated from the

respective VFP table and can be scaled according to the length or depth span of the segment.

A program, PROSPER [31], can be used to calculate VFP tables, using a choice of multi-phase flow correlations to calculate the pressure losses within the tubing string.

This study uses "Petroleum Experts 2" correlation which combines the best features of existing correlations. It uses the Gould *et al.* [32] flow map and the Hagedorn and Brown [33] correlation in slug flow, and Duns and Ros [34] for mist flow. In the transition regime, a combination of slug and mist results is used.

4.4.8 Multi-segment Well Model

The multi-segment well model provides a detailed description of fluid flow in the wellbore and improves modeling of multi-phase flow. This model is specially designed for horizontal and multi-lateral wells.

The detailed description of the fluid flowing conditions within the well is obtained by dividing the well bore into a number of segments. A single-bore well will just consist of a series of segments arranged in sequence along the well bore.

Each segment consists of a node and a flowpath to its parent segment's node. A segment's node is positioned at the end that is furthest away from the wellhead as illustrated in Figure 4.8.
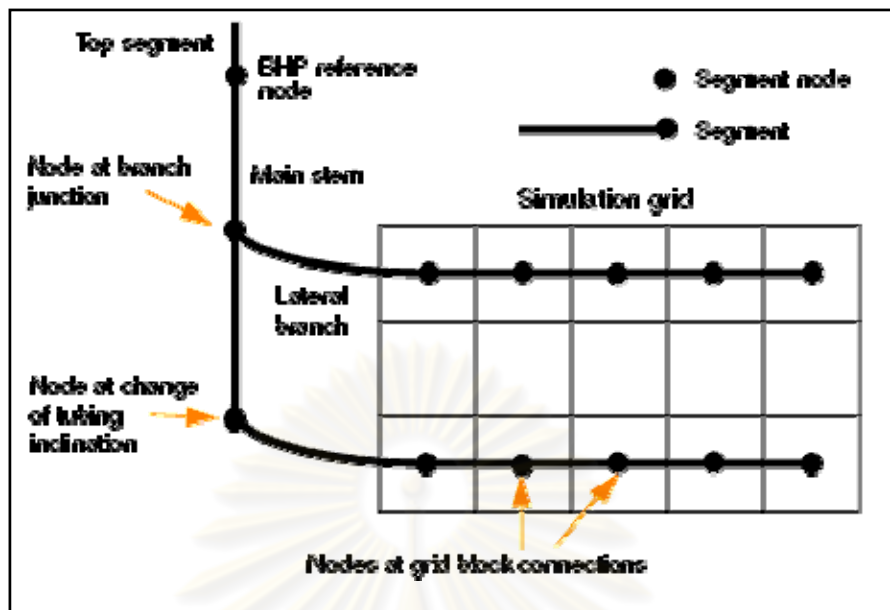
Figure 4.8: A multi-lateral, multi-segment well [22].

Each segment has a specified length, diameter, roughness, area and volume and also has its own set of independent variables to describe the local fluid conditions which are the fluid pressure, the total flow rate and the flowing fractions of water and gas.

The pressure drop is derived from pre-calculated VFP tables. Use of pre-calculated pressure drop tables can produce more accurate pressure gradients than the homogeneous flow treatment used in the other well models.

The top segment of the well is special. Its node corresponds to the well's bottomhole reference depth, so that the top segment's pressure is the same as the well's bottomhole pressure. Since there is no parent segment above it, no pressure losses are calculated across the top segment. It is best to model the pressure loss between this point and the tubing head in the standard way with a VFP table.

CHAPTER V

SIMULATION RESULTS

The base case simulation which is a non-fractured horizontal well in a low permeability gas condensate reservoir was modeled to obtain appropriate reservoir permeability for evaluating the productivity improvement when a horizontal well is hydraulically fractured.

A hydraulically fractured horizontal well was then modeled to evaluate the effects of various factors from fracture spacing, fracture half-length, fracture width, fracture permeability to number of fracture on well productivity

Economy analysis was performed in order to investigate the feasibility of hydraulic fracturing project.

5.1 Non-Fractured Well Simulation Results

5.1.1 Effect of reservoir permeability

To obtain a comparative assessment of the effect of reservoir characteristics, five reservoir cases were built with different permeabilities: 0.2, 0.4, 0.6, 0.8 and 1 mD. Figure 5.1 illustrates the non-fractured horizontal well simulation model. The five cases were simulated with a constant flow rate of 10,000 Mscf/D.
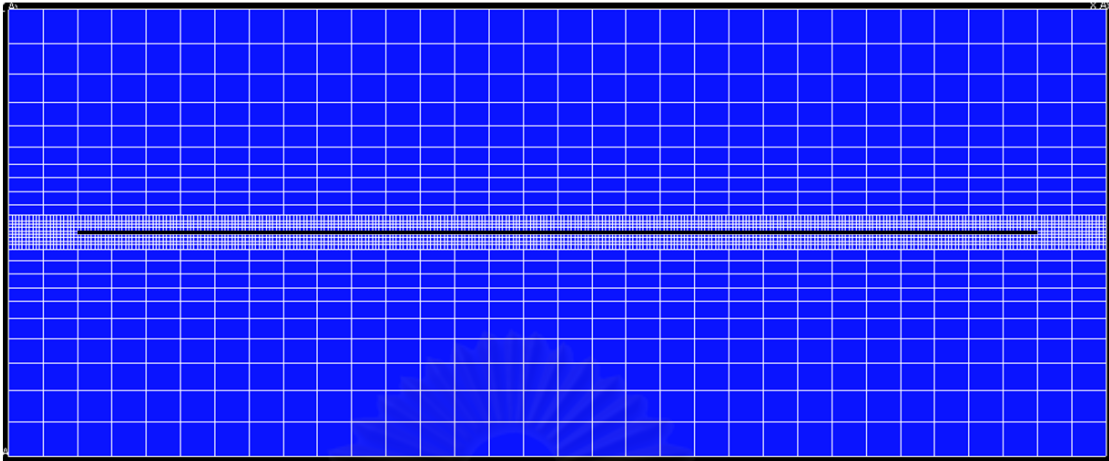
Figure 5.1: Areal view of the non-fractured horizontal well simulation model.

Figure 5.2 shows that gas production rate for a reservoir permeability of 1 mD is greater than that for the other cases. After 452 days of production at a constant rate of 10,000 Mscf/D, the rate declines sharply and goes below that for the other cases due to depletion. Note that the reservoir with permeability of 0.2 mD cannot sustain a plateau of 10,000 Mscf/D.

Figure 5.2: Gas rates of the non-fractured horizontal well for different reservoir permeabilities.

Figures 5.3 and 5.4 show that cumulative gas production and recovery factor for a reservoir permeability of 1 mD are greater than that for the other cases. However, recovery factor only slightly increases when reservoir permeability increases.
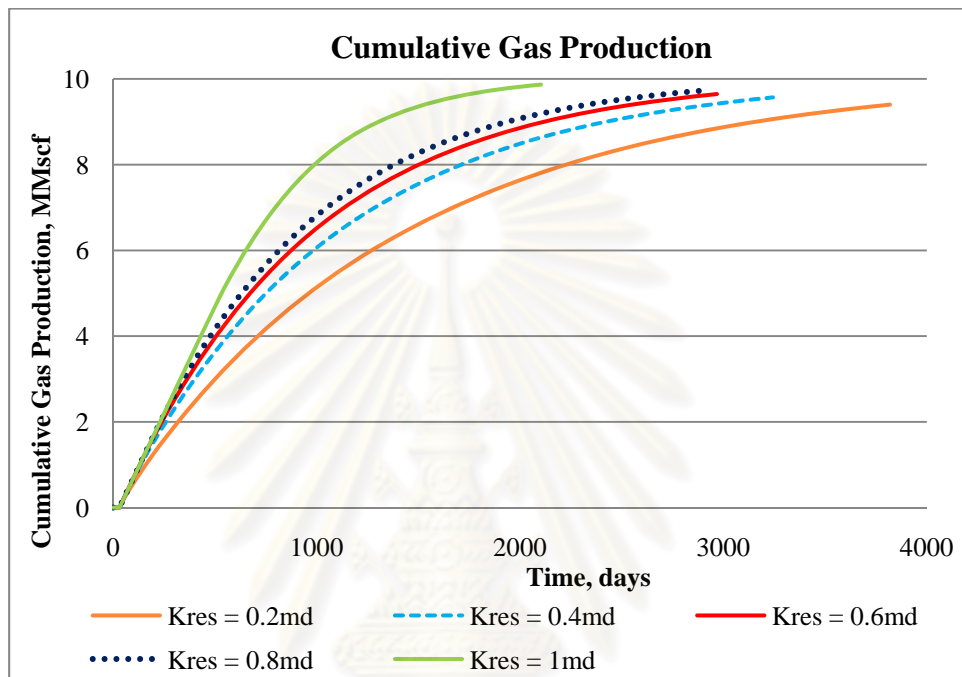
Figure 5.3: Cumulative gas production for different reservoir permeabilities.
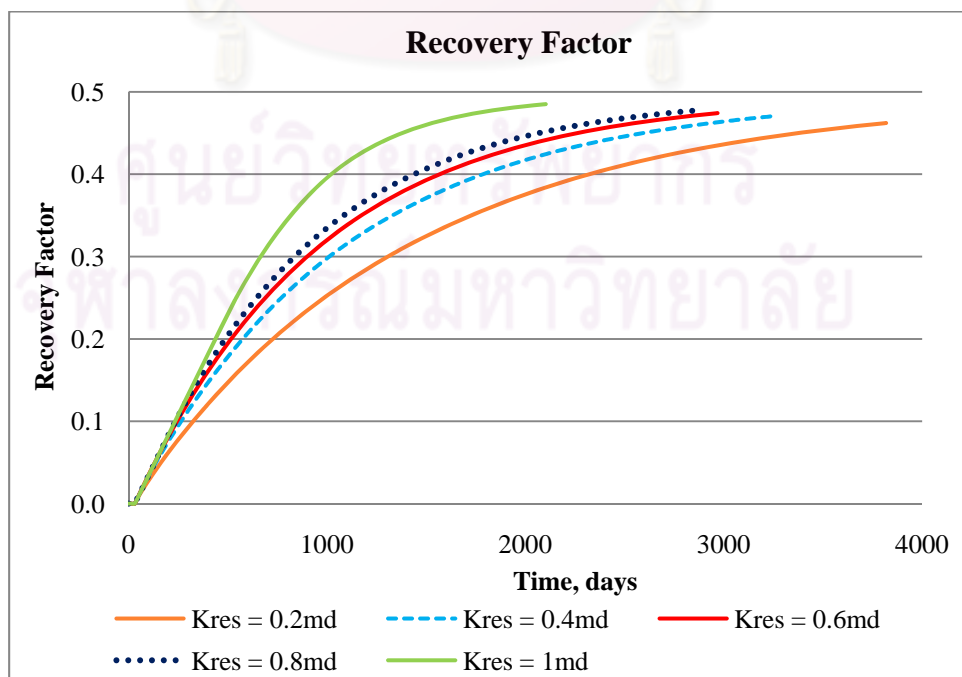
Figure 5.4: Gas recovery factor for different reservoir permeabilities.

Figure 5.5 shows that production time for the reservoir permeability of 0.2 mD is 3818 days and the production time for the reservoir permeability of 1 mD is 2103 days which is 1715 days less than that of the former case.
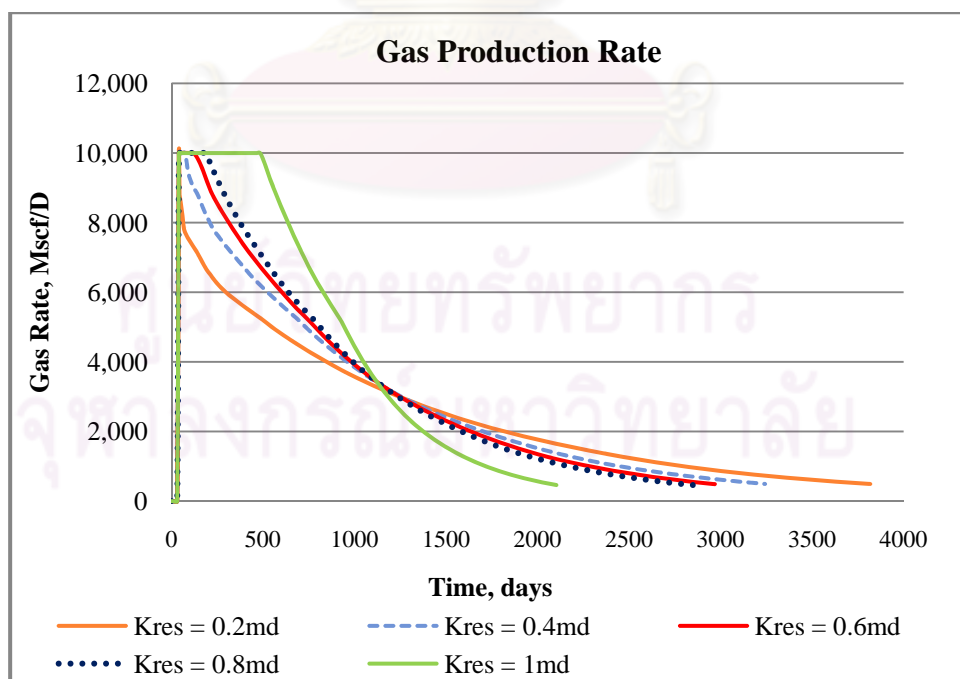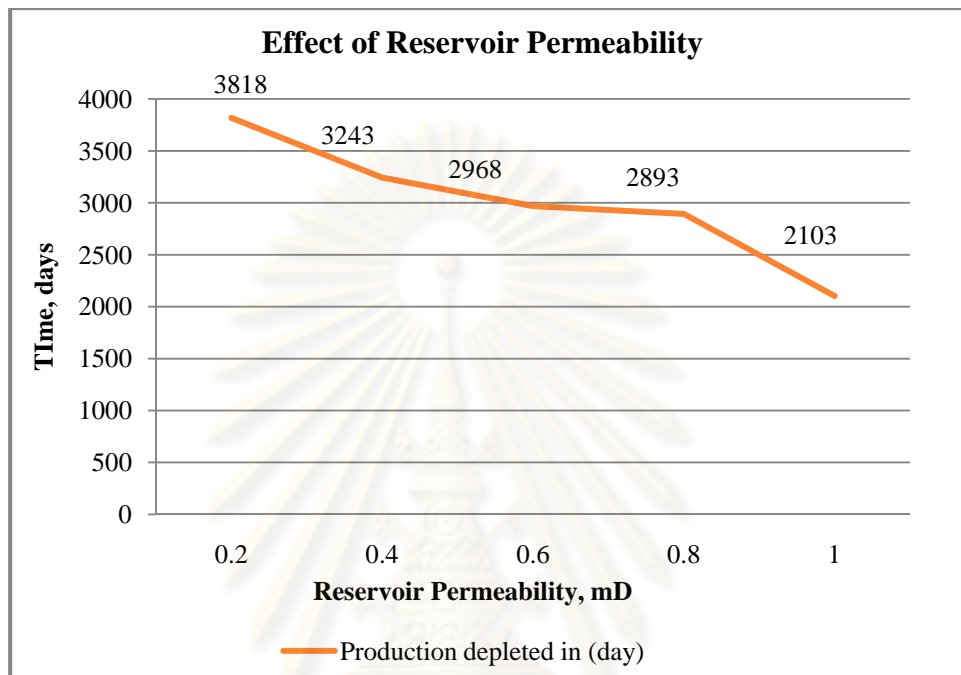

Figure 5.5: Production time of the non-fractured horizontal well for different reservoir permeabilities.

Figures 5.6 and 5.7 show that plots of condensate production rate and cumulative condensate production show similar trend with plots of gas production rate and cumulative gas production.

Figure 5.6: Condensate production rate for different reservoir permeabilities.

Figure 5.7: Cumulative condensate production for different reservoir permeabilities.

Table 5.1 summarizes the important results. It shows that reservoir permeability has a significant effect on the gas production time. To obtain a comparative assessment of hydraulic fracturing, a reservoir permeability of 0.2 mD,

which is the worst case, was used to simulate and study the improvement when a horizontal well is hydraulically fractured.

Table 5.1: Effect of reservoir permeability

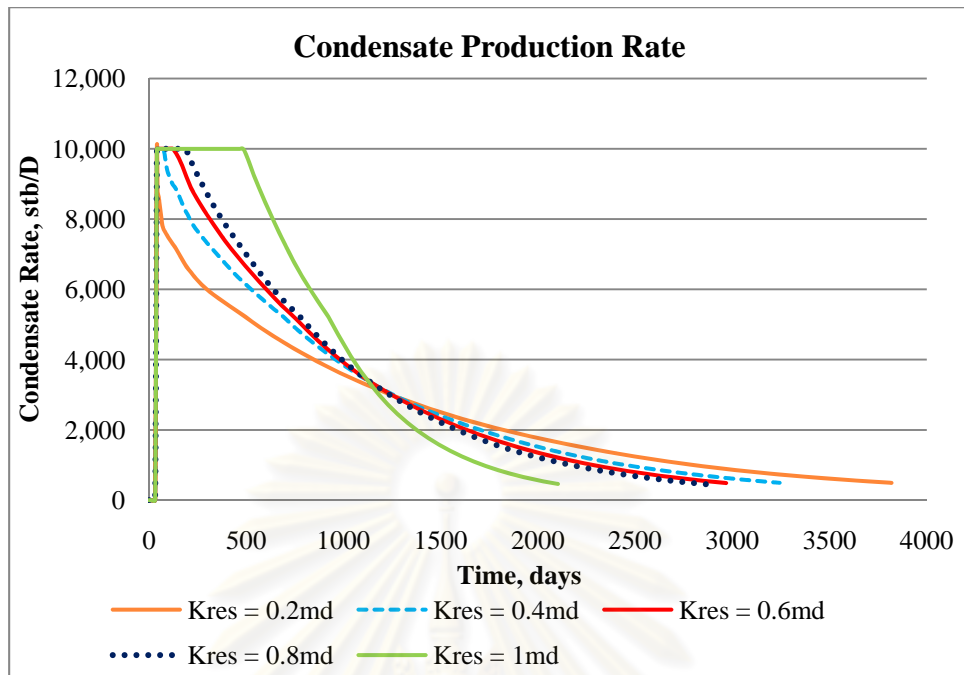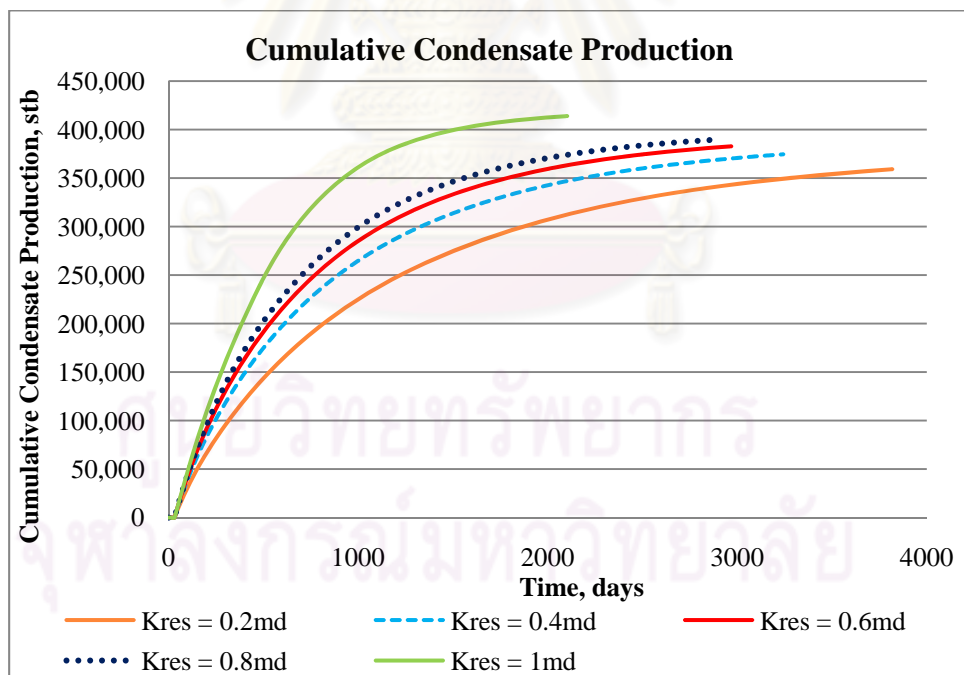| Reservoir permeability (mD)	Gas recovery factor	Cumulative gas production (Mscf)	Cumulative condensate production (stb)	Production time (days)
0.2	0.462	9,401,612	359,089	3,818
0.4	0.470	9,569,324	374,438	3,243
0.6	0.474	9,646,985	382,816	2,968
0.8	0.478	9,727,966	389,760	2,893
1.0	0.485	9,869,309	413,982	2,103

5.2 Fractured Well Simulation Results

5.2.1 Effect of fracture spacing

To understand the productivity enhancement of hydraulic fracturing, a hydraulically fractured horizontal well was simulated with gas production rate of 10,000 Mscf/D. Four cases were built with different fracture spacings: 200, 300, 400 and 600 ft as illustrated in Figures 5.8, 5.9, 5.10 and 5.11, respectively. The fracture half-length of 600 ft, fracture width of 0.2 ft and fracture permeability of 100,000 mD were used in all cases. The performances of these four cases were compared with that of non-fractured well.
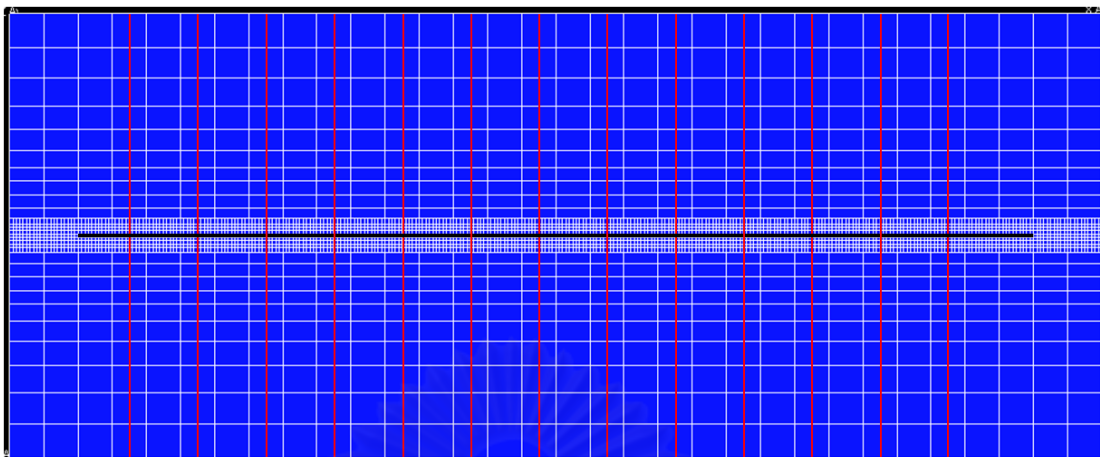
Figure 5.8: Areal view of the simulation model with fracture spacing of 200 ft.
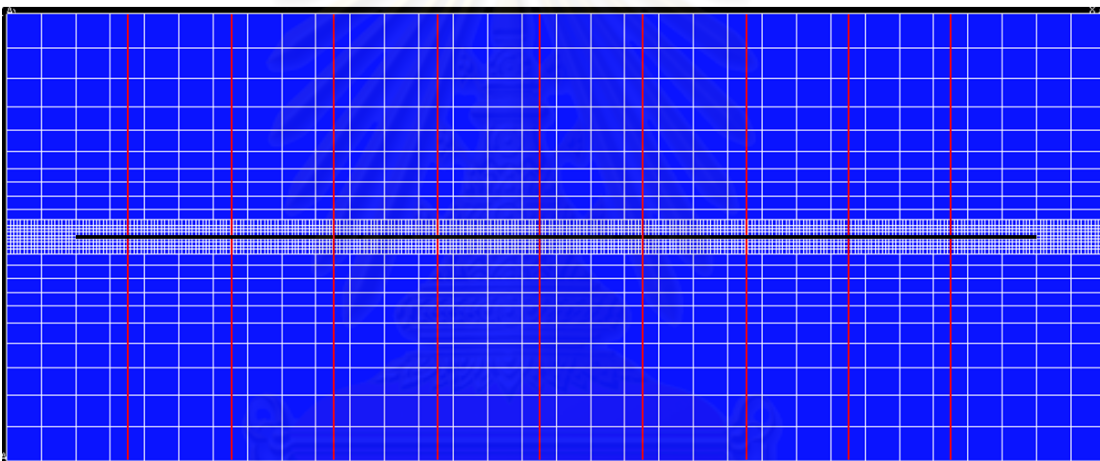
Figure 5.9: Areal view of the simulation model with fracture spacing of 300 ft.
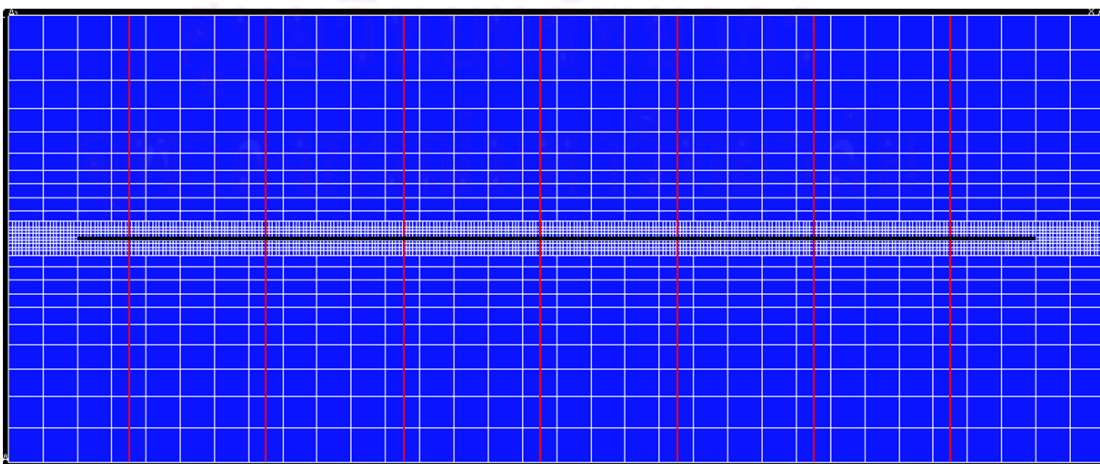
Figure 5.10: Areal view of the simulation model with fracture spacing of 400 ft.
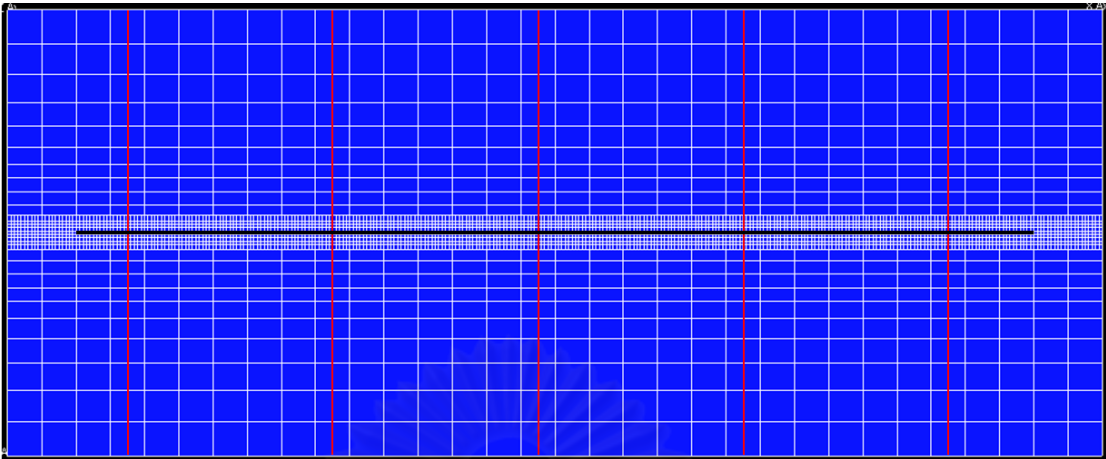
Figure 5.11: Areal view of the simulation model with fracture spacing of 600 ft.

Figure 5.12 shows that hydraulic fracturing improves productivity. There is a plateau in the gas rate for all fractured cases compared to no plateau in the non-fractured case. For the fracture spacing of 200 ft, the gas rate is constant at 10,000 Mscf/D up to 134 days.
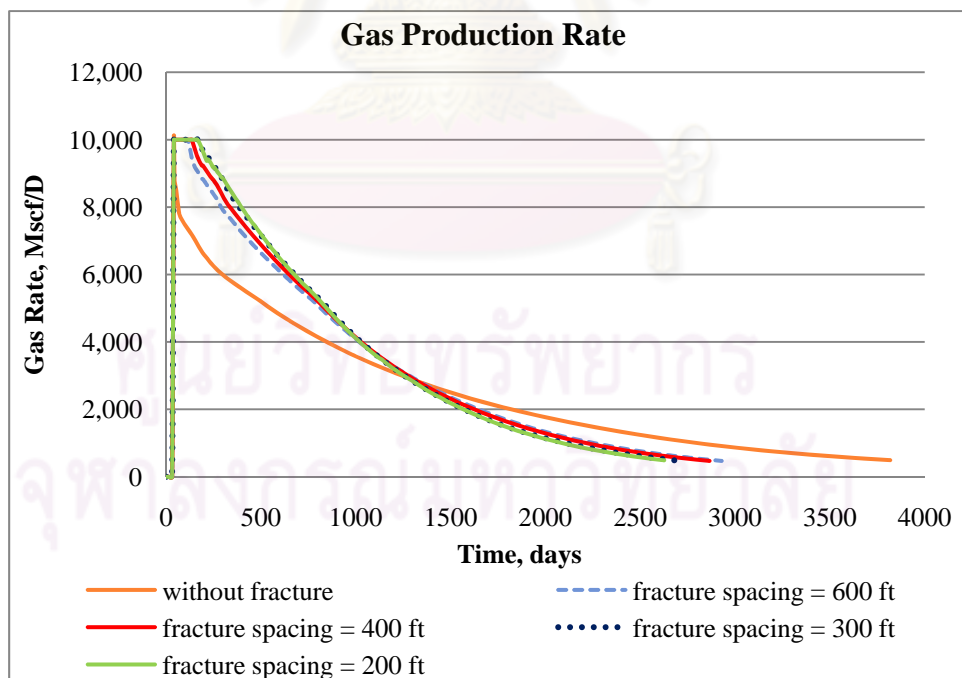
Figure 5.12: Gas rate for different fracture spacings when maximum gas rate is fixed at 10,000 Mscf/D.

Figure 5.13 shows that when the maximum gas rate is not fixed, hydraulic fracturing causes the gas rate to go up above 10,000 Mscf/D in all cases. For the fracture spacing of 200 ft, the gas rate goes up to 14,810 Mscf/D.
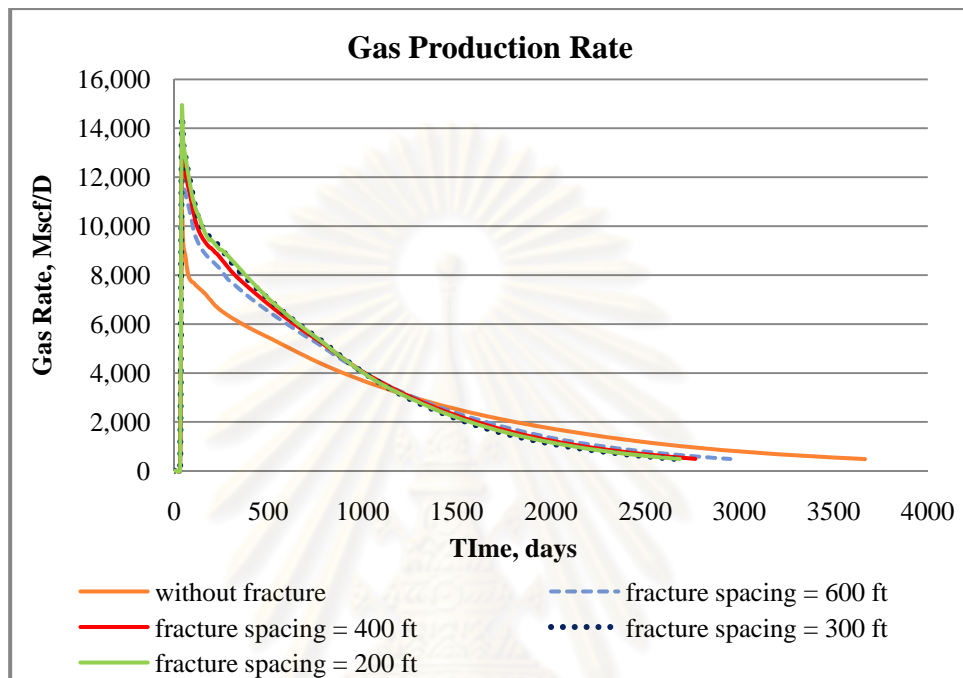
Figure 5.13: Gas rate for different fracture spacings when maximum gas rate is not fixed.

Figures 5.14 and 5.15 show that cumulative gas production and gas recovery factor increase in all fractured cases. For the fracture spacing of 200 ft, the gas recovery factor increases to 0.478. However, gas recovery factor only slightly increases when fracture spacing decreases.
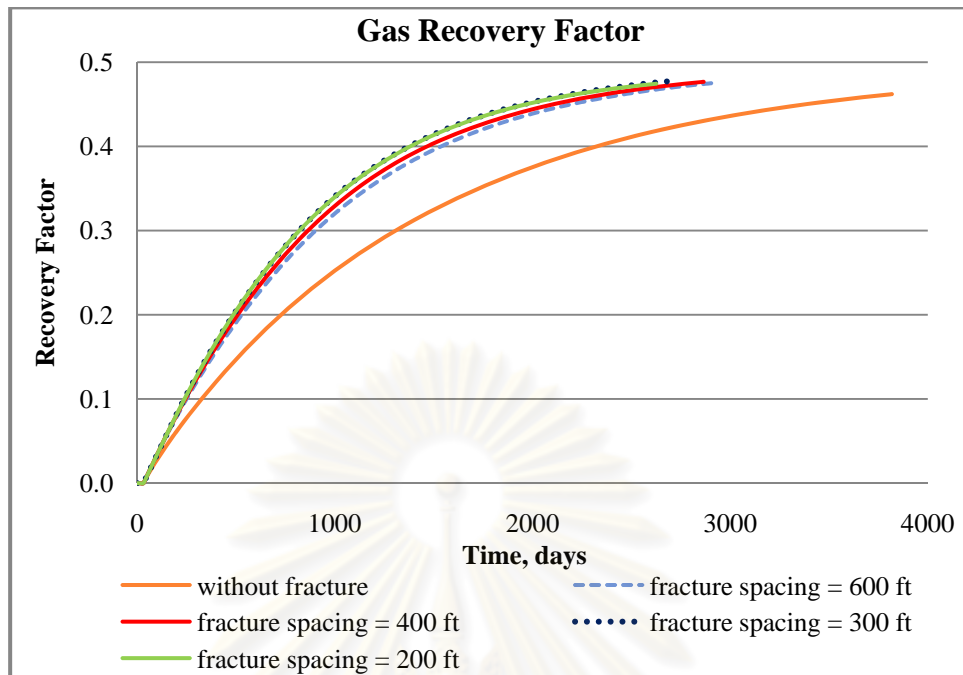
Figure 5.14: Gas recovery factor for different fracture spacings.
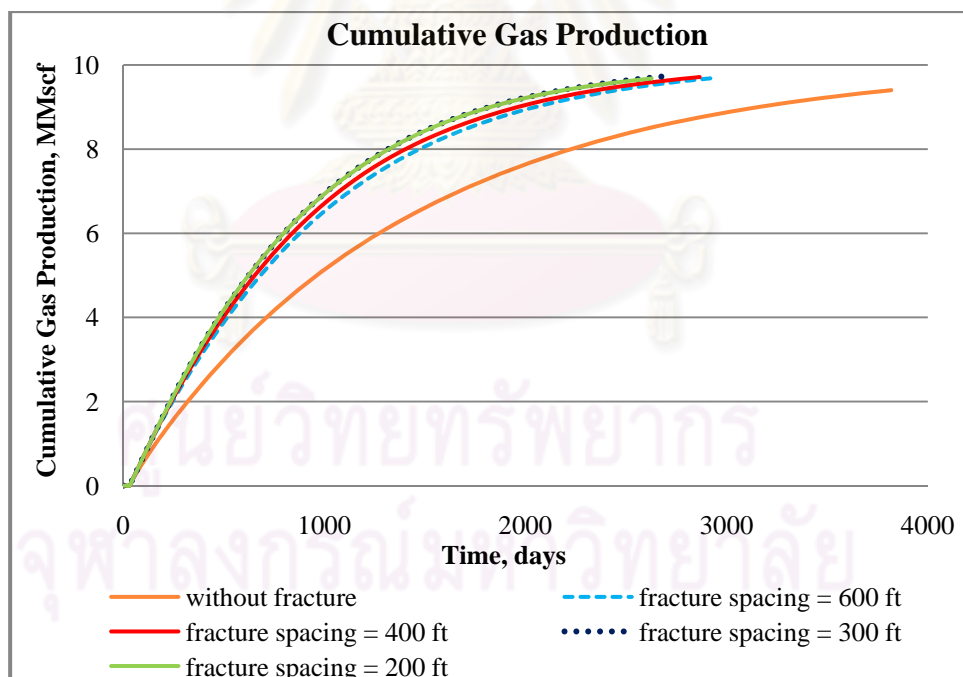
Figure 5.15: Cumulative gas production for different fracture spacings.

From Figure 5.15, the productivity of the fractured horizontal wells is slightly greater than that for the non-fractured well. However, Figure 5.16 clearly shows that production time of the fractured wells is much less than that of the non-fractured well.

The production time for the case with fracture spacing of 200 ft decreases by 1192 days compared to that of the non-fractured case.

Effect of Fracture Spacing
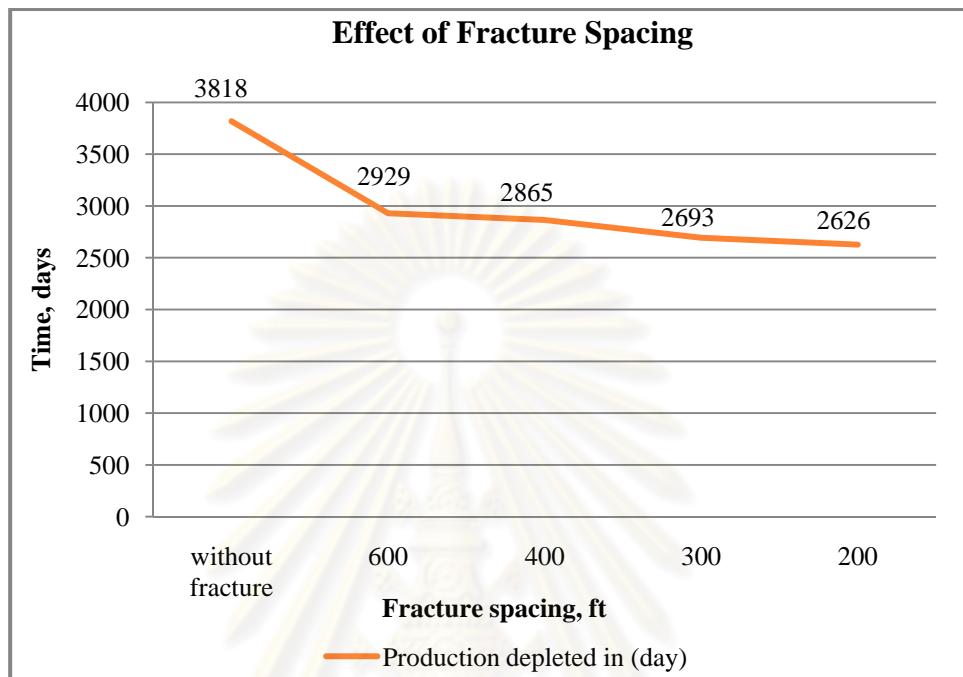
Figure 5.16: Production time for different fracture spacings.

Plots of condensate rate and cumulative condensate production show similar trend as shown in Figures 5.17, 5.18 and 5.19. Cumulative condensate production increases in all fractured cases. For the fracture spacing of 200 ft, the cumulative condensate production increases to 411,582 stb.
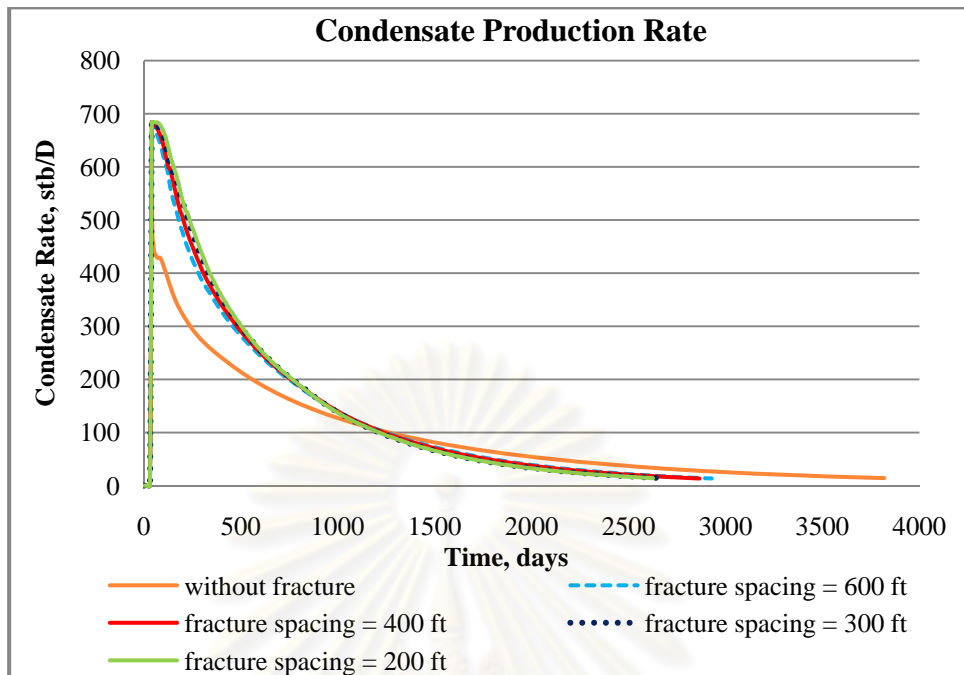
Figure 5.17: Condensate production rate for different fracture spacings.
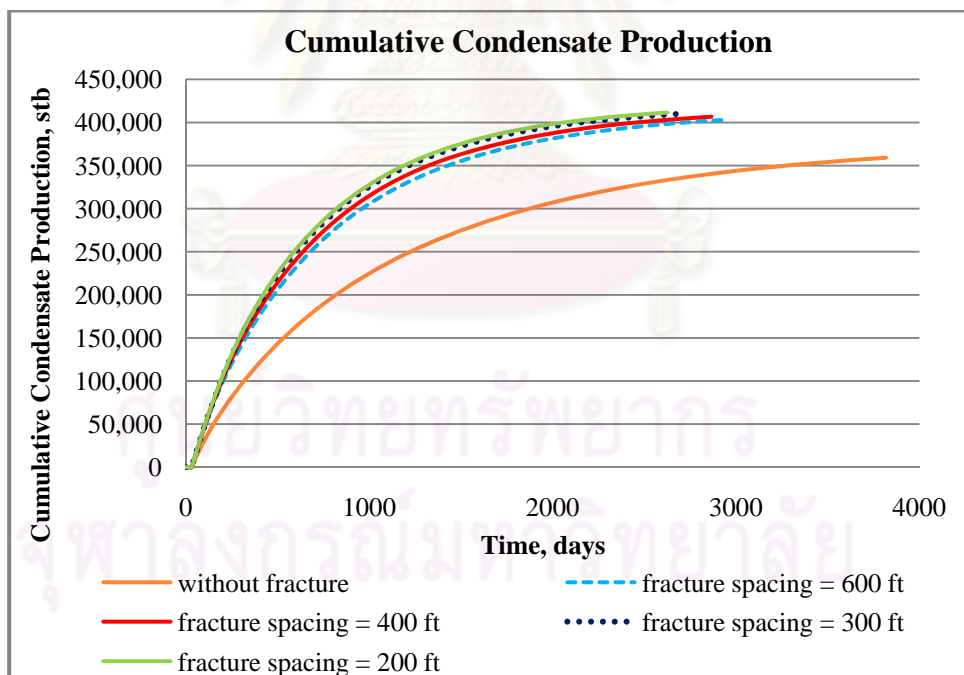
Figure 5.18: Cumulative condensate production versus time for different fracture spacings.
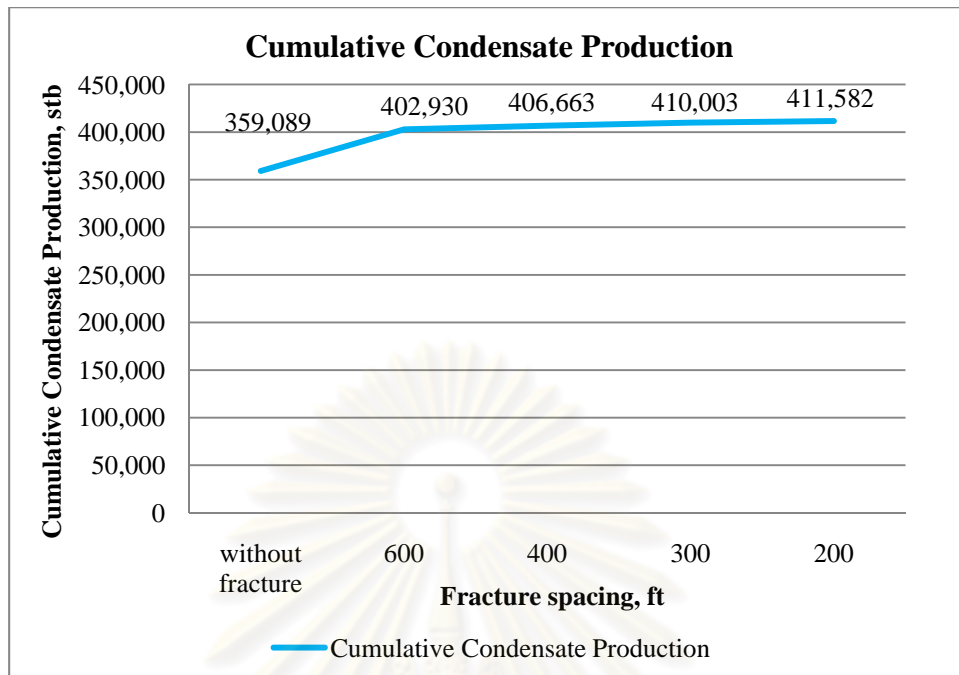
Figure 5.19: Cumulative condensate production for different fracture spacings.

For a tight gas condensate reservoir, well productivity increases as fracture spacing decreases. Table 5.2 summarizes the important results. It can be seen from the table that the fracture itself and fracture spacing have small impact on the gas recovery increment, but the amount of time required to produce gas from the reservoir reduces as the fracture spacing is less.

Condensate recovery increases as spacing becomes smaller. There is a big improvement in cumulative condensate production for fractured cases compared to non-fractured case. The cumulative condensate production for the case with fracture spacing of 200 ft increases by 14.62% when compared with non-fractured case. However, increment is quite small when comparing among fractured cases.

Table 5.2: Effect of fracture spacing.

Fracture spacing	Gas recovery factor	Cumulative gas production (Mscf)	Percent-age increase (%)	Cumulative condensate production (stb)	Percent-age increase (%)	Product-ion time (days)
No fracture	0.462	9,401,612	-	359,089	-	3,818
600	0.476	9,686,306	3.03	402,930	12.21	2,929
400	0.477	9,714,827	3.33	406,663	13.25	2,865
300	0.478	9,733,976	3.53	410,003	14.18	2,693
200	0.479	9,778,210	4.01	411,582	14.62	2,626

5.2.2 Effect of fracture half-length

Fracture half-length will affect the contact area between well and the reservoir. Increasing the half-length will have a direct impact on production. In this study, the objective is to investigate the effects of fracture half-length on well productivity by varying fracture half-length from case to case. Four simulation models were run with seven fractures along the horizontal well of different fracture half-lengths: 50, 200, 400 and 600 ft as illustrated in Figures 5.20, 5.21, 5.22 and 5.23, respectively. Other parameters which are fracture spacing of 400 ft, fracture width of 0.2 ft and fracture permeability of 100,000 mD were kept constant. The performances of the four cases were compared with that of non-fractured well. The models were simulated at a production rate of 10,000 Mscf/D.

Figure 5.20: Areal view of the simulation model with fracture half-length of 50 ft.
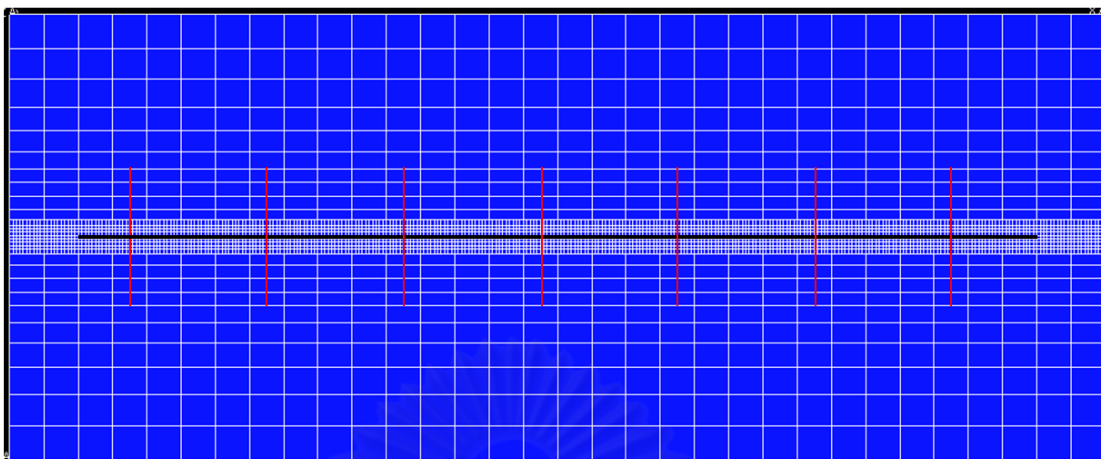
Figure 5.21: Areal view of the simulation model with fracture half-length of 200 ft.
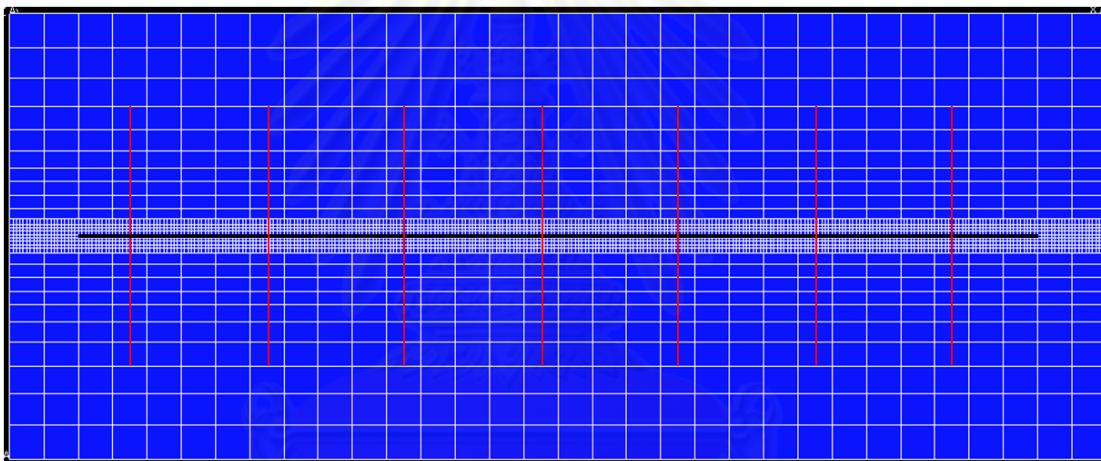
Figure 5.22: Areal view of the simulation model with fracture half-length of 400 ft.
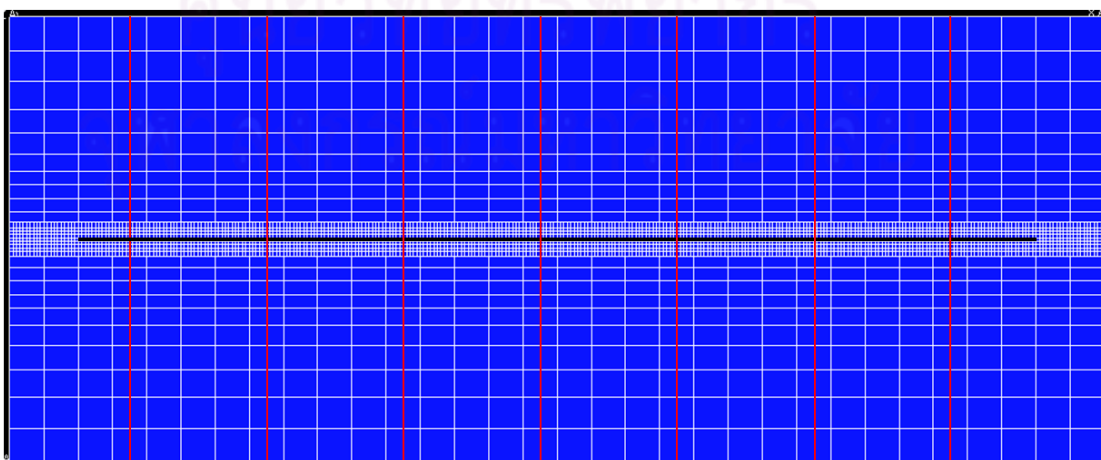
Figure 5.23: Areal view of the simulation model with fracture half-length of 600 ft.

Figures 5.24, 2.25 and Table 5.3 show that the time required to produce gas significantly decreases as the fracture half-length increases. Gas and condensate recovery increase as length of fracture half-length becomes larger. Length of fracture half-length has small impact on gas recovery, but large impact on condensate recovery. The cumulative condensate production for the case with fracture half-length of 600 ft increases by 13.25% when compared with non-fracture case.

Figure 5.24: Production time for different fracture half-lengths.

Figure 5.25: Cumulative condensate production for different fracture half-lengths.

Table 5.3: Effect of fracture half-length.

Fracture half-length	Gas recovery factor	Cumulative gas production (Mscf)	Percent-age increase (%)	Cumulative condensate production (stb)	Percent-age increase (%)	Product-ion time (days)
No fracture	0.462	9,401,612	-	359,089	-	3,818
50	0.467	9,491,013	0.95	363,292	1.17	3,693
200	0.473	9,621,756	2.34	385,896	7.47	3,073
400	0.475	9,681,505	3.00	402,191	12.00	2,924
600	0.477	9,714,827	3.33	406,663	13.25	2,865

5.2.3 Effect of fracture width

In this case study, the objective is to investigate the effects of fracture width on well productivity by varying fracture width from case to case. Four simulation models were run with seven fractures along the horizontal well of different fracture widths: 0.02083, 0.05, 0.1 and 0.2 ft. Other parameters which are fracture spacing of 400 ft, fracture half-length of 600 ft, and fracture permeability of 100,000 mD were

kept constant. Their performances were compared with that of non-fractured well. The models were simulated at a production rate of 10,000 Mscf/D.
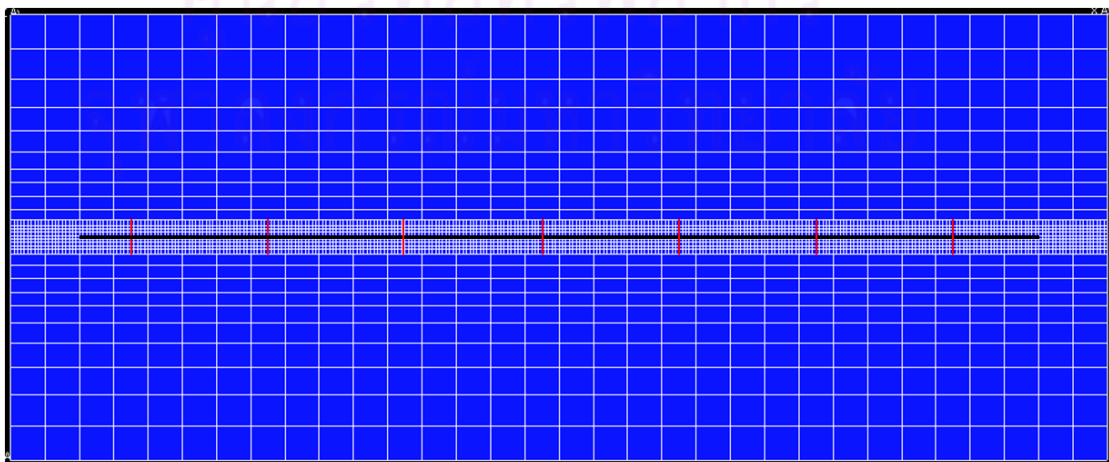
Figures 5.26, 5.27 and Table 5.4 show that the time required to produce gas significantly decreases as the fracture width increases. Gas and condensate recovery increase as fracture width becomes larger. Fracture width has small impact on gas recovery, but large impact on condensate recovery. The cumulative condensate production for the case with fracture width of 0.2 ft increases by 13.25% when compared with non-fracture case.

Figure 5.26: Production time for different fracture widths.
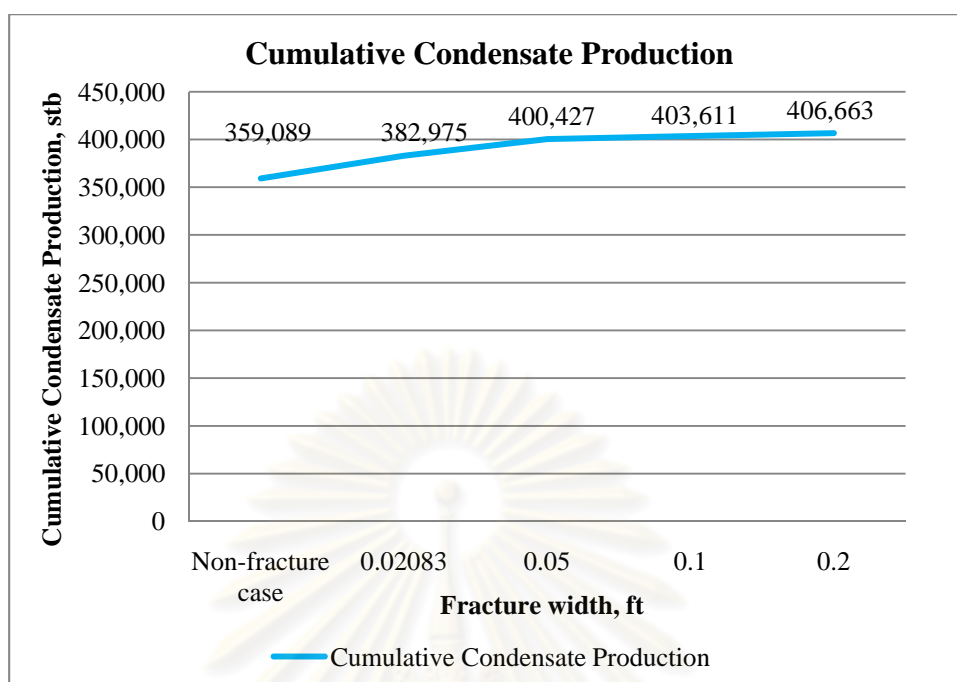
Figure 5.27 : Cumulative condensate production for different fracture widths.

Table 5.4: Effect of fracture width.

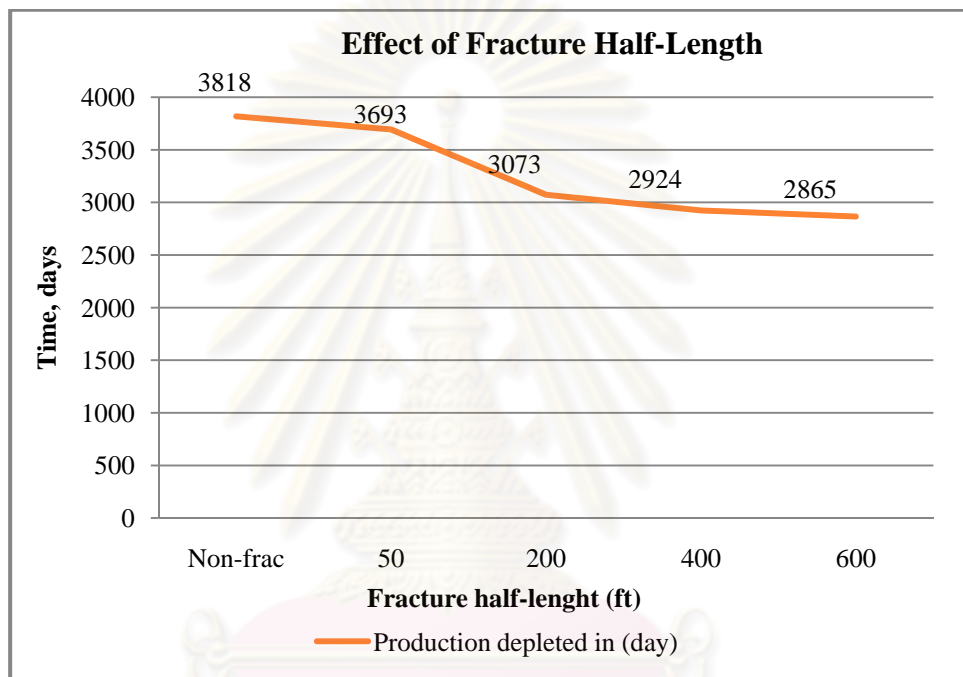| Fracture width	Gas recovery factor	Cumulative gas production (Mscf)	Percent-age increase (%)	Cumulative condensate production (stb)	Percent-age increase (%)	Product-ion time (days)
No fracture	0.462	9,401,612		359,089	-	3,818
0.02083	0.467	9,498,543	1.03	382,975	6.65	3,497
0.05	0.473	9,627,010	2.40	400,427	11.51	3,259
0.1	0.474	9,656,074	2.71	403,611	12.40	3,044
0.2	0.477	9,714,827	3.33	406,663	13.25	2,865

5.2.4 Effect of fracture permeability

In this case study, the objective is to investigate the effects of fracture permeability on well productivity by varying fracture permeability from case to case. Seven fractures were modeled with four different fracture permeabilities: 1,000, 10,000, 50,000 and 100,000 mD. The fracture spacing of 400 ft, fracture half-length of 600 ft, and fracture width of 0.2 ft were kept constant. Their performances were

compared with that of non-fractured well. The models were simulated at a production rate of 10,000 Mscf/D.

Figures 5.28, 5.29 and Table 5.5 show that the time required to produce gas significantly decreases as the fracture permeability increases. Gas and condensate recovery increase as fracture permeability becomes larger. Fracture permeability has small impact on gas recovery, but large impact on condensate recovery. The cumulative condensate production for the case with fracture permeability of 100,000 mD increases by 13.25% when compared with non-fracture case.

Figure 5.28: Production time for different fracture permeabilities.
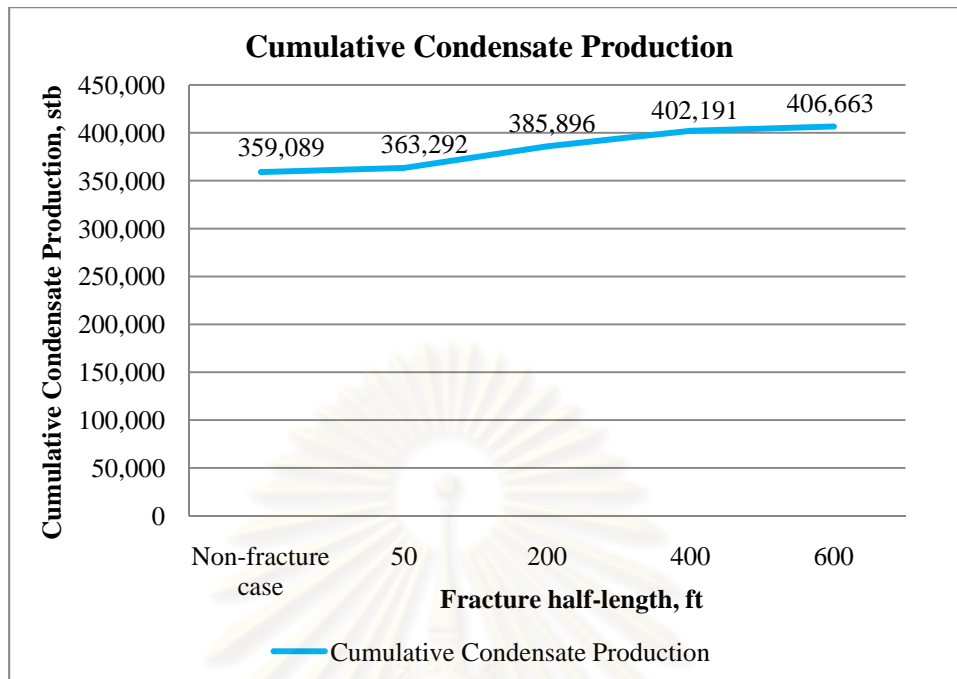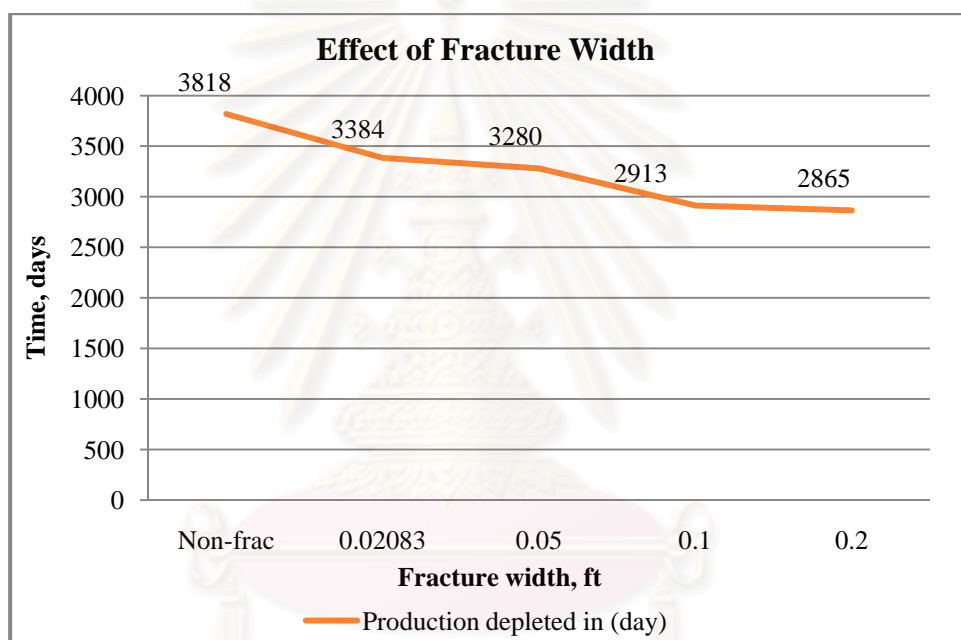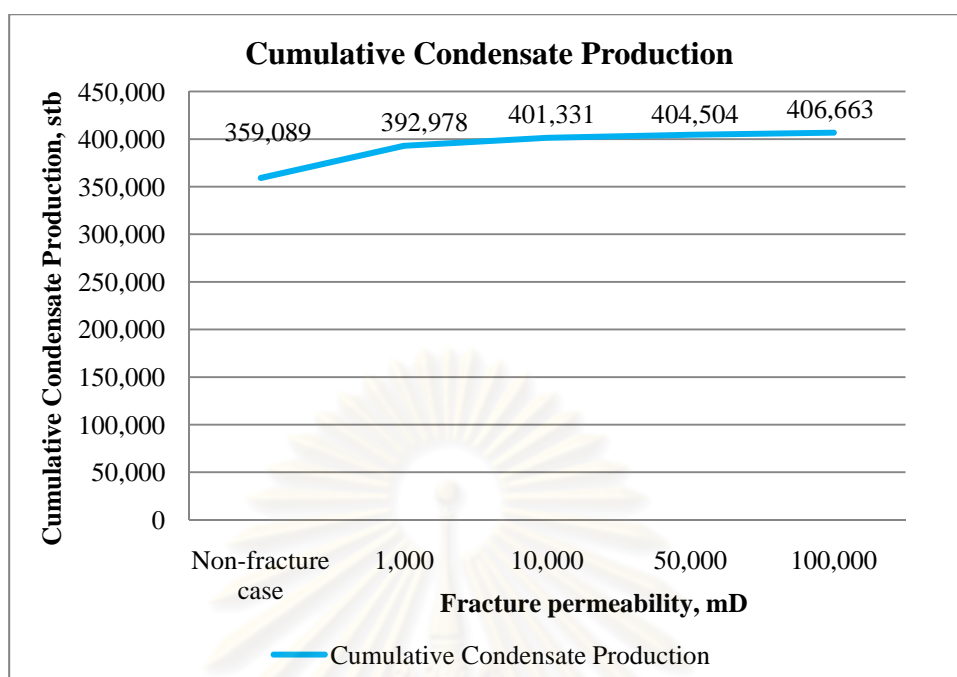
Figure 5.29 : Cumulative condensate production for different fracture permeabilities.

Table 5.5 : Effect of fracture permeability.

Fracture permea-bility	Gas recovery factor	Cumulative gas production (Mscf)	Percent-age increase (%)	Cumulative condensate production (stb)	Percent-age increase (%)	Product-ion time (days)
No fracture	0.462	9,401,612	-	359,089	-	3,818
1,000	0.470	9,568,445	1.78	392,978	9.44	3,384
10,000	0.474	9,667,069	2.82	401,331	11.76	3,280
50,000	0.475	9,677,944	2.94	404,504	12.65	2,913
100,000	0.477	9,714,827	3.33	406,663	13.25	2,865

5.2.5 Effect of number of fracture

To understand effect of number of fracture, fractures with the same properties were modeled. Three simulation models were run with different numbers of fracture: one, four and seven fractures, along the horizontal well. Fracture half-length of 600 ft, fracture width of 0.2 ft and fracture permeability of 100,000 mD were kept constant. Fractures were modeled at the middle of the horizontal well with constant fracture spacing of 400 ft. Figures 5.30, 5.31 and 5.32 illustrate the simulation models. Their

performances were compared with that of non-fractured well. The models were simulated at a production rate of 10,000 Mscf/D.
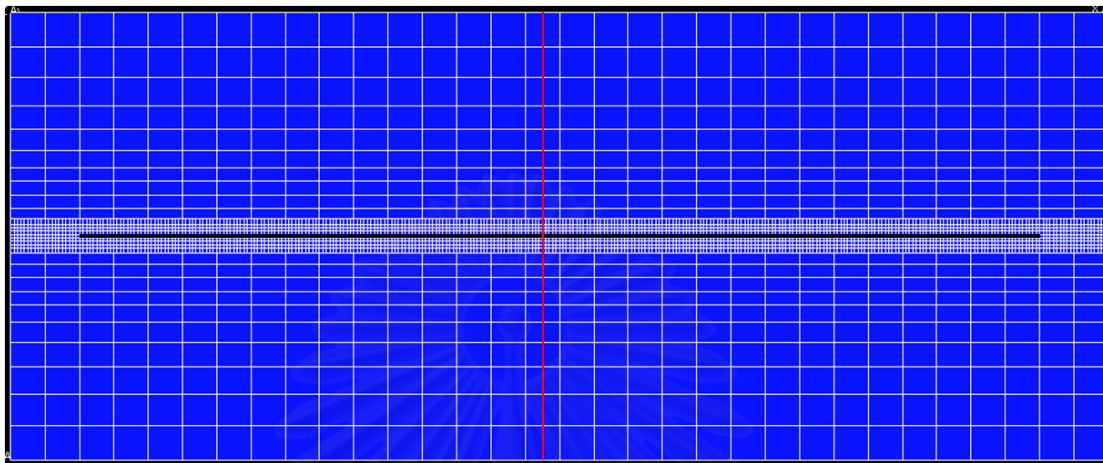
Figure 5.30: Areal view of simulation model with one hydraulic fracture.
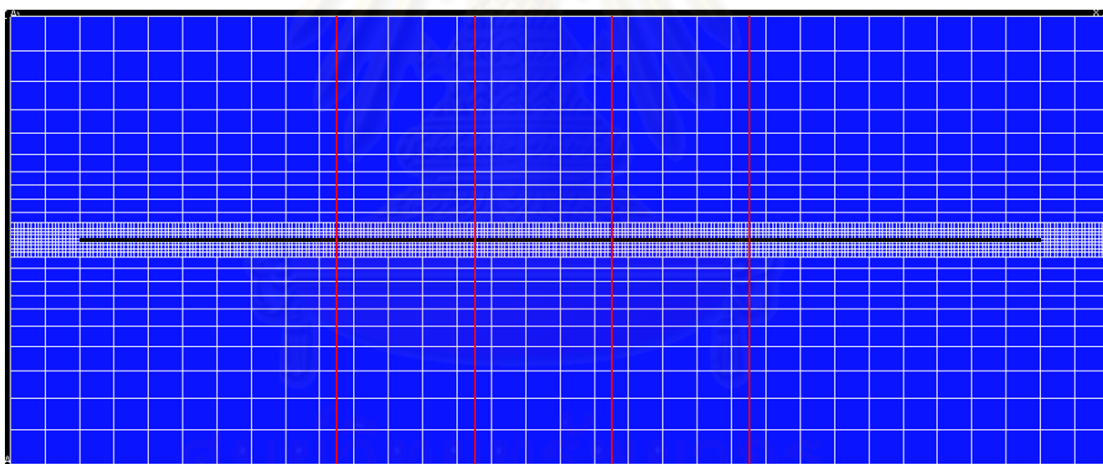
Figure 5.31: Areal view of simulation model with four hydraulic fractures.
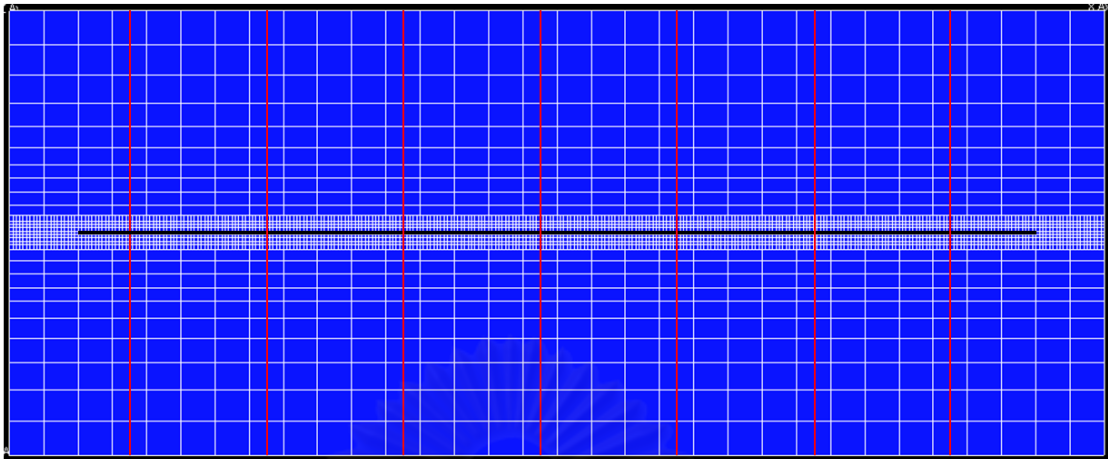
Figure 5.32: Areal view of simulation model with seven hydraulic fractures.

Figures 5.33, 5.34 and Table 5.6 highlight the fact that the time required to produce gas significantly decreases as number of fracture increases. Gas and condensate recovery increase as number of fracture increases. Number of fracture has small impact on gas recovery, but large impact on condensate recovery. The cumulative condensate production for the case with 7 fractures increases by 13.25% when compared with non-fracture case.
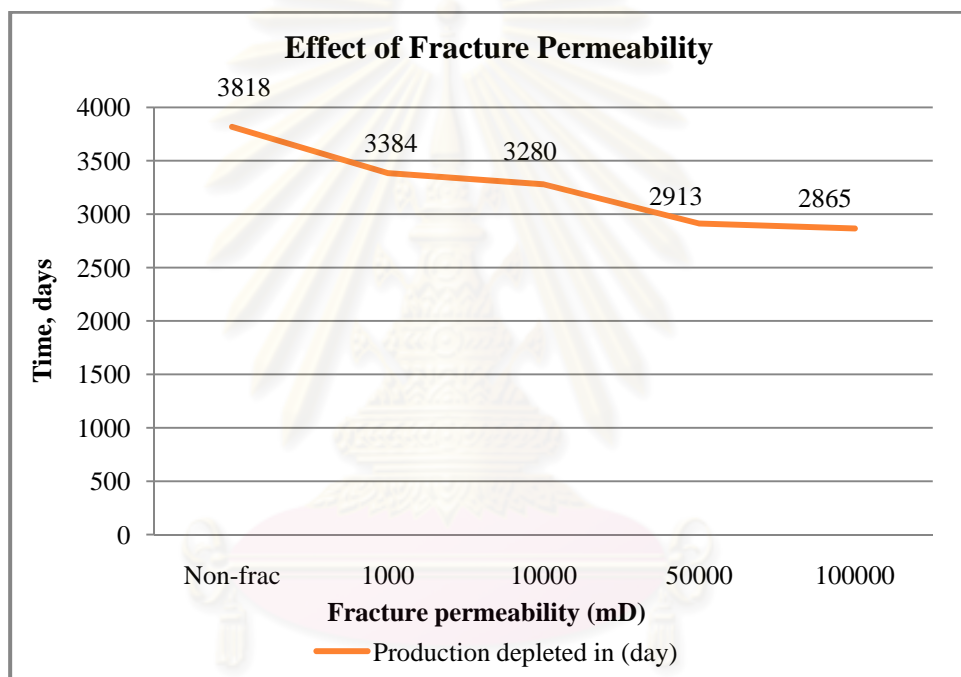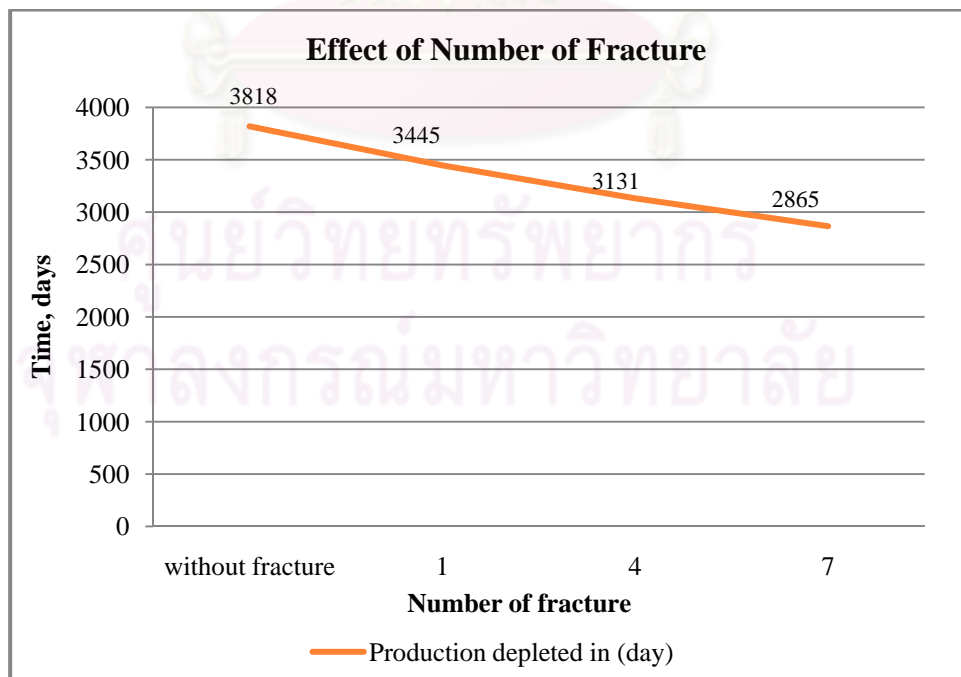

Figure 5.33: Production time for different numbers of fractures.
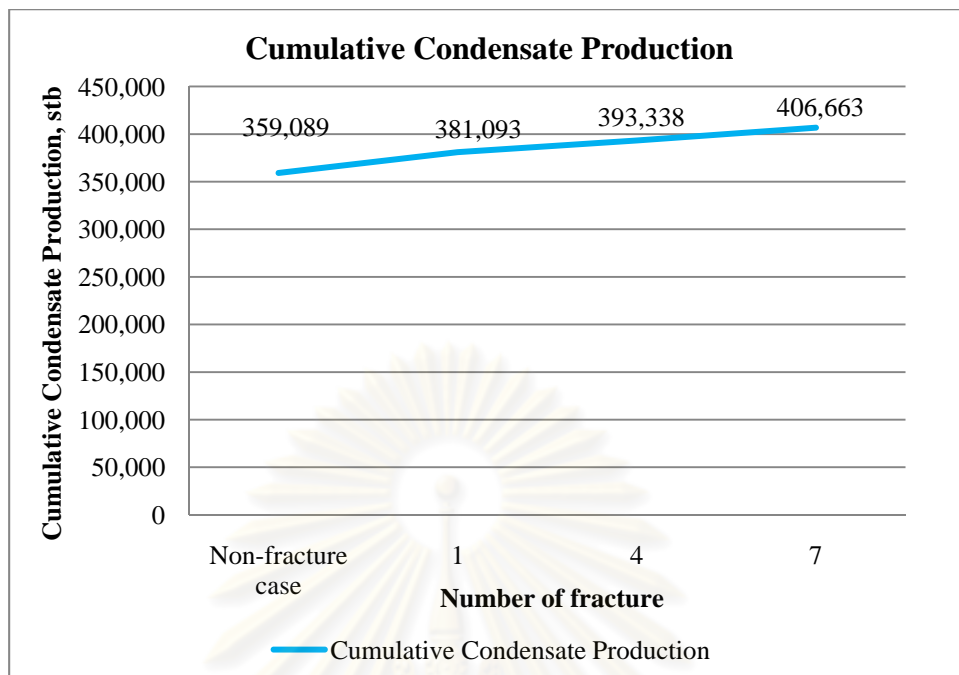
Figure 5.34: Cumulative condensate production for different number of fractures.

Table 5.6: Effect of number of fractures.

Number of fracture	Gas recovery factor	Cumulative gas production (Mscf)	Percent-age increase (%)	Cumulative condensate production (stb)	Percent-age increase (%)	Product-ion time (days)
No fracture	0.462	9,401,612	-	359,089	-	3,818
1	0.467	9,504,313	1.09	381,093	6.13	3,445
4	0.472	9,619,335	2.31	393,338	9.54	3,131
7	0.477	9,714,827	3.33	406,663	13.25	2,865

5.3 Condensate Saturation Profile

In this section, the objective is to study condensate saturation profiles around non-fractured and fractured well. Seven fractures were modeled with fracture spacing of 400 ft, fracture half-length of 600 ft, fracture width of 0.2 ft and fracture permeability of 100,000 mD. Fracture conductivity is 166.67. Its result was compared with that of non-fractured well. The models were simulated at a production rate of 10,000 Mscf/D.

Figures 5.35 and 5.36 show condensate saturation profile at the end of production for fractured well compared with non-fractured well away from the wellbore in the y- and z- directions, respectively. It can be seen that condensate saturation for fractured well decreases in both directions.
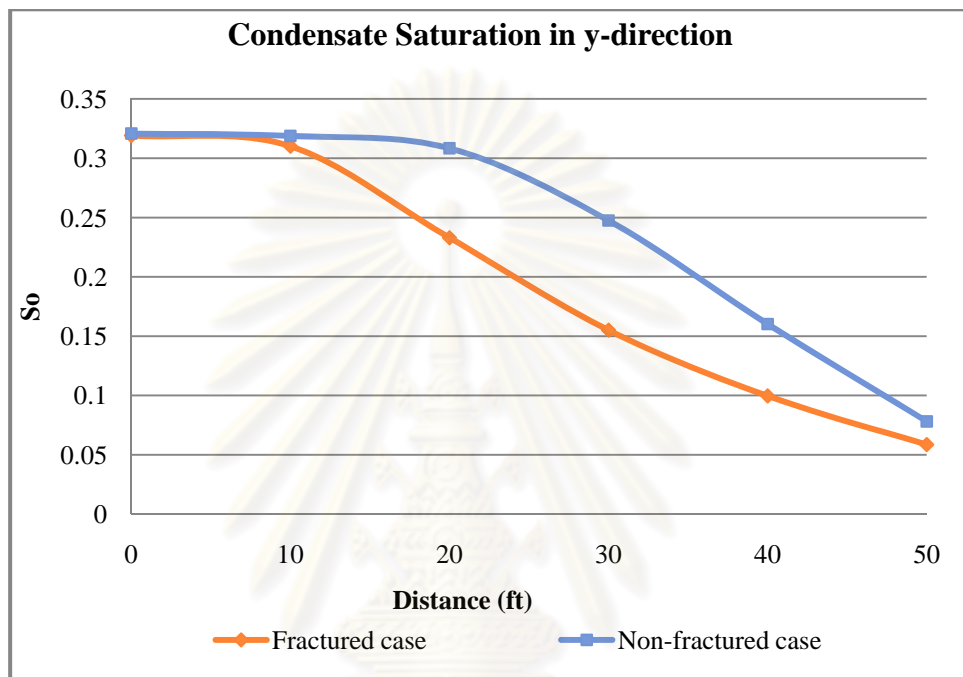
Figure 5.35: Condensate saturation profile in the y- direction.
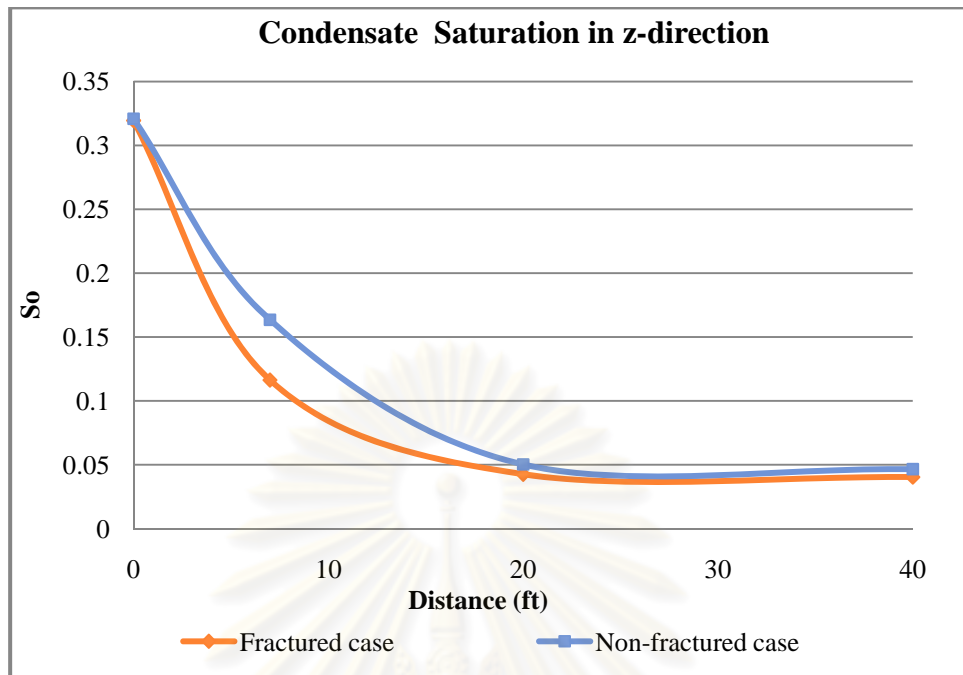
Figure 5.36: Condensate saturation profile in the z- direction.

Figures 5.37 and 5.38 illustrate the condensate saturation profiles around non-fractured and fractured well after 208 days. Condensate saturation is scaled from 0 (blue) to 0.5 (red). As shown in the figures, the condensate saturation profiles are different for the two cases. The figures show that hydraulic fracturing reduces condensate saturation near the wellbore because of decrease in pressure drawdown. The condensate bank size around the well also decreases.

This can be illustrated further by plotting the pressure profiles as shown in Figures 5.39 and 5.40. Pressure is scaled from 683.4 psia (blue) to 3505.8 psia (red). For the fractured case, the wellbore grid has pressure of 2252 psia after 208 days of production which is higher than that of the non-fractured case which has pressure of 1822 psia.
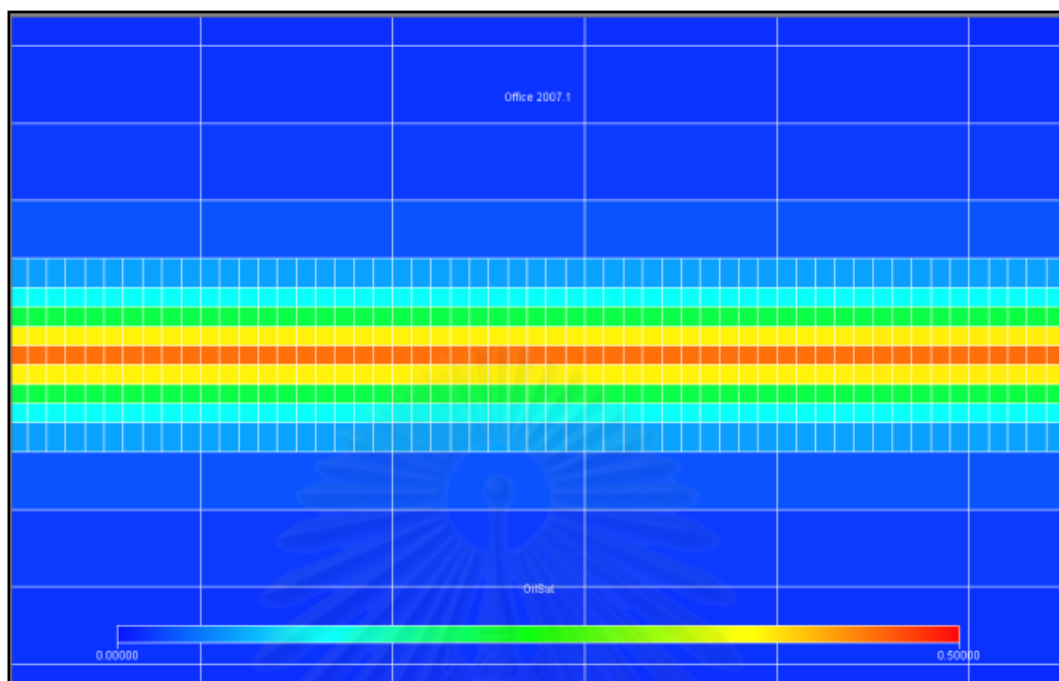
Figure 5.37: Areal view of condensate saturation for the non-fractured case after 208 days of production.
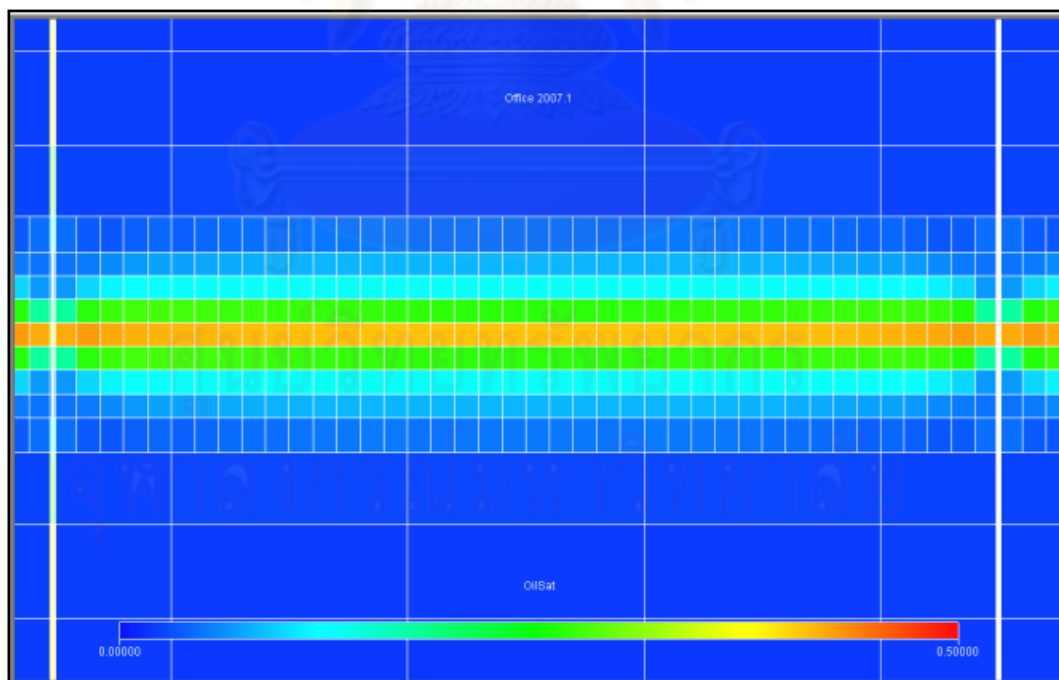
Figure 5.38: Areal view of condensate saturation for the fractured case after 208 days of production.
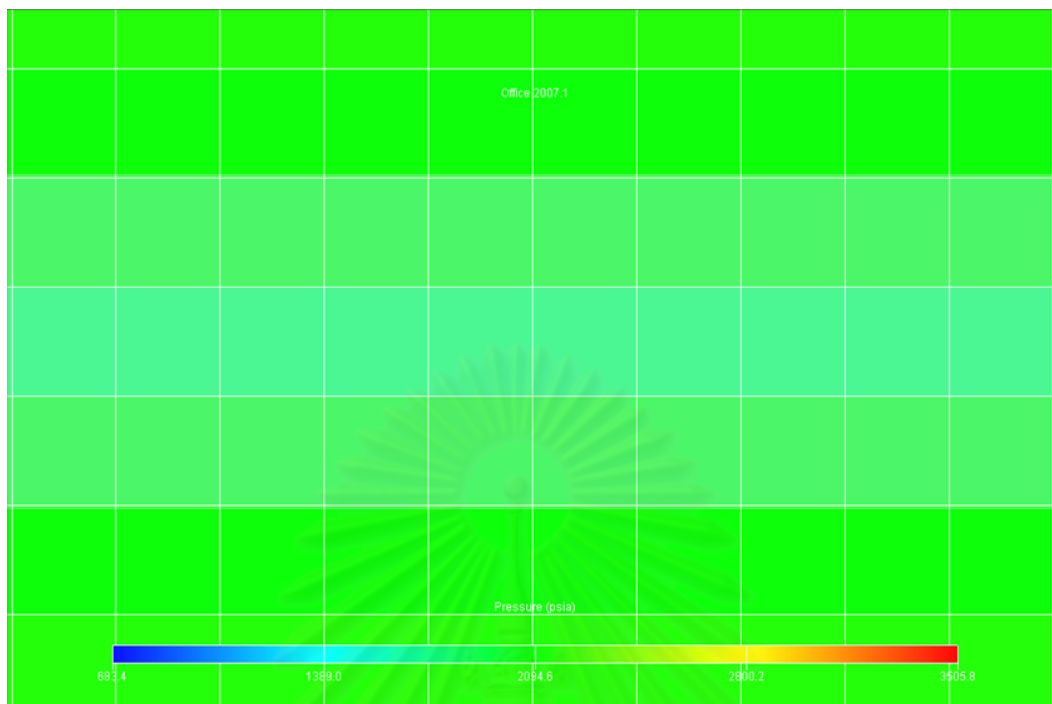
Figure 5.39: Areal view of pressure profile for the non-fractured case after 208 days of production.
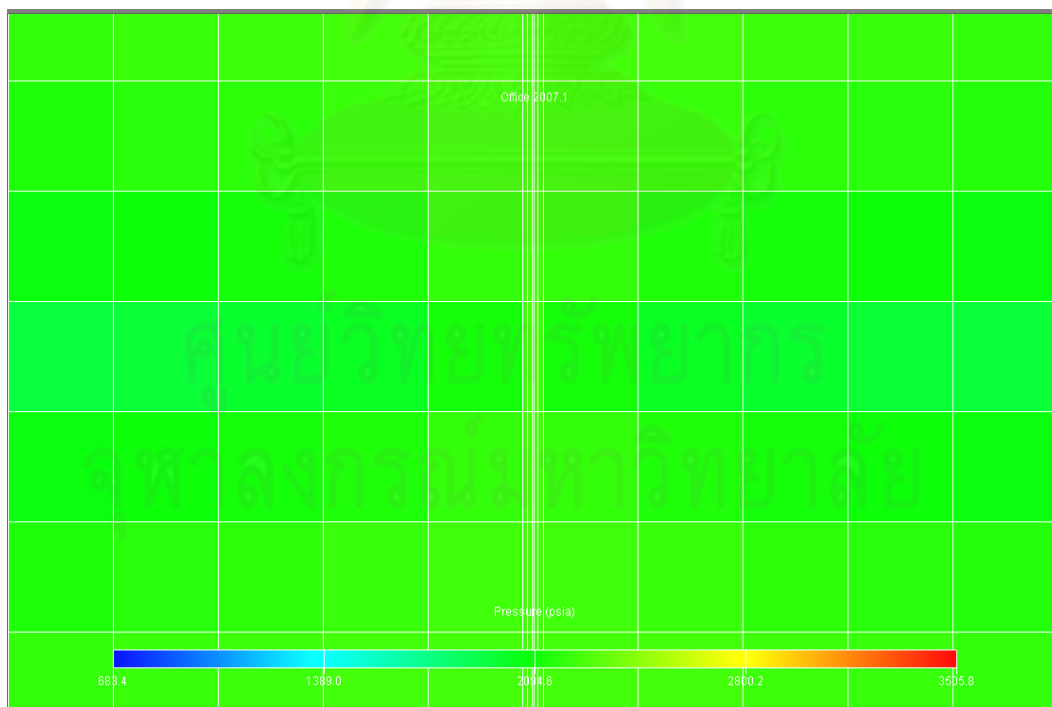
Figure 5.40: Areal view of pressure profile for the fractured case after 208 days of production.

5.4 Economy Analysis

The simulation models in Section 5.2.5 which have different number of fracture: one, four and seven fractures are selected for economy analysis. All three cases have fracture half-length of 600 ft, fracture width of 0.2 ft and fracture permeability of 100,000 mD. Fractures are modeled at the middle of the horizontal well with constant fracture spacing of 400 ft. The models are simulated at a constant gas production rate of 10,000 Mscf/D. The results are compared with the non-fractured case.

The economy analysis is used to compare among four cases: non-fractured horizontal well, horizontal well with one, four and seven hydraulic fractures. The results of different cases are presented to provide a margin of freedom in making decision on how many fractures in horizontal well would provide optimum productivity.

The hydraulic fracturing cost is a function of type and cost of frac fluid and proppant used, pumping cost, fixed cost to cover equipment hire and other expenses. The cost is highly variable depending upon location, equipment requirement, material costs and pumping services availability.

For the current effort, the economy analysis in this study is based on the following assumption.

1. The cost is invested at the beginning of the project.
2. Fixed OPEX costs are 150 \$/MMscf and 3 \$/stb.
3. Fixed cost of production well equals to 5,000,000 \$.
4. Discount rate is constant at 15%.
5. Gas price equals to 7 \$/MMbtu which equals to 7000 \$/MMscf.
6. Oil price equals to 50 \$/stb.
7. For one fracture, volume of proppant used is 2,000 ft^3. The cost of proppant is assumed to be 20 $\$/ft^3$
8. The hydraulic fracturing costs related to frac fluid, pumping and service costs have been bundled and assigned as a cost of 5$\$/ft^3$ of proppant volume used.
9. The cost of equipment hire is assumed to be a fixed cost of 150,000 \$.

The estimated hydraulic fracturing costs for each case with proppant volume used are shown in Table 5.7.

Table 5.7: Estimated hydraulic fracturing costs.

Number of fracture	Proppant volume (ft^3)	Proppant cost ($)	Non-proppant cost ($)	Equipment cost ($)	Total cost ($)
1	2,000	40,000	10,000	150,000	200,000
4	8,000	160,000	40,000	150,000	350,000
7	14,000	280,000	70,000	150,000	500,000

Annual cash flow, cumulative gas production, cumulative condensate production, and NPV are illustrated in Figures 5.41, 5.42, 5.43, and 5.44, respectively. The annual cash flow tables for all cases are shown in Tables 5.8, 5.9, 5.10, and 5.11.
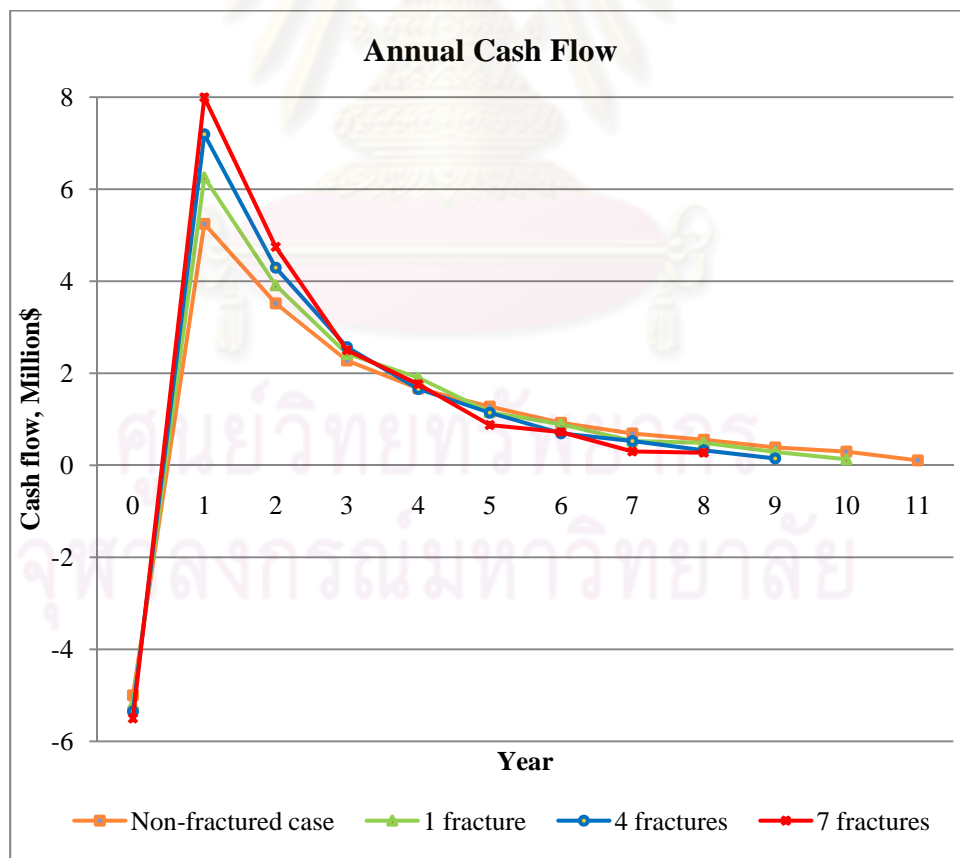
Figure 5.41: Annual cash flow.
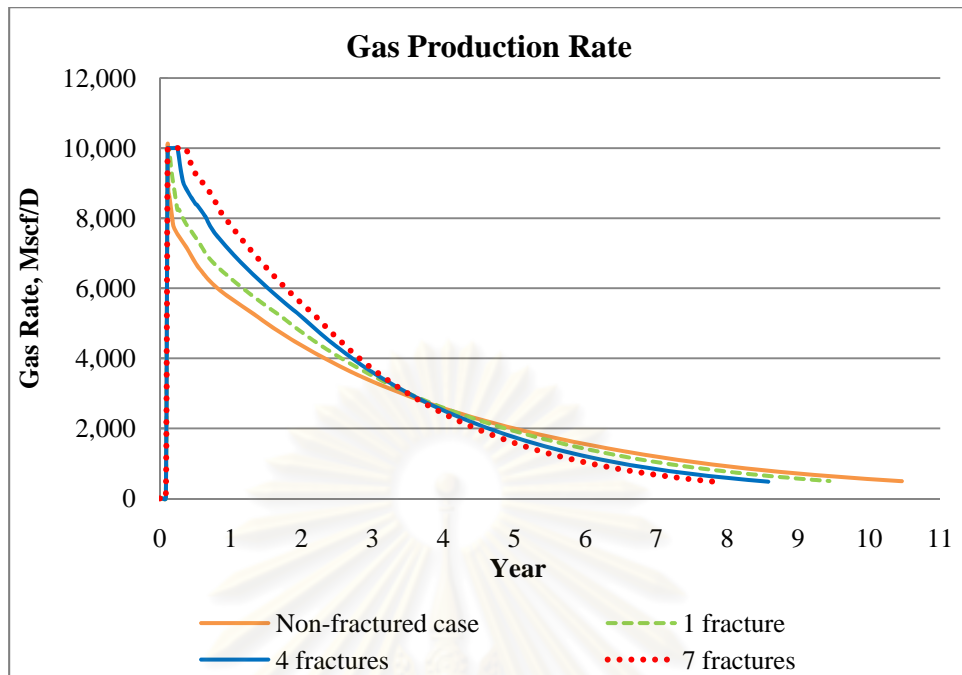
Figure 5.42: Gas production rate for different number of fractures.
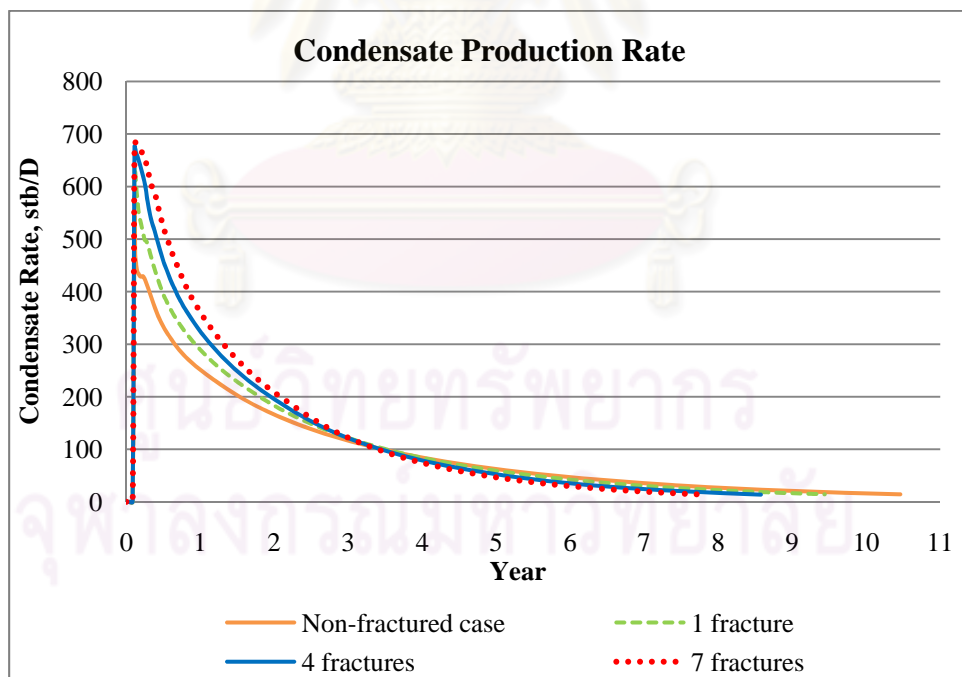
Figure 5.43: Condensate production rate for different number of fractures.
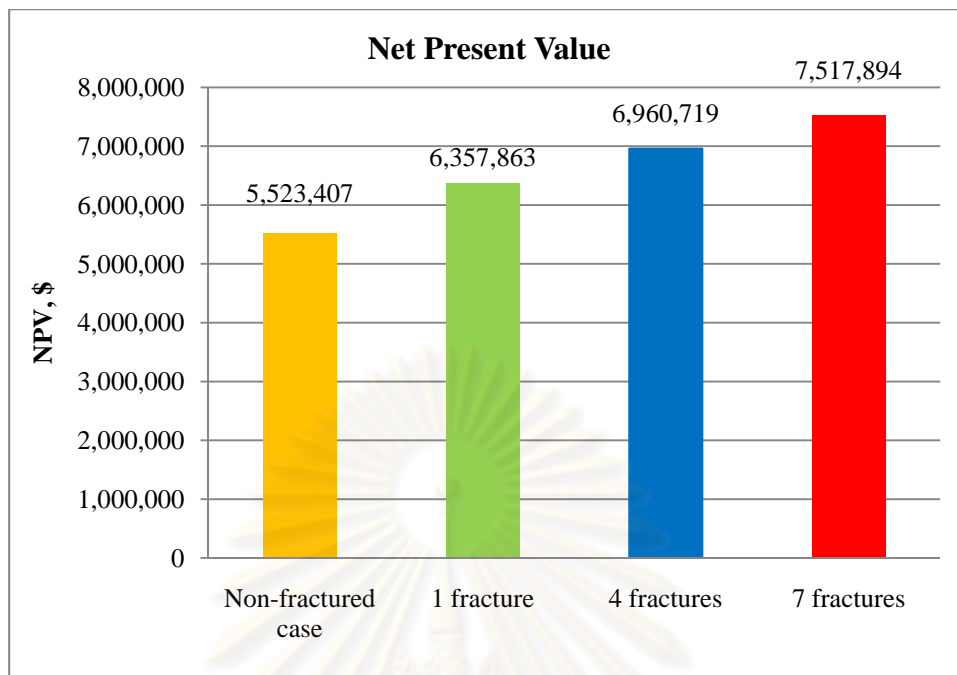
Figure 5.44 : Net present value.

The success of hydraulic fracturing is measured from value of the increase in cumulative gas and condensate production and income and the decrease of production time. From the economic analysis, the results can be summarized as follows:

1. Figure 5.41 compares annual cash flow of different cases during a period of 11 years. In year 0, the seven-fracture case has the highest investment cost and the non-fractured case has the lowest investment cost. From year 1 to 3, the seven-fracture case has the highest income because of higher gas and condensate production as shown in Figures 5.42 and 5.43. The non-fractured case has the lowest income because of lower gas and condensate production. From year 4 to 8, the income of the seven-fracture case turns to be the lowest because gas production rates decline after high gas production at early time. The one-fracture and four-fracture cases have the same trends.

2. From Figure 5.44, all cases have positive net present values. The one-fracture, four-fracture and seven-fracture cases have higher NPV than the non-fractured case.

3. From the figures above, the non-fractured, one-fracture, four-fracture and seven-fracture cases have production time of 11, 10, 9 and 8 years,

respectively. This highlights the fact that increasing number of fracture significantly decreases production time.

4. The NPV and hydraulic fracturing cost trade-off helps designing optimum number of fracture for a hydraulic fracturing stimulation.

Table 5.8: Annual cash flow for non-fractured case.

	Year												Total
	0	**1**	**2**	**3**	**4**	**5**	**6**	**7**	**8**	**9**	**10**	**11**	
Annual Gas Production (MMscf)	0.000	2.236	1.834	1.327	1.048	0.848	0.638	0.490	0.324	0.299	0.232	0.124	9.402
Annual Oil Production (stb)	0.000	111,304.44	74,558.31	48,228.06	35,315.28	27,041.63	19,527.94	14,611.34	11,755.22	8,239.00	6,277.72	2,230.25	359,089.19
Gas price ($/MMscf)	7,000	7,000	7,000	7,000	7,000	7,000	7,000	7,000	7,000	7,000	7,000	7,000	
Oil price ($/stb)	50	50	50	50	50	50	50	50	50	50	50	50	
Revenue (Million$)	0.000	5.581	3.741	2.421	1.773	1.358	0.981	0.734	0.590	0.414	0.316	0.112	18.020
Producer well cost (Million$)	5.000	0.000	0.000	0.000	0.000	0.000	0.000	0.000	0.000	0.000	0.000	0.000	5.000
Total CAPEX (Million$)	5.000	0.000	0.000	0.000	0.000	0.000	0.000	0.000	0.000	0.000	0.000	0.000	5.000
Fixed OPEX (Million$)	0.000	0.334	0.224	0.145	0.106	0.081	0.059	0.044	0.035	0.025	0.019	0.007	1.079
Hydraulic fracturing (Million$)	0.000	0.000	0.000	0.000	0.000	0.000	0.000	0.000	0.000	0.000	0.000	0.000	0.000
Total OPEX (Million$)	0.000	0.334	0.224	0.145	0.106	0.081	0.059	0.044	0.035	0.025	0.019	0.007	1.079
Total expense (Million$)	5.000	0.334	0.224	0.145	0.106	0.081	0.059	0.044	0.035	0.025	0.019	0.007	6.079
Cash Flow (Million$)	-5.000	5.247	3.517	2.276	1.667	1.277	0.922	0.690	0.555	0.389	0.297	0.106	11.942
NPV (Million$)	**5.523**												

Table 5.9: Annual cash flow for one-fracture case.

	Year												Total
	0	**1**	**2**	**3**	**4**	**5**	**6**	**7**	**8**	**9**	**10**	**11**	
Annual Gas Production (MMscf)	0.000	2.465	1.981	1.403	1.104	0.878	0.548	0.460	0.328	0.242	0.096	0.000	9.504
Annual Oil Production (stb)	0.000	132,754.94	82,938.23	51,321.11	40,381.50	24,396.88	18,913.47	11,177.43	10,342.00	6,128.50	2,739.22	0.000	381,093.28
Gas price ($/MMscf)	7,000	7,000	7,000	7,000	7,000	7,000	7,000	7,000	7,000	7,000	7,000	-	
Oil price ($/stb)	50	50	50	50	50	50	50	50	50	50	50	-	
Revenue (Million$)	0.000	6.655	4.161	2.576	2.027	1.226	0.950	0.562	0.519	0.308	0.138	0.000	19.121
Producer well cost (Million$)	5.000	0.000	0.000	0.000	0.000	0.000	0.000	0.000	0.000	0.000	0.000	0.000	5.000
Total CAPEX (Million$)	5.000	0.000	0.000	0.000	0.000	0.000	0.000	0.000	0.000	0.000	0.000	0.000	5.000
Fixed OPEX (Million$)	0.000	0.399	0.249	0.154	0.121	0.073	0.057	0.034	0.031	0.018	0.008	0.000	1.145
Hydraulic fracturing (Million$)	0.200	0.000	0.000	0.000	0.000	0.000	0.000	0.000	0.000	0.000	0.000	0.000	0.200
Total OPEX (Million$)	0.200	0.399	0.249	0.154	0.121	0.073	0.057	0.034	0.031	0.018	0.008	0.000	1.345
Total expense (Million$)	5.200	0.399	0.249	0.154	0.121	0.073	0.057	0.034	0.031	0.018	0.008	0.000	6.345
Cash Flow (Million$)	-5.200	6.256	3.912	2.422	1.905	1.153	0.893	0.528	0.488	0.290	0.129	0.000	12.776
NPV (Million$)	6.358												

Table 5.10: Annual cash flow for four-fracture case.

	Year												Total
	0	**1**	**2**	**3**	**4**	**5**	**6**	**7**	**8**	**9**	**10**	**11**	
Annual Gas Production (MMscf)	0.000	2.775	2.201	1.534	1.083	0.712	0.579	0.339	0.286	0.111	0.000	0.000	9.619
Annual Oil Production (stb)	0.000	152,694.19	91,058.01	54,399.46	35,095.78	24,199.00	14,667.56	11,174.34	6,890.00	3,159.79	0.000	0.000	393,338.13
Gas price ($/MMscf)	7,000	7,000	7,000	7,000	7,000	7,000	7,000	7,000	7,000	7,000	-	-	
Oil price ($/stb)	50	50	50	50	50	50	50	50	50	50	-	-	
Revenue (Million$)	0.000	7.654	4.568	2.731	1.762	1.215	0.737	0.561	0.347	0.159	0.000	0.000	19.734
Producer well cost (Million$)	5.000	0.000	0.000	0.000	0.000	0.000	0.000	0.000	0.000	0.000	0.000	0.000	5.000
Total CAPEX (Million$)	5.000	0.000	0.000	0.000	0.000	0.000	0.000	0.000	0.000	0.000	0.000	0.000	5.000
Fixed OPEX (Million$)	0.000	0.458	0.274	0.163	0.105	0.073	0.044	0.034	0.021	0.009	0.000	0.000	1.181
Hydraulic fracturing (Million$)	0.350	0.000	0.000	0.000	0.000	0.000	0.000	0.000	0.000	0.000	0.000	0.000	0.350
Total OPEX (Million$)	0.350	0.458	0.274	0.163	0.105	0.073	0.044	0.034	0.021	0.009	0.000	0.000	1.531
Total expense (Million$)	5.350	0.458	0.274	0.163	0.105	0.073	0.044	0.034	0.021	0.009	0.000	0.000	6.531
Cash Flow (Million$)	-5.350	7.196	4.295	2.567	1.657	1.142	0.693	0.528	0.326	0.149	0.000	0.000	13.203
NPV (Million$)	**6.961**												

Table 5.11: Annual cash flow for seven-fracture case.

	Year												Total
	0	1	2	3	4	5	6	7	8	9	10	11	
Annual Gas Production (MMscf)	0.000	3.010	2.266	1.689	0.971	0.829	0.433	0.314	0.202	0.000	0.000	0.000	9.715
Annual Oil Production (stb)	0.000	169,677.86	100,674.64	53,017.44	37,356.15	18,497.22	15,326.38	6,333.62	5,779.38	0.000	0.000	0.000	406,662.69
Gas price ($/MMscf)	7,000	7,000	7,000	7,000	7,000	7,000	7,000	7,000	7,000	-	-	-	
Oil price ($/stb)	50	50	50	50	50	50	50	50	50	-	-	-	
Revenue (Million$)	0.000	8.505	5.050	2.663	1.875	0.931	0.769	0.319	0.290	0.000	0.000	0.000	20.401
Producer well cost (Million$)	5.000	0.000	0.000	0.000	0.000	0.000	0.000	0.000	0.000	0.000	0.000	0.000	5.000
Total CAPEX (Million$)	5.000	0.000	0.000	0.000	0.000	0.000	0.000	0.000	0.000	0.000	0.000	0.000	5.000
Fixed OPEX (Million$)	0.000	0.509	0.302	0.159	0.112	0.056	0.046	0.019	0.017	0.000	0.000	0.000	1.221
Hydraulic fracturing (Million$)	0.500	0.000	0.000	0.000	0.000	0.000	0.000	0.000	0.000	0.000	0.000	0.000	0.500
Total OPEX (Million$)	0.500	0.509	0.302	0.159	0.112	0.056	0.046	0.019	0.017	0.000	0.000	0.000	1.721
Total expense (Million$)	5.500	0.509	0.302	0.159	0.112	0.056	0.046	0.019	0.017	0.000	0.000	0.000	6.721
Cash Flow (Million$)	-5.500	7.995	4.747	2.503	1.762	0.875	0.723	0.300	0.273	0.000	0.000	0.000	13.680
NPV(Million$)	7.518												

CHARPTER VI

CONCLUSIONS AND RECOMMENDATIONS

6.1   Conclusions

Many horizontal wells have been drilled in gas condensate, but a few of them have been hydraulically fractured to improve gas and condensate recovery. Also, there are not many researches showing successful use of hydraulic fracturing for horizontal wells in gas condensate reservoirs.

Successful use of hydraulic fracturing requires reservoir simulation study which incorporates all available data to justify economic success. Reservoir simulation in this thesis takes into account all important factors used in various reviewed researches to accurately estimate results.

Results found in this thesis obtain better understanding of effect of hydraulic fracturing on gas and condensate recovery. This thesis also helps in planning the well and designing the optimum hydraulic fracture to maximize gas and condensate recovery and leads to the decision to perform hydraulic fracturing for horizontal wells.

In this study, reservoir simulator is used as a tool to investigate productivity improvement when horizontal well is hydraulic fractured with different design parameters.

Firstly, a non-fractured horizontal well in a low permeability gas condensate reservoir was simulated. The effect of reservoir permeability was studied.

Secondly, a hydraulically fractured horizontal well was then modeled to evaluate the effects of fracture spacing, fracture half-length, fracture width, fracture permeability and number of fractures on well productivity

Then, condensate saturation profile for the hydraulically fractured horizontal well was investigated.

Finally, economy analysis was performed in order to investigate the feasibility of hydraulic fracturing project.

From the simulation results for different cases, the following comments can be made:

1. In a low permeability gas condensate reservoir, a hydraulic fracturing increases gas production rate. There is a plateau in the gas production rate for a hydraulically fractured horizontal well compared to no plateau in the non-fractured horizontal well.

2. Hydraulic fracturing reduces the pressure drawdown, leading to less condensate dropout near the wellbore and more condensate produced at surface.

3. Cumulative gas production slightly increases in all fractured cases when compared to a non-fractured horizontal well while cumulative condensate production greatly increases in all fractured cases when compared to a non-fractured horizontal well.

4. All fracture design parameters: fracture spacing, fracture half-length, fracture width, fracture permeability and number of fractures have small impact on the gas recovery increment. However, they have significant impact on condensate recovery increment.

5. The amount of time required to produce gas and condensate from the reservoir significantly reduces as the fracture spacing decreases or any of these parameters: fracture half-length, fracture width, fracture permeability and number of fracture increases.

6. The NPV and hydraulic fracturing cost trade-off helps designing optimum number of fracture for hydraulic fracturing.

7. The results can be used as guideline to optimize the hydraulic fracturing design for a horizontal well in gas condensate reservoirs.

6.2 Recommendations

The following points are recommendations for future study:

1. Nowadays tools do not adequately describe hydraulic fractures that are the key to development of tight gas or gas condensate reservoirs. Fractures are described as linear smooth channels of uniform width. However, real fractures are rough and branching. Development of simulation tools will improve our ability to describe fractures complexity and increase understanding of hydraulic fracturing.

2. The full-field simulation with real field data should be studied to confirm productivity improvement from hydraulic fracturing.

3. Study of longitudinally fractured horizontal well should be done to better understand the impact of longitudinal fractures on the performance of horizontal well.

4. ECLIPSE 300 compositional simulation should be used to take into account the change in fluid composition as gas and condensate is produced from the reservoir.

References

[1] Chen, H. L., Wilson, S. D., and Monger-McClure. Determination of Relative Permeability and Recovery for North Sea Gas Condensate Reservoir. Paper SPE 30769 presented at the 1995 SPE Annual Technical Conference and Exhibition, Dallas, Texas, U.S.A., 22-25 October 1995.

[2] Boom, W., Wit, K., Zeelenberg, J.P.W., Weeda, H.C., and Maas, J.G. On the Use of Model Experiments for Assessing Improved Gas condensate Mobility Under Near-Wellbore Flow Conditions. Paper SPE 36714 presented at the 1996 SPE Annual Technical Conference and Exhibition, Denver, Colorado, U.S.A., 6-9 October 1996.

[3] Settari, A., Bachman, R.C., Hovem, K., and Paulson, S.G. Productivity of Fractured Gas Condensate Wells – A Case Study of Smorbukk Field. Paper SPE 35604 presented at the 1996 Gas Technology Conference, Calgary, Canada, 28 April - 1 May 1996.

[4] Fevang, P.Ø., and Whitson, C.H. Gas Condensate Relative Permeability for Well Calculations. Paper SPE 56476 presented at the 1999 SPE Annual Technical Conference, Houston, Texas, U.S.A., 3-6 October 1999.

[5] Wheaton, R.J., and Zhang, H.R. Condensate Banking Dynamics in Gas Condensate Fields: Compositional Changes and Condensate Accumulation Around Production Wells. Paper SPE 62930 presented at the 2000 SPE Annual Technical Conference and Exhibition, Dallas, Texas, U.S.A., 1-4 October 2000.

[6] Luo, K., et al Experimental Investigation in Revaporization of Retrograde Condensate by Lean Gas Injection. Paper SPE 68683 presented at the 2000 SPE Asia Pacific Oil and Gas Conference, Jakarta, Indonesia, 17-19 April 2000.

[7]   Chowdhury, N.S, Sharma, R., Pope, G.A., and Sepehrnoori, K. A Semi-
      Analytical Method to Predict Well Deliverability in Gas Condensate
      Reservoirs. Paper SPE 90320 presented at the 2004 SPE Annual
      Technical Conference, Houston, Texas, U.S.A., 26-29 September 2004.

[8]   Hashemi, A., and Gringarten, A.C. Comparison of Well Productivity Between
      Vertical, Horizontal and Hydraulically Fractured Wells in Gas condensate
      Reservoirs. Paper SPE 94178 presented at the 2005 SPE Europec/EAGE
      Annual Conference, Madrid, Spain, 13-16 June 2005.

[9]   Holditch, S.A. Optimization of Well Spacing and Fracture Length in Low
      Permeability Gas Reservoirs. Paper SPE 7496 presented at the 1978 SPE
      Annual Technical Conference, Houston, Texas, U.S.A., 1-3 October 1978.

[10] Baig, T., and Droegemueller, U. Productivity Assessment of Fractured and Non-
      Fractured Wells in a Lean/Intermediate Low Permeability Gas Condensate
      Reservoir. Paper SPE 93136 presented at the 2005 SPE Europe/EAGE
      Annual Conference held in Madrid, Spain, 13-16 June 2005.

[11] Medeiros, F., Ozkan, E., and Kazemi, H. Productivity and Drainage Area of
      Fractured Horizontal Wells in Tight Gas Reservoirs. Paper SPE 108110
      presented at the 2008 SPE Rocky Mountain Oil and Gas Technology
      Symposium, Denver, Colorado, U.S.A., 16-18 April 2008.

[12] George, W., et al Simultaneous Hydraulic Fracturing of Adjacent Horizontal
      Wells in the Woodford Shale. Paper SPE 119635 presented at the 2009
      SPE Hydraulic Fracturing Technology Conference, Woodlands, Texas,
      U.S.A., 19–21 January 2009.

[13] Ehrl, E., and Schueler, S.K. Simulation of a Tight Gas Reservoir with Horizontal Multifractured Wells. Paper SPE 65108 presented at the 2000 SPE European Petroleum Conference held in Paris, France, 24-25 October 2000.

[14] Alberto, C., Loris, T., Roberto, L.C., Brad, M., and Jim, A. Multiple Transverse Fracturing in Open Hole Allows Development of a Low Permeability Reservoir in the Foukanda Field, Offshore Congo. Paper SPE 119140 presented at the 2009 SPE Hydraulic Fracturing Technology Conference , Woodlands, Texas, U.S.A., 19–21 January 2009.

[15] Byung, L., Aramco, S., Steve, D., and Kirk, B. Optimization of Multiple Hydraulic Fractures for Open Hole Horizontal Wells by Numerical Modeling – Saudi Arabia Case Study. Paper SPE 124406 presented at the 2009 SPE Annual Technical Conference and Exhibition held in New Orleans, Louisiana, U.S.A., 4-7 October 2009.

[16] Coghlan, G., and Holland, B. The Chiswick Field: Long Horizontal Wells and Innovative Fracturing Solutions in a Low Permeability, Sandstone, Gas Reservoir in the North Sea. Paper SPE 124067, presented at 2009 SPE Annual Technical Conference and Exhibition held in New Orleans, Louisiana, U.S.A., 4-7 October 2009.

[17] Lolon, E.P., Cipolla, C.L., Weijers, L., Hesketh, R.E., and Grigg, M.W. Evaluating Horizontal Well Placement and Hydraulic Fracture Spacing/Conductivity in the Bakken Formation, North Dakota. Paper SPE 124905 presented at the 2009 SPE Annual Technical Conference and Exhibition held in New Orleans, Louisiana, U.S.A., 4-7 October 2009.

[18] Li, F., et al Understanding Gas-Condensate Reservoirs. Oilfield Review (Winter 2005-2006), page 14–27, 2005.

[19] Henry, D. The Distribution of Water. The Public Fountains of the City of Dijon, 1856.

[20] Forchheimer, P. Wasserbewegung durch Boden. ZVD1, 1901.

[21] Geertsma, J. Estimating the Coefficient of Inertial Resistance in Fluid Flow through Porous Media. SPEJ, page 445-450, October 1974.

[22] Schlumberger Information Solutions. ECLIPSE Reference Manual 2007.1 and ECLIPSE Technical Description 2007.1.

[23] Blom, S.M.P., and Hagoort, J. How to Include the Capillary Number in Gas Condensate Relative Permeability Functions?. Paper SPE 49268, presented at the 1998 SPE Annual Technical Conference and Exhibition held in New Orleans, Louisiana, U.S.A., 27-30 September 1998.

[24] Brady, B., Elbel, J., Mack, M., Morales, H., Nolte, K. and Poe, B. Cracking Rock: Progress in Fracture Treatment Design. Schlumberger Oilfield Review, October 1992.

[25] Michael P.C. Analysis of Mechanisms and Procedures for Producing Favourable Shapes of Hydraulic Fractures. Paper SPE 9260, presented at the 55th Annual Fall Technical Conference and Exhibition of the Society of Petroleum Engineering of AIME. Held in Dallas, Texas, U.S.A. 21-24 September 1980.

[26] Montgomery, K.T., Holditch, S.A., and Berthelot, J.M. Effects of Fracture Fluid Invasion on Cleanup Behavior and Pressure Buildup Analysis. Paper SPE 20643, presented at the 1990 SPE Annual Technical Conference and Exhibition, Houston, Texas, U.S.A. 23-26 September 1990.

[27] Encana Corporation. Hydraulic Fracturing Explained.

[28] Shaoul, J.R., Behr, A., and Mtchedlishvili, G. Developing a Tool for 3D Reservoir Simulation of Hydraulically Fractured Wells. Paper SPE 108321, presented at the 2005 SPE International Petroleum Technology Conference, Doha, Qatar, 21-23 November 2005.

[29] Erwin, K., Ibrahim, S. A., Krishna, B., and Martin, F.C. Compositional Simulation of Well Performance for Fractured and Multiple Fractured Horizontal Wells in Stratified Gas Condensate Reservoirs. Paper SPE 37995, presented at the 1997 SPE Reservoir Simulation Symposium held in Dallas, Texas, U.S.A., 8-11 June 1997.

[30] Peaceman, D.W. Representation of a Horizontal Well in Numerical Simulation. Paper SPE 21217, presented at the 11th SPE Symposium on Reservoir Simulation, Anaheim, California, U.S.A. 17-20 February 1991.

[31] Petroleum Experts. PROSPER Single Well Systems Analysis user guide version 9.1.

[32] Gould, T.L., Tek, M.R., and Katz, D.L. Two-Phase Flow Through Vertical, Inclined, or Curved Pipe. JPT, page 915-925, August 1974.

[33] Hagedorn, A.R., and Brown, K.E. Experimental Study of Pressure Gradients Occuring During Continuous Two-Phase Flow in Small-Diameter Vertical Conduits. JPT, page 475-484, April 1965.

[34] Duns, H.J., and Ros, N.C.J. Vertical Flow of Gas and Liquid Mixtures in Wells. Proc., Sixth World Petroleum Congress, Frankfurt, page 451, 1963.

Vitae

Kuntol Chinrungkhakul was born in Chiang Rai, Thailand on 20th January 1985. He completed his high school education at Samakkhi Witthayakhom School, Chiang Rai, Thailand in 2003. He entered Chulalongkorn University, Bangkok, Thailand in June 2003. He received his Bachelor of Engineering in Computer Engineering from the Faculty of Engineering, Chulalongkorn University in 2007. In June 2007, he continued his studies in the Master of Petroleum Engineering program at the Department of Mining and Petroleum Engineering, Faculty of Engineering, Chulalongkorn University.